

TECTONO-GEOMORPHIC EVOLUTION OF THE INTERMONTANE  
BASINS AND QUATERNARY DEFORMATION IN THE  
SCHUPPEN BELT IN PARTS OF THE DIMAPUR  
AND PEREN DISTRICTS, NAGALAND



by

**J. N. MOIYA**

Submitted  
In partial fulfillment of the requirement of the Degree of  
Doctor of Philosophy in Geology  
Nagaland University

## NAGALAND UNIVERSITY

May 2019

### DECLARATION

I, Miss J.N. Moiya, hereby declare that the subject matter of this thesis is the record of work done by me, that the contents of this thesis did not form basis of the award of any previous degree to me or to the best of my knowledge to anybody else, and that the thesis has not been submitted by me for any research degree in any other University/Institute.

This is being submitted to the Nagaland University for the degree of Doctor of Philosophy in Geology.

  
Candidate

  
Head

  
Supervisor

  
17/5/2019  
Co-Supervisor

HEAD  
Department of Geology  
Nagaland University, Kohima

*NAGALAND*



*UNIVERSITY*

*Glenn T. Thong*  
*Professor of Geology*

☎ : 0370-2240515  
Mobile : 09436000479  
E-mail : [glen2t03@yahoo.com](mailto:glen2t03@yahoo.com)  
[nagalandslide@yahoo.com](mailto:nagalandslide@yahoo.com)

*Dated Kohima the 17<sup>th</sup> May 2019*

## **CERTIFICATE**

The thesis presented by Miss J.N. Moiya, M.Sc., bearing Registration No. 601/2014 (20<sup>th</sup> May 2014) embodies the results of investigations carried out by her under my supervision and guidance.

I certify that this work has not been presented for any degree elsewhere and that the candidate has fulfilled all conditions laid down by the University.

(G.T. THONG)  
Supervisor



**WADIA INSTITUTE OF HIMALAYAN GEOLOGY**  
(An Autonomous Institute of Department of Science & Technology,  
Govt. of India) 33, General Mahadeo Singh Road,  
Dehradun-248 001 Uttarakhand, India

**Dr. Khayingshing Luirei**  
M.Sc., Ph.D.  
**Scientist - E**

Phone: 91+135-2525405  
Email: ashing\_luirei@wihg.res.in

---

Dated Dehradun, 17<sup>th</sup> May 2019

**CERTIFICATE**

The thesis presented by Miss J.N. Moiya, M.Sc., bearing Registration No. 601/2014 (20<sup>th</sup> May 2014) embodies the results of investigations carried out by her under my supervision and guidance.

I certify that this work has not been presented for any degree elsewhere and that the candidate has fulfilled all conditions laid down by the University.

(DR. KHAYINGSHING LUIREI)  
Co-Supervisor



## ACKNOWLEDGEMENTS

This thesis is the result of guidance, support and help received from various individuals and organization. I would like express my sincere gratitude and appreciation in humble acknowledgement.

I extend my heartfelt gratitude to my Supervisor Dr. Glenn T. Thong, Professor of Geology, Nagaland University and Co-Supervisor Dr. Khayingshing Luirei, Scientist 'E', Wadia Institute of Himalayan Geology, Dehradun, for their supervision, guidance, and encouragement in various ways. I am indebted for their help and support in preparation and completion of the thesis.

I sincerely thank Dr. Girish Ch. Kothiyari, Scientist, Institute of Seismological Research, Raisan, Gandhinagar for extending all help in chronological data analysis. I am greatly obliged for the valuable suggestions in improving the quality of my research work.

I would like to thank the Nagaland University for giving me the opportunity to pursue my doctoral degree as well as granting the Non-NET fellowship.

I am extremely thankful to the Faculty of the Geology Department, Nagaland University, Prof. B.V. Rao, Prof. S.K. Singh, Dr. V. Rino, Dr. S.K. Srivastava, Dr. T. Walling and Dr. C.M. Khuman for their constant guidance and support and also all the Non-Teaching Staff of the Department for rendering their help in various ways.

I owe deepest gratitude to Mr. Limasanen Longkumer for constantly assisting me during field and laboratory works and also thank all my colleagues, Ms. Anettsungla, Mrs. Aienla Ozukum, Ms. Imlirenla Jamir, Mr. A. Moalong Kichu, Mr. R. Peseyie, Mr. Wathang Rengma and Mr. Kenyelo for their words of encouragement and advice.

I am extremely thankful to Dr. Supongtemjen, Nagaland GIS and Remote Sensing Centre, Department of Planning and Coordination, Kohima for help received in Remote Sensing and GIS during my initial research work.


I am grateful to the Geological Survey of India, Dimapur for facilitating the access and provision of the data.

I would like to express my heartfelt thanks to Prof. Thong's family for their hospitality and generosity.

My sincere gratitude goes to Ms. Mary K. Liezietsu, Assistant Professor, Department of Anthropology, Kohima Science College, Jotsoma for her constant support and help.

Lastly, I express my love and gratitude to my parents, siblings, friends and dear ones for their constant support and blessings that have made the completion of my thesis possible.

Praise the Almighty for His grace

  
J. N. Moiya

## PARTICULARS OF CANDIDATE

NAME OF CANDIDATE : Miss J. N. Moiya

DEGREE : Ph.D.

DEPARTMENT : Geology

TITLE OF DISSERTATION :  
**Tectono-geomorphic evolution of the intermontane basins and Quaternary deformation in the Schuppen Belt in parts of the Dimapur and Peren districts, Nagaland**

DATE OF ADMISSION : 30/8/2013

APPROVAL OF RESEARCH PROPOSAL : 16<sup>th</sup> June 2014

REGISTRATION NUMBER AND DATE : 601/2014 (20.05.2014)

  
Head of Department

HEAD  
Department of Geology  
Nagaland University, Kohima

## BIODATA OF THE CANDIDATE

### I. Papers Published

1. **Moiya, J.N.**, Luirei, K., Longkumer, L., Kothiyari, G.C and Thong, G.T., 2019 Late Quaternary deformation in parts of the Belt of Schuppen of Dimapur and Peren districts, Nagaland, NE India. **Geological Journal**, <https://doi.org/10.1002/gj.3413>, pp. 1-20.
2. Longkumer, L., Luirei, K., **Moiya, J.N.** and Thong. G.T., 2019. Morphotectonics and neotectonic activity of the Schuppen Belt of Mokokchung, Nagaland, India. **Journal of Asian Earth Sciences** <https://doi.org/10.1016/j.jseaes.2018.11.010>, vol. 170, pp. 138-154.

### II. Oral Presentations / Abstracts Published

1. Morphotectonic analysis of watershed in Schuppen Belt in parts of Dimapur and Peren districts, Nagaland. National Seminar on Geology, Geochemistry, Tectonics, Energy and Mineral Resources of North East India. Organized by Department of Geology, Nagaland University, Kohima Campus, Meriema (9-11 November, 2016).
2. Analysis of geomorphic indices using GIS to decipher tectonic activity in Dimapur and Peren districts of Nagaland. Research Conclave '19, An Amalgamation of Academia, Industry & Start-Up. Organized by Students' Academic Board, IIT, Guwahati (14-17 March, 2019) - **Best Presentation Award**.

### III. Workshop / Training Attended

1. National Workshop on Active Fault Mapping. Sponsored by Ministry of Earth Sciences, New Delhi. Organized by Department of Geology, Mizoram University, Aizawl (3-5 May, 2014).
2. Regional Workshop for Young Earth Scientists on Tectonics, Sedimentation and Geohazards, with Special Reference to North East India. Conducted by Department of Geology Nagaland University, Kohima Campus, Meriema (16-21 November, 2015).
3. National Workshop on Geoinformatics in Geology. Organized by Department of Geological Sciences, Gauhati University, Guwahati, Assam (20-25 June, 2016).
4. National Workshop on Sequence Stratigraphy and Basin Analysis. Conducted by Department of Geology, Nagaland University, Kohima Campus, Meriema (26-30 November, 2018).

## PREFACE

This study has been carried out in parts of the Dimapur and Peren districts within the Belt of Schuppen, a complex thrust zone. This thrust fold belt is riddled with joints, faults and other lineaments. The complex setting is due to varied tectonic activity in numerous phases. An attempt has been made in this study to determine the tectonic activity in this region through the applications of GIS and remote sensing. Emphasis was given to identification of the morphotectonic features and computation of the various morphometric parameters in conjunction with field observations and chronologic data to validate the evidences of tectonic movements.

The study has been arranged in seven chapters in the thesis, which are as follows:

**Chapter 1:** This chapter introduces the subject and gives an overview of the study area with details of location and accessibility, climate, geomorphology and drainage, while spelling out the objectives and giving a brief background of previous works.

**Chapter 2:** The general geology and tectonic setup of Nagaland and the study area are discussed here.

**Chapter 3:** All the materials and methods used for the research are discussed in detail in this chapter.

**Chapter 4:** The computed results of the morphometric parameters are discussed and suitable deductions made.

**Chapter 5:** This chapter deals with the morphotectonic features of the study area. Emphasis is laid on the strath and fluvial terraces to decipher tectonic movements through sediment deformation and river migration. All findings, including that obtained from topographic profiles, are discussed at length and appropriate interpretations made.

**Chapter 6:** This chapter deals with chronologic dates obtained from sediments of fluvial terraces, which are used to determine the ages of sediments and timing of deformations.

**Chapter 7:** All the results of the above work are summarized and concluded here.

# CONTENTS

	Page No.
<i>Declaration</i>	i
<i>Certificate of Supervisor</i>	ii
<i>Certificate of Co-Supervisor</i>	iii
<i>Acknowledgements</i>	iv
<i>Particulars of the Candidate</i>	v
<i>Biodata of the Candidate</i>	vi
<i>Preface</i>	vii
<i>List of Tables</i>	viii
<i>List of Figures</i>	ix-x
<b>CHAPTER 1</b>	
<b>INTRODUCTION</b>	<b>1-8</b>
1.1 Location and accessibility	2
1.2 Climate	2
1.3 Geomorphology	4
1.4 Drainage	4
1.5 Objectives	4
1.6 Review of literature	5
<b>CHAPTER 2</b>	
<b>GEOLOGY AND TECTONIC SETUP</b>	<b>9-25</b>
2.1 Tectono-stratigraphy	9
2.1.1 Naga Metamorphics	9
2.1.1.1 Nimi Formation	11
2.1.2.2 Saramati Formation	11
2.1.2 Naga Ophiolite Belt	12
2.1.2.1 Salumi Formation	12
2.1.2.2 Phokpur/Jopi Formation	12
2.1.3 Inner Fold Belt	13
2.1.3.1 Kohima Synclinorium	13
2.1.3.2 Patkai Synclinorium	13
2.1.4 Belt of Schuppen	14
2.2 Cenozoic Sequences in the Inner Fold Belt	14
2.2.1 Disang Group	14
2.2.1.1 Lower Disang Formation	15
2.2.1.2 Upper Disang Formation	16
2.2.2 Barail Group	16
2.2.2.1 Laisong/Naogaon Formation	17
2.2.2.2 Jenam/Baragolai Formation	17
2.2.2.3 Renji/Tikak Parbat Formation	18
2.2.3 Surma Group	18
2.2.3.1 Bhuban Formation	19
2.2.3.1a <u>Lower Bhuban Formation</u>	19
2.2.3.1b <u>Middle Bhuban Formation</u>	19
2.2.3.1b <u>Upper Bhuban Formation</u>	19
2.2.3.2 Bokabil	19
2.2.4 Tipam Group	20
2.2.4.1 Tipam Sandstone Formation	20
2.2.4.2 Girujan Clay Formation	20

2.2.5	Dupi Tila Group	21
2.2.6	Dihing Group	21
2.3	Geology and structure of the study area	21
2.3.1	Lithostratigraphy	21
2.3.1.1	Chathe Alluvium	22
2.3.2	Structure	23
2.3.2.1	Thrust	23
2.3.2.2	Fault	24
2.3.2.3	Anticline	24
<b>CHAPTER 3</b>	<b>METHODOLOGY</b>	<b>26-32</b>
3.1	Morphometric analysis	26
3.1.1	Drainage analysis	26
3.1.2	Longitudinal profile	27
3.1.3	Stream length gradient index	27
3.1.4	Steepness index	27
3.1.5	Asymmetry factor	28
3.1.6	Transverse topographic symmetry factor	28
3.1.7	Basin elongation ratio	28
3.1.8	Channel sinuosity	29
3.1.9	Mountain front sinuosity	29
3.1.10	Valley floor width to valley height ratio	30
3.1.11	Hypsometric curve and hypsometric integral	30
3.2	Optical Chronology	31
3.2.1	Fieldwork	31
3.2.2	Laboratory work	31
<b>CHAPTER 4</b>	<b>MORPHOMETRIC ANALYSIS</b>	<b>33-51</b>
4.1	Drainage Analysis	34
4.1.1	Drainage Pattern	34
4.2.2	Drainage order and orientation	35
4.1.3	Drainage density	36
4.2	Geomorphic indices	37
4.2.1	Longitudinal profile	37
4.2.2	Stream length gradient index	38
4.2.3	Steepness index	39
4.2.4	Asymmetry factor	41
4.2.5	Transverse topography symmetry factor	42
4.2.6	Basin elongation ratio	43
4.2.7	Channel sinuosity	45
4.2.8	Mountain front sinuosity	46
4.2.9	Valley floor width to valley height ratio	47
4.2.10	Hypsometric curve and hypsometric integral	48
<b>CHAPTER 5</b>	<b>MORPHOTECTONICS</b>	<b>52-74</b>
5.1	Seismotectonics	54
5.2	Lineaments	54
5.3	Faults	55
5.4	River anomalies	58
5.5	Strath and valley-fill terraces	59

	5.5.1	Unpaired terraces	60
	5.5.2	Faulted terraces	62
	5.5.3	Folded terraces	65
	5.5.4	Tilted terraces	67
	5.6	Folded mountain front	68
	5.7	Topographic profiles	69
	5.8	Evolution of intermontane basins	72
<b>CHAPTER 6</b>	<b>OPTICAL CHRONOLOGY AND TIMING OF FLUVIAL AGGRADATION</b>		<b>75-83</b>
	6.1	Applications	76
	6.2	Mechanism	78
	6.3	Single aliquot regenerative dose	78
	6.4	Bleaching	79
	6.5	Measurement of equivalent dose	79
	6.6	Determining the dose rate	79
	6.7	Dating results	80
	6.8	Timing of deformation	81
<b>CHAPTER 7</b>	<b>SUMMARY AND CONCLUSIONS</b>		<b>84-89</b>
	7.1	Summary	84
	7.2	Conclusions	87
	<b>REFERENCES</b>		<b>90-101</b>

## LIST OF TABLES

<b>Table 2.1</b>	Stratigraphy of Nagaland (after Imchen et al., 2014)
Table 2.2	Stratigraphic succession of the study area (after Moiya et al., 2019)
<b>Table 4.1</b>	Asymmetry factor
<b>Table 4.2</b>	Transverse topography symmetry factor
<b>Table 4.3</b>	Basin elongation ratio
<b>Table 4.4</b>	Channel sinuosity
<b>Table 4.5</b>	Mountain front sinuosity index
<b>Table 4.6</b>	Valley floor width to valley height ratio
<b>Table 6.1</b>	Application in sedimentary environments for OSL dating
<b>Table 6.2</b>	OSL chronology (modified after Moiya et al., 2019)



## LIST OF FIGURES

- Fig. 1.1** Map of the study area (modified after Moiya et al., 2019)
- Fig. 2.1** Geological map of the study area (modified after Chakraborty and Sarma 1982; Chakradhar and Gaur, 1985; Moiya et al., 2019)
- Fig. 4.1** (a) Drainage map of the study area - (a1) Dendritic pattern, (a2) Parallel pattern, (a3) Trellis pattern, (a4) Rectangular pattern (b) Drainage orientation of the various drainage orders (modified after Moiya et al., 2019)
- Fig. 4.2** Drainage density map showing high values within the Belt of Schuppen (modified after Moiya et al., 2019)
- Fig. 4.3** (a) Profiles of Bara Manglu, Langlong, Khova, Chathe, and Jharnapani rivers; (b) Knickpoints observed along the longitudinal profile, stream length gradient index and steepness index of the five major rivers of the study area (modified after Moiya et al., 2019)
- Fig. 4.4** Asymmetry factor, transverse topography symmetry factor and basin elongation ratio map with T orientation showing a prominent NE-SW direction (modified after Moiya et al., 2019)
- Fig. 4.5** Channel sinuosity, mountain front sinuosity and valley floor width to valley height ratio (modified after Moiya et al., 2019)
- Fig. 4.6** Hypsometric curve and hypsometric integral
- Fig. 5.1** Tectono-geomorphologic map of the study area (modified after NGISRSC, 2014)
- Fig. 5.2** Seismotectonic map of NE India (after Nandy, 2000 and earthquake epicenters from USGS, 1915-2016)
- Fig. 5.3** Lineament map of the study area showing prominent trend NE-SW and NW-SE trends; higher densities are noted in the thrust zones (modified after Moiya et al., 2019)
- Fig. 5.4** (a) Chathe Fault and local faults observed in the study area (b) Depression along the Chathe Fault (c) Trace of Chathe Fault (after Moiya et al., 2019)
- Fig. 5.5** (a) Google Earth image showing palaeochannels (b) Topographic highs-1,2,3 (c) Chathe River course during (1921-23), (d) Chathe River showing stream capture and migration (1981-83) (after Moiya et al., 2019)
- Fig. 5.6** (a-d) Unpaired levels of strath terrace observed in study area (modified after Moiya et al., 2019)

- Fig. 5.7** Fault- displaced Quaternary sediments near Sanis-Chongliyimsen Thrust (after Moiya et al., 2019)
- Fig. 5.8** (a) Strath terraces along the Chathe River (b, c) Chathe Alluvium and Dihing displaced by normal fault (d) Faulting within Dihing (4) Normal fault dislocating Dihing and overlying Chathe Alluvium(after Moiya et al., 2019)
- Fig. 5.9** (a) Displacement at various locations of the strath terraces along AH1 (b) Numerous fault dislocating the bedrock and younger sediments (c) Fault observed in the Girujan bedrock with displacement extending into the overlying Chathe Alluvium (after Moiya et al., 2019)
- Fig. 5.10** Fill terrace displaced by normal fault along the Chathe River (after Moiya et al., 2019)
- Fig. 5.11** Displacement of Jenam bedrock and overlying fluvial deposits
- Fig. 5.12** (a) Three levels of strath terraces along the banks of Bara Manglu River (b) Folded Jenam bedrock affected by normal fault, (c) Slickensides on bedrock
- Fig. 5.13** (a) Folded bedrock and sediments (b) Sheared sandstone bed exposed near Naga Thrust zone (after Moiya et al., 2019)
- Fig. 5.14** Tilted terrace observed along the AH1 (after Moiya et al., 2019)
- Fig. 5.15** Tilted sediments along the Langlong River
- Fig. 5.16** (a) Folded mountain front (b) inclined Surma bedrock with tilted pebbles (modified after Moiya et al., 2019)
- Fig. 5.17** (a) Cross-sections (b) Development of two intermontane basins within BoS (c) Topographic profiles sections a-a', b-b', c-c', d-d' and e-e'
- Fig. 5.18** Development of Medziphema and Jalukie intermontane basins within the thrust plane of the BoS
- Fig. 6.1** Flow chart shows procedure to measure De (left) and the dose rate (right) are combined to calculate a luminescence age
- Fig. 6.2** OSL sample sites of the study area (modified after Moiya et al., 2019)

## CHAPTER: 1

### INTRODUCTION

The tectonically complex structural framework of NE India owes its development to the collision of the Indian and Eurasian plates during the Alpine orogenesis (Molnar and Tapponnier, 1975; Aier et al., 2011). Merging of these plates generated strong compressional forces that led to the subduction of the Indian Plate under the Burma (Myanmar) microplate, the eastern extension of the Eurasian Plate, during middle Eocene (Aier et al., 2011; Moiya et al., 2019). The northern collision resulted in the formation of the Himalayan mountain ranges while the eastern collision-subduction gave rise to the Indo-Myanmar Ranges (IMR) (Olympa and Kumar, 2015). The Eastern Himalaya and Indo-Burmese arcs represent the subduction margin between the Indian and Eurasian plates (Singh, 2017).

The IMR, forming the western fringe of the Burma microplate (Najman et al., 2019), is an arc-shaped tectonic belt that is classified into three tectonic blocks including the Arakan-Yoma Hills, Chin Hills and Naga Hills (Singh, 2017). The Indo-Burma orogenic belt including NE India falls in the Alpine-Himalayan earthquake belt. Earthquake mechanisms and tectonics in the region suggests predominance of thrust faulting similar to the Himalayan region (Rastogi et al., 1973). The ongoing stresses between the Indian Plate and Burma microplate are evident from seismic activity in this region.

Seismically, the northeastern region lies in the Zone-V category of the seismic zonation map (India), which is regarded as very active (Bhatia et al., 1999; Devi, 2012). This region has experienced two great earthquakes; the first in the Shillong Plateau region in 1897 with a magnitude of 8.7 and the other in the Assam Syntaxis zone in 1950 with a magnitude of 8.6. Besides these two great earthquakes, the region was affected by numerous large earthquakes of magnitudes  $\geq 7.0$  in Assam (1869, 1906, 1930, 1941, 1943), Meghalaya (1923), Nagaland (1932), Arunachal Pradesh (1947, 1954, 1957) and Manipur (1988) (Devi, 2012; Olympa and Kumar, 2015).

In order to better understand the vigorous tectonic processes of this region with a complex geological history, extensive fieldwork was carried out to observe morphotectonic signatures in conjunction with morphometric analysis using geomorphic indices. The present study includes scrutiny of Survey of India (SoI) topographic maps satellite data, field studies, determination of geomorphic indices, and optically stimulated luminescence (OSL) dating of samples to decipher the role of tectonic activity in development of various landforms.

### **1.1 Location and accessibility**

Nagaland is a mountainous state in NE India with an area of 16,579 km<sup>2</sup>. It is bounded by the states of Assam (west), Arunachal Pradesh (north) and Manipur (south) and shares an international boundary with Myanmar (east). Dimapur, also known as the gateway of Nagaland, is the commercial hub of the state, with a well-connected network of roads. The only railhead and airport of Nagaland are located in Dimapur district. Dimapur is surrounded by Kohima district (east) and Peren district (south) of Nagaland and Karbi Anglong (west) and Golaghat districts (north) of Assam. Peren, about 80 km from Dimapur, is connected to Dimapur and Kohima by a network of roads. It is bounded by the Dimapur district (northeast), Kohima district (east) Karbi Anglong district (west) and Tamenglong district of Manipur (south).

The study area, with an area of 1,335 km<sup>2</sup>, falls in the Dimapur and Peren districts of Nagaland. It lies within 25°30' and 25°57'N latitudes and 93°32' and 94°00'E longitudes (Fig. 1.1), with elevations varying from 122 m to 2722 m above mean sea level (asl). The study area lies within the Belt of Schuppen (BoS), which comprises strike-slip faults, normal faults and thrusts. The BoS is designated after the schuppen structure of the Alps, which usually implies possessing similar shape and strata that dip in the same direction (Suess, 1904). The BoS is bounded between the Inner Fold Belt (IFB) in the southeast and Assam Valley in the northwest. The study area extends in both directions beyond the BoS to enable computations for Morphometric analysis.

### **1.2 Climate**

In the study area, July is the warmest and January is the coldest month of the year. The average temperature recorded during summer is 28.6°C in Dimapur district and

22.5°C in Peren district. During winter, the average temperature is about 16.6°C and 11.7°C in Dimapur and Peren districts respectively. Summer in Peren district is sultry in the valley region and pleasant in the higher hills while Dimapur district experience hot and humid weather. During winter, frost and mist are common over the hill ranges of Peren, making it quite chilly but is moderately cold in the valleys. The rainy season in these districts begins from mid-May and ends in September. The average annual rainfall is 1560 mm in Dimapur and 2056 mm in Peren.

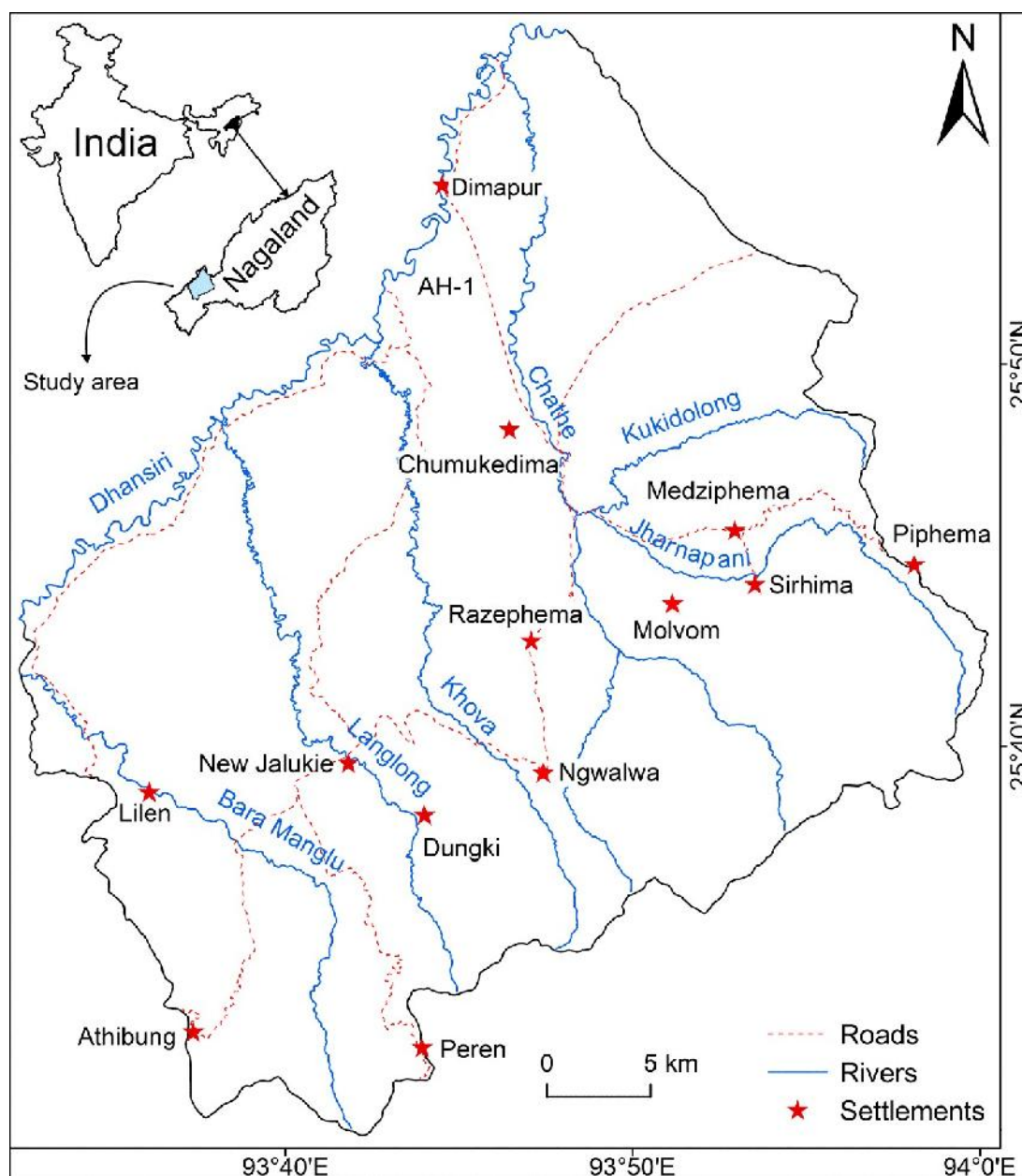


**Figure 1.1:** Map of the study area (modified after Moiya et al., 2019)

### **1.3 Geomorphology**

The study area exhibits diverse landform characteristics from plains to valleys and moderate to high hills. In the plains of Dimapur, older and younger alluvium covers major portion of the area. Extensive plains formed by several pediments are encountered near the frontal thrust zones. Towards Chumukedima, as the Naga-Patkai Range is approached from Dimapur, drastic change in morphological features is observed. Structural landforms such scarps, parallel and strike ridges with highly dissected structural hills, valleys and steep waterfalls are seen along the Naga Thrust zone. Medziphema consists of broad intermontane valleys enclosed by moderately to highly dissected hills. Towards Razhephema, moderately to highly dissect hills and high-level terraces are observed. Oxbow lakes are observed along the banks of the Dhansiri River. Most of the landforms within the BoS of Peren district are younger than Tertiary. It consists of newer and older alluvium. The older alluvium covers an extensive area in the Jalukie intermontane valley. The intermontane valley is surrounded by low to highly dissected hills. Depositional landforms such as alluvial fans, valley fills and piedmont slopes are also observed.

### **1.4 Drainage**

The present study area is demarcated towards the north by the River Dhansiri. The major tributaries of the Dhansiri River in the study area are the Chathe (Diphupani), Jharnapani, Bara Manglu, Langlong and Khova rivers that flow along a northerly direction. The drainage network, up to a 7<sup>th</sup> order stream, includes drainage patterns such as dendritic, trellis, parallel, as well as rectangular. Numerous joints, faults, thrust and lineaments are associated with the alignment of drainage, pointing to structural control. Meandering channels are mostly found to be constrained in the plains of Dimapur. Palaeochannels are commonly observed in the present area.

### **1.5 Objectives**

The objectives may be summarised as follows:

1. Determination of ongoing tectonic activity in the area
2. Identification of various lithotypes
3. Computation of morphometric parameters
4. Determination of morphotectonic setup of the area

5. Determination of the morphostratigraphy of the Quaternary landforms
6. Interpretation of geological history of the study area

## **1.6 Review of literature**

Evans (1932, 1964) and Mathur and Evans (1964) provided comprehensive description of the Cenozoic succession and structural framework of Nagaland and the north-eastern region. The complicated framework of NE India and its adjoining region was extensively studied. Brunnschweiler (1966) and Mitchell and Mckerrow (1975) explained the tectonic history and evolution of the IMR. Molnar and Tapponnier (1975) focused on the stratigraphy and sedimentation history of NE India and Burma. Banerjee (1979) described the basin arrangement of NE India and Burma. Ranga Rao (1983) studied the geology of the Assam-Arakan Basin and its adjoining region while Acharyya (1986) explained the development of IMR that resulted from plate collision. Bhattacharjee (1997) discussed the tectonics of the Indo-Burman basin, while Najman et al. (2019) studied uplift of the IMR. Naik (1998) explained the tectonostratigraphic evolution of NE India and Nandy (2000) elucidated the geodynamics of NE India and the adjoining region. Kent and Dasgupta (2004) studied the structural evolution of tectonic belt of Assam; Htay (2016) investigated the tectonic setting of the ophiolite belt of Myanmar.

The north-eastern region of India is considered to be an active tectonic region. Seismotectonics of the region was extensively investigated by Rastogi et al. (1973), Bhatia et al. (1999), Bureau of Indian Standards (BIS) (2002), Devi (2012), Talukdar and Barman (2012), Bora et al. (2013), Talukdar (2013), Olympa and Kumar (2015), Bora (2016) and Singh (2017). USGS seismic data shows high occurrence of earthquakes in NE India and its adjoining regions.

Geological studies in the Naga Hills were initiated by Mallet (1876), who investigated some coal reserves of Nagaland. The Directorate of Geology and Mining, Nagaland (DGM) (1978) carried out studies on the geology and mineral resources of Nagaland. Systematic geological mapping was undertaken in various parts of Nagaland by the officers of the Geological Survey of India (GSI) in Mon (Naganimora-Tamlu areas), Tuensang and Mokokchung districts (Sen and Krishna, 1975), Tuli, Merangkong and Changtongya areas of Mokokchung district (Sarma and Bharatiya, 1978), Tening-Impai-Intuma area of Kohima district (Prasad and Sarma,

1981), Medziphema-Khonoma-Pulomi area of Kohima district (Prasad and Sarma, 1983), Peren-Pedi-Benreu area of Peren subdivision, Kohima district (Sarma and Chakraborty, 1981), Peren-Puilwa-Tesangki area and Kohima district (Chakraborty and Sarma, 1982), Fakimile-Thanameir-Saramati area of Tuensang district (Bhattacharyya and Sanwal, 1985), Jalukie and parts of Kohima district (Chakradhar and Gaur, 1985), Maromi-Akuluto-Suruhuto area of Zunheboto district (Devdas and Gandhi, 1986), part of Kohima district (Chakradhar et al., 1986; Verma, 1989), Chiephobozou and Tukuleqa areas of Kohima and Zunheboto districts (Sahu and Venkataswamy, 1989), parts of Kohima, Mokokchung, Tuensang, Zunheboto and Phek districts (Shitiri, and Mishra, 1999) and Dzükou valley of Kohima district and Tening subdivision of Peren district (Shitiri, 2008). These works led to upgradation of the stratigraphy of Nagaland. Besides geological mapping, Mitra and Choudhary, (1969, 1970) also worked on the geology and coal resources in some parts of Tuensang and Mokokchung districts. Madhav (1989) worked on Quaternary and geomorphology of Kohima, Wokha, Mokokchung and Mon districts. Agrawal and Kacker (1980), Chattopadhyay et al. (1983), Singh et al. (1983), Acharyya et al. (1986), Agrawal and Ghose (1986), Ghose et al. (1987), Ghose and Agrawal (1989), Acharyya et al. (1990), Bhattacharjee (1991), Ghose et al. (2010), Watitemsu (2014), Fareeduddin and Dilek (2015) and Jain and Bhowmik (2016) studied the Naga Ophiolite Belt (NOB). Vidyadharan et al. (1986) studied part of the Naga Metamorphics. The GSI (2011) investigated the geology and mineral resources of Nagaland. Imchen et al. (2014) studied the tectonic setting of parts of the IFB.

The BoS has been a subject of keen interest to many authors who have investigated various issues associated with the thrusts. Ranga Rao and Murthy (1980) studied the origin of Naga Thrust. Roy and Kacker (1982, 1986) gave a tectonic description of the Orogenic Belt of Naga Hills and focused on the deformation mechanism of the BoS. Ranga Rao (1983) states that the BoS is bounded on the west by a complex set of intersecting faults called the Naga Thrust. Ranga Rao and Samanta (1987) dwelt on the structural style of the BoS. Srinivasan (2007) discussed the structures and seismic pattern of the belt. Saha (2011) explained gravity and magnetic anomalies, while Ghosh et al. (2014) mapped part of the terrain using geospatial technology.



Morphotectonics deals with the development of landscapes due to tectonic movements (Scheidegger, 2004). Investigations on morphotectonics, neotectonics and active tectonic features were carried out by Bull (1977), Ollier (1981), Keller and Rockwell (1984), Keller (1986), and Argyriou (2012). Neotectonic studies from drainage movements (Audemard, 1999; Perucca et al., 2013) and lineaments (Dalati, 2000; Kumanan, 2001; Ni et al., 2016) have been effective in the deduction of active tectonic structures. The Nagaland GIS and Remote Sensing Centre (NGISRSC) (2014) mapped the geomorphology and lineaments of Nagaland. River terraces are good geomorphic indicators of neotectonic movements (Molnar et al., 1994). Bull (1990) worked on stream-terrace genesis while Starkel (2003) studied climatically controlled terraces in uplifted mountain areas. Luirei et al. (2017) studied the relationship between Quaternary river terraces and transverse faults developed along folded mountain fronts.

Luminescence dating of sediments was carried out extensively by various authors (Prescott and Stephan, 1982; Aitken, 1985, 1998; Huntley et al., 1985; Godfrey-Smith et al., 1988; Hütt et al., 1988; Rhodes, 1988; Hütt and Jaek, 1989; Smith et al., 1989; Smith et al., 1990; Perkins and Rhodes, 1994; Olley et al., 1998; Galbraith et al., 1999; Murray and Wintle, 2000, 2003; Murray and Olley, 2002; Rhodes et al., 2003; Tsukamoto et al., 2003; Bailey and Arnold, 2006; Wintle and Murray, 2006; Wallinga et al., 2007; Duller, 2008; Fuchs and Owen, 2008; Preusser et al., 2008; Rittenour, 2008; Roy, 2013; Sohbati, 2013). Applications of optically stimulated luminescence dating have proven to be valid evidence for neotectonic investigations (Pazzaglia et al., 1998; Lave and Avouac, 2000; Kothyari and Luirei, 2016). Glaciation in the Lahul Himalaya (Owen et al., 1997), development of the Kashmir intermontane basins in the Himalaya (Burbank and Johnson, 1983), the evolution of the St. Laurent Mountain (Chrucinska et al., 2004), faulting along the northern Himalayan front (Kumar et al., 2010) and evolution of Holocene coastal dunes (Alappat, 2011) are some studies based on chronologic dating of sediments.

Morphometric analysis is a functional tool to decipher the role of tectonic activity (Kulkarni, 2015). The geomorphic approach of drainage basin analysis was initiated by Horton (1932, 1945) followed by Strahler (1952), Schumm (1956) and Hack (1957, 1973). The relationship of drainage patterns with subsurface structures has been explained by Jackson et al. (1998), Schumm et al. (2000), Valdiya and

Narayana (2007), Slattery (2011) and Radaideh et al. (2016). Drainage density is intimately associated with lithology, climate and tectonism (Gregory and Gardiner, 1975; Hou and Han, 1997; Tucker et al., 2001; Han et al., 2003; Garrote et al., 2008; Faghih et al., 2015). Geomorphic indices have been studied globally to infer active tectonism (Leopold et al., 1964; Bull and McFadden, 1977; Keller and Pinter, 1996, 2002; Whipple and Tucker, 1999; Snyder et al., 2000; Burbank and Anderson, 2001; Wobus et al., 2003; Pinter, 2005; Sreedevi et al., 2005; Pérez-Peña et al., 2008, 2009; Tsodoulos et al., 2008; Figueroa and Knott, 2010; Bhattacharya et al., 2013; Pareta and Pareta, 2011; Whipple et al., 2013; Morrish, 2015). The application of geomorphic indices to decipher neotectonic activity has proven to be very productive (Hare and Gardner, 1985; Hou and Han, 1997; Kirby and Whipple, 2001, 2003; Bhatt et al., 2007; Elias, 2013). Cox (1994) used drainage-basin asymmetry to determine tilt in Quaternary tectonic blocks while Azor et al. (2002) used geomorphic indices to determine active fold growth. Chen et al. (2003) based their work on tectonic implications through analysis of stream gradient and hypsometric. El Hamdouni et al. (2008) used geomorphic indices to study tectonic movements while Troiani and Della Seta (2008) applied stream length gradient index to prove ongoing neotectonic activity. Sulaksana (2017) used quantitative analysis to study active faults.

Aier et al. (2011), Bezbaruah et al. (2016), Longkumer et al. (2019) and Moiya et al. (2019) studied tectonic activity in the BoS. Mathew (2016) carried out morphotectonic analysis to study the evolution of Sarawak basin. Burbank and Johnson (1983), Zhu et al. (2006), Streit et al. (2015), Sinha and Sinha (2016), Longkumer et al. (2019), Moiya et al. (2019) and Saroli et al. (2019) used strath terraces to decipher tectonic movements in the evolution of intermontane basins. Aier et al. (2011) and Moiya et al. (2019) have notably contributed to the evolution of the Medziphema intermontane basin of the BoS.

## **CHAPTER: 2**

### **GEOLOGY AND TECTONIC SETUP**

The Naga Hills on the eastern margin of the Indian subcontinent represents the northernmost segment of the IMR (Ranga Rao and Murthy, 1980). It is composed of Mesozoic and Cenozoic sediments (Mathur and Evans, 1964). Cenozoic development of the Himalayan belt during continental collision, causing subduction of the Indian Plate under that of the Burma microplate is considered synchronous with the origin of the Naga Hills orogenic belt (Roy and Kacker, 1982). Morphotectonically, the Naga Hills orogenic belt is enclosed by tectonic provinces of the Indo-Myanmar belt towards the east, Assam Valley and Karbi Anglong Hills towards the west, Eastern Himalayan fold belt in the north and the Chin Hills and Arakan-Yoma in the south (Mitchell and McKerrow, 1975; Roy and Kacker, 1982).

#### **2.1 Tectonostratigraphy**

The tectonic framework of Nagaland encompasses four geotectonic units from east to west (Ghose et al., 1987) namely, the Naga Metamorphic, NOB, IFB and the BoS. Various workers including Mathur and Evans (1964), DGM (1978) and Ghose et al. (2010) contributed to the stratigraphic setup of Nagaland (Table 2.1).

##### **2.1.1 Naga Metamorphics**

The geotectonic unit of metamorphic rocks encountered on the eastern fringes of Nagaland adjacent to Myanmar was designated the Naga Metamorphics by Brunnschweiler (1966), who considered it as Pre-Mesozoic. It is composed of quartzite, limestone, phyllite, marble, sheared granite, mica schist, granitoid gneiss and minor serpentinites (Roy and Kacker, 1982; Watitemsu, 2014). The Naga Metamorphics has been compared with the Chaung Magyi Series of Burma on the basis of the folded nature displayed by the metasediments (Roy and Kacker, 1982). The lithounit also bear resemblance with the Lower Palaeozoic sequences of Myanmar (Roy and Kacker, 1982). This Pre-Cenozoic basement ‘subnappe’ are thrust over the Naga Hill Ophiolite (Brunnschweiler, 1966), with thrust planes marking the

boundary (Vidyadharan et al., 1986). The Naga Metamorphics include the Nimi and Saramati formations.

**Table 2.1:** Stratigraphy of Nagaland (after Imchen et al., 2014)

Age	Group	Litho-formations		
		Outer and Intermediate Hills	Eastern High Hills	
Recent - Pleistocene		Alluvium and high level terraces		
	Dihing	Boulder beds		
-----Unconformity-----				
Mio-Pliocene	Dupi Tila	Namsang Beds		
-----Unconformity-----				
Miocene	Tipam	Girujan Clay Tipam Sandstone		
	Surma	Upper Bhuvan Lower Bhuvan		
-----Unconformity-----				
Oligocene	Barail	Renji	<u>Jopi / Phokphur Formation</u> Tuffaceous shale, sandstone, greywacke, grit and conglomerate. Minor limestone and carbonaceous matter	
		Jenam		Baragolai
		Laisong		Naogaon
Upper Cretaceous - Eocene	Disang	Upper	Shale/slate/phyllite with calcareous lenses in basal sections and invertebrate and plant fossils in upper sections with brine springs	
		Lower		
-----Base not seen-----		-----Fault/Thrust-----		
Chert Kimmeridgian to mid-Tithonian  Middle Jurassic - Cretaceous	Ophiolite Complex	<u>Zepuhu Formation</u> Marine sediments (shale, phyllite, greywacke, iron-rich sediments, chert and limestone with radiolaria and coccoliths), volcanics (basalt, spilite, volcanoclastics), metabasics, greenschist, glaucophane schist/ glaucophane-bearing metachert, eclogite), layered cumulate sequence (peridotite, pyroxenite, gabbroids, plagiogranite, anorthosite), and peridotite tectonite and serpentinite associated with deposits of podiform chromite and nickeliferous magnetite, minor Cu-Mo sulphides associated with late felsic intrusions and some dolerite dykes		
		-----Fault/Thrust-----		
Pre-Mesozoic (?)	Naga Metamorphic Complex	<u>Nimi Formation</u> Weakly metamorphosed limestone, phyllite, quartzite and quartz-sericite schist  <u>Naga Metamorphics</u> Mica schist, granitoid gneiss and feldspathic metagreywacke with tectonic slices of ophiolite in variable dimensions		

#### *2.1.1.1 Nimi Formation*

The Nimi Formation, named after Nimi village, is assigned an Upper Cretaceous - Lower Eocene age. It consists of limestone, schists, phyllite, feldspathic and schistose quartzite (GSI, 2011). This formation, overridden by the Saramati Formation (Bhattacharya and Sanwal, 1985; GSI, 2011), is supposed to be a detached fraction of the Burmese continental crust (DGM, 1978). Brunnschweiler (1966) mentioned the resemblance of the Pansat Beds of Myanmar with those of the Nimi Formation, while Singh et al. (1983) opines that the facies of Pokhungri Formation and the Nimi Formation are similar. This formation has been subjected to three phases of deformations as evident by the presence of deformation and intense mylonitisation by cataclastic sediments (GSI, 2011).

#### *2.1.1.2 Saramati Formation*

The Saramati Formation, named after the Saramati peak by Acharyya et al. (1982), occur on the eastern part of the NOB. It is made up of tectonic slices of metasediments (GSI, 2011) and bears a higher grade of metamorphism than the Nimi Formation (Bhattacharya and Sanwal, 1985; GSI, 2011). It consists of argillaceous and arenaceous rock units such as schistose, quartzite, quartz-mica schist and carbonaceous phyllites (Bhattacharya and Sanwal, 1985). This formation has been tentatively allocated a Pre-Cretaceous age (GSI, 2011; Fareeduddin and Dilek, 2015). The Saramati Formation consists of a dominantly arenaceous lower unit and an argillaceous upper unit (Bhattacharya and Sanwal, 1985). The lower member is observed to the east of Thanameir village in Kiphire district. It consists of alternations of foliated feldspathic quartzites and muscovite-biotite schist. The presence of rounded epidote grains, which usually occurs as accessory mineral indicates the sedimentary nature (GSI, 2011). The upper member observed in the Fakimile and Thanameir areas, consists of sericite schist and sericite-muscovite schist with intercalations of quartzite. This younger member does not possess any fossil (GSI, 2011) and bears a thrust contact with the Nimi Formation (Bhattacharyya and Sanwal, 1985).

### 2.1.2 Naga Ophiolite Belt

The NOB is a discontinuous linear patch of the western ophiolite belt of Myanmar (Htay, 2016) exposed along the eastern part of Nagaland that is enclosed by the Zepuhu Thrust (west) and Nimi Thrust (east) (Agrawal and Kacker, 1980). It occurs as relics of the Tethyan oceanic crust and upper mantle along the IMR northern segment (Ghose et al., 2010) and represents a suture zone of the Indian-Eurasian plate collision (Acharyya et al., 1990; Bhattacharjee, 1991). It consists of diverse igneous, sedimentary and metamorphic rocks ranging in age from Middle Jurassic to Upper Cretaceous (Ghose and Agrawal, 1989; Bhattacharjee, 1991). The NOB belt, trending N-S, is considered the eastern extension of the Indus-Tsangpo suture zone (Jain and Bhowmik, 2016), which is made up of units juxtaposed haphazardly along the fault zone or as slices between Disang rocks.

The ophiolite suite is categorized into six lithological units such as, ultramafic complex, gabbroic complex, dolerite dykes, ultramafic volcanic complex, plagiogranite and Salumi Formation (GSI, 2011). On basis of fossil assemblages obtained from the cherts of Waziho and Ziphu areas, a Maestrichtian age is indicated. The litho-units of the NOB show signs of tectonic slicing, fracturing, shearing, mylonitization, silicification and tectonic agglomeration (Bhattacharjee, 1991). The ophiolites are tectonically dismembered, pointing to Alpine-Himalayan movements during Late Eocene - Early Oligocene (Roy and Kacker, 1982).

#### 2.1.2.1 Salumi Formation

The Salumi Formation, named after Salumi village, overlying the rock units of the ophiolite suite is distributed in patches. It consists of shale, claystone, thin interbedded chert, phyllite and limestone intercalated with volcanics. This formation assigned a Maestrichtian age (GSI, 2011), is exposed in the Luthur-Salumi, Ziphu, Mollen and Waziho areas.

#### 2.1.2.2 Phokphur /Jopi Formation

The ophiolite-derived clastics imbricated with ophiolitic rocks have been designated the Phokphur or Jopi Formation (Acharyya, 1986). The Jopi Formation derived from the Jopi-Mollen ridge (Agrawal and Ghose, 1986), lies nonconformably above the ophiolite. Based on flora and shallow marine fauna records, this formation is allocated

a Late Eocene - Oligocene age (Ghose et al., 2010) and is considered equivalent to the Barail Formation (Watitemsu, 2014). It consists of thick piles of alternating sequences of conglomerate, grit, sandstone, subgreywacke, siltstone, clay, shale and minor limestone (Acharyya et al., 1990; Ghose et al., 2010); it also bears volcanoclastics, tuffaceous wacke and minor volcanics (Acharyya et al., 1990).

### 2.1.3 Inner Fold Belt

Occupying the central part of Naga Hills, the IFB of Upper Cretaceous - Eocene age is confined between the Disang Thrust (west) and NOB (east) (Chattopadhyay et al., 1983). Lithologically, it includes sequences of splintery shale, slate and phyllite interbedded with sandstone. The IFB is characterized by two synclinoria, the Kohima Synclinorium (south) and Patkai Synclinorium (north), which continues southward forming a part of the Burmese arc (Mathur and Evans, 1964).

#### 2.1.3.1 Kohima Synclinorium

The Kohima Synclinorium occupies the southern part of the IFB, southwest of Kohima, with a slight southerly pitch trending approximately N-S (Evans, 1964). The northern limb of this synclinorium that forms the Barail Range of North Cachar Hills extends south-westward beyond Haflong, and turns westward, fringing the eastern extension of the Meghalaya Plateau. The southern limb extends into west Manipur, east Cachar and east Mizoram. The Changrung-Zungki-Lanye Thrust and Halflong-Disang Thrust mark the eastern and western limits of the Kohima Synclinorium (Naik, 1998). Lithological variation can be observed in the Kohima Synclinorium. The underlying Disang occupy the rims while the Barail are dominant towards the southern limb; the younger Surma sediments occupy the core of this synclinorium (Ranga Rao, 1983)

#### 2.1.3.2 Patkai Synclinorium

The Patkai Synclinorium occupies the northern part of the IFB. It is the northeastern continuation of the Kohima Synclinorium (Roy and Kacker, 1982), covering an extensive area in the intermediate hills of Nagaland. It comprises the Disang and Barail groups (Banerjee, 1979). The Disang Group is exposed along the rims of this synclinorium while the Barail mark the highest ground of the Patkai Synclinorium.

The Disang Thrust marks the boundary between the Patkai Synclinorium and BoS (Mathur and Evans, 1964).

#### 2.1.4 Belt of Schuppen

The BoS is a closely spaced NE-SW trending linear belt of imbricate thrust slices with numerous NW-SE normal faults running perpendicular to it (Mathur and Evans, 1964) along with occurrence of anticlinal folds towards the hanging walls of the thrusts (Ranga Rao and Samanta, 1987, Moiya et al., 2019). The BoS is a morphotectonic unit of the Assam-Arakan belt (Roy and Kacker, 1986), due to collision between the Indian and Eurasian plates (Burma microplate) (Roy and Kacker, 1986; Saha, 2011). It is considered a probable area for future great earthquakes (Srinivasan, 2007). Seismic surveys by the Oil and Natural Gas Corporation Ltd. suggests that the extension of the Assam shelf is overlain by the BoS (Roy and Kacker, 1986). Deformation in the BoS is similar to that of the Alpine-Himalayan and Pliocene-Quaternary movement (Roy and Kacker, 1986).

Mathur and Evans (1964) suggested the presence of more than eight thrust sheets, which override each other in an en-echelon fashion in the BoS. Four to five thrusts with some local thrusts have been recognized (Roy and Kacker, 1986; Ranga Rao and Samanta, 1987; Bhattacharjee, 1991). The BoS in Nagaland is about 20-25 km wide and more than 200 km long. It is composed of sediments ranging in age from Oligocene to Holocene and comprises two major thrusts, viz., the Naga Thrust (northwest) and Disang Thrust (southwest) (Roy and Kacker, 1986). The Naga and Disang thrusts merge near Haflong (Mathur and Evans, 1964; Roy and Kacker, 1986). The northern end of the BoS moved downwards towards the west along the Mishmi Thrust of Arunachal Himalaya causing the “S” shaped bending of the BoS while the southernmost end moved upwards, towards the east along the E-W trending Dauki Fault. The Mishmi Thrust and Dauki Fault mark the northern and southern termination of the BoS, respectively (Srinivasan, 2007).

## 2.2 Cenozoic sequences of the Inner Fold Belt and Belt of Schuppen

### 2.2.1 Disang Group

The Disang Formation was named by Mallet (1876) after the Disang Valley of Upper Assam, for a thick monotonous succession of splintery shales interbedded with



subordinate sandstones as well as thin bands of siltstone (Sahu and Venkataswamy, 1989; Ghosh et al., 2014). The Disang bear a thrust contact with the ophiolite (GSI, 2011). This group of Tertiary rock sequences range from Upper Cretaceous to Eocene age and is extensively spread in the intermediate hill regions of the IFB (Shitiri and Mishra, 1999). However, it is lacking in the BoS. This group of rocks is overlain by the Laisong Formation of the Barail Group by a gradational contact. As the amount of arenaceous sediments increases towards the Upper Disang Group, distinguishing between these two becomes complicated (Shitiri and Mishra, 1999). Towards the downthrown block of the Haflong-Disang Thrust, the Lower Disang Formation composed of argillaceous sediments has a tectonic contact with the Jenam Formation of the Barail Group (Chakradhar et al., 1986). The Disang shale bears rich remnants of fossiliferous assemblage and plant fragments (GSI, 2011). Fossil assemblages such as lamellibranch and mollusc are recorded from New Ngwalwa area near the Disang Thrust (Chakradhar and Gaur, 1985). Ferruginous nodules present in some Disang shale point to spheroidal weathering (Chakradhar et al., 1986).

The stratigraphy sequence is not entirely recognized owing to its complicated folded structure (GSI, 2011). However, based on identification of an upper arenaceous stratum and basal argillaceous, the Disang Group is classified into two lithounits: Upper Disang Formation and Lower Disang Formation (Imchen et al., 2014). The contact between the two formations is gradational and at some places faulted and thrust (Sahu and Venkataswamy, 1989).

#### 2.2.1.1 Lower Disang Formation

The Upper Cretaceous Lower Disang Formation comprises dark grey, argillaceous shale that exhibit fine laminations intercalated with thin layers of siltstone and sandstone (Bhattacharjee, 1991). In some localities, phyllite and phyllitic shale dominate this formation, which mostly occurs in the cores of anticlines (Devdas and Gandhi, 1986). The shales are moderately to highly carbonaceous; occasionally fine grained sandstone occurs in certain areas, especially at the junction of faults. The beds are commonly crumpled and squeezed. The Lower Disang rocks shows foliation, folding and faulting, indicating ongoing structural deformation. These rocks were deposited in shallow to deep marine environments (Bhattacharjee, 1997). Sedimentary structures displayed by the Lower Disang Formation include parallel laminations,

planar cross-stratification and cross bedding (GSI, 2011). This formation has yielded fossils assemblages such as foraminifers, lamellibranchs and molluscs (Chakradhar and Gaur, 1985).

#### 2.2.1.2 Upper Disang Formation

The Upper Disang Formation, confined between the Disang Thrust and the NOB belt, is considered as Lower to Middle Eocene in age (Bhattacharjee, 1997). The Upper Disang is predominantly argillaceous and includes sequences of dark grey to black shale with sandstone and siltstone (Verma, 1989) and conglomerate (Bhattacharjee, 1991). Thicknesses of sandstone vary, which makes it difficult in identification of the overlying younger sediments of the Barail Group (Shitiri, 2008). The occurrences of conglomerate signify shallower deposition. Fragments of ophiolite are noted in this formation (Bhattacharjee, 1997). The Upper Disang exhibit numerous sedimentary structures such as, rhythmic bedding, graded bedding, ripple marks, load casts, flute casts and groove casts (GSI, 2011).

#### 2.2.2 Barail Group

The Barail Group is named after the Barail Range in the North Cachar Hills of Assam for an arenaceous suite of rocks (DGM, 1978). The Barail comprise primarily of sequences of sandstone intercalated with very thin shale and siltstone (Chakraborty and Sarma, 1982) and coal seams (Sarma and Chakraborty, 1981; Bhattacharjee, 1997). The Barail sandstones are hard, compact and massive bedded, and extensively jointed (Shitiri and Mishra, 1999). These rocks of Upper Eocene - Oligocene age overlie the Disang Group (Roy and Kacker, 1986). Along the eastern extremity of the Kohima Synclinorium, the Barail are disconformably overlain by the Surma Group (Prasad and Sarma, 1983). The Barail Group of rocks is the oldest of the Tertiary sequence occurring in the BoS. This group of rocks exhibits a number of sedimentary structures such as ripple marks, load casts, flute marks, sole marks, current bedding, etc. (Prasad and Sarma, 1983).

The Barail Group is divided into three formations, the Laisong, Jenam and Renji in the south and southwest of Nagaland, whereas in the north and northeast of Nagaland, the equivalents of these formations are the Naogaon, Baragolai and Tikak Parbat (Evans, 1932).

#### *2.2.2.1 Laisong / Naogaon Formation*

The Laisong / Naogaon formations of Late Eocene-early Oligocene consist of very hard, grey, thinly to massive bedded, fine to medium grain sandstones with intercalations of silty shale and carbonaceous shale (Mathur and Evans, 1964). Dominantly arenaceous (Verma, 1989), occasionally thin streaks of coal (Roy and Kacker, 1986) and conglomerate are encountered in the Laisong Formation (Shitiri, 2008). This formation bears a gradational contact with the older Disang sediments (Chakradhar and Gaur, 1985). Sedimentary structures associated with this unit are ripples, load casts, asymmetric ripples, cross lamination, cross bedding, burrow mark and flute marks (Prasad and Sarma, 1981; Chakradhar and Gaur, 1985; Shitiri, 2008). The Naogaon Formation is widely found in the north-eastern region of Nagaland, covering extensive areas composed of alternation of shale, sandy shale and sandstone, occasionally with carbonaceous shale. Coal seams are not seen in this formation. The Naogaon Formation is sandwiched between the Kongan Thrust and Disang Thrust (Mitra and Choudhary, 1969). This formation has a gradational contact with the older Disang Group (Sen and Krishna, 1975; Sarma and Bharatiya, 1978).

#### *2.2.2.2 Jenam / Baragolai Formation*

The Jenam Formation consists of alternations of shale, sandy shale and carbonaceous shales, interbedded with sandstone and silt (Verma, 1989; Shitiri, 2008). The sandstones are thinly to thickly bedded (Verma, 1989). This formation bears a gradational contact with the Laisong and Renji formations (Evans, 1964; Ranga Rao, 1983). The Jenam Formation also bears a tectonic contact with the Disang Group towards the downthrown block, east of Piphema (Chakradhar and Gaur, 1985). The Jenam are characterised by a lower argillaceous and an upper arenaceous sequence (Evans, 1932). Plant matter and sedimentary structures such as ripple marks and current bedding are found in the sandstone (Chakradhar and Gaur, 1985; Ghosh et al., 2014). Trochamina species of the foraminiferida family and Lygopodiumsporites of lycopodiaceae are found in this formation (Ghosh et al., 2014).

The Baragolai consists of argillaceous shale with thin layers of clay and coal seams (Mathur and Evans, 1964; Mitra and Choudhary, 1970). The shales are mostly thinly bedded, grey to bluish grey and sometimes carbonaceous (Mitra and

Choudhary, 1970). The Baragolai Formation bears a gradational contact with the Naogaon and Tikak Parbat formations.

#### *2.2.2.3 Renji / Tikak Parbat Formation*

The Renji Formation is the youngest member of the Barail Group and is composed primarily of massive, thick bedded, ferruginous sandstones intercalated with minor shale. These sandstone exhibits tabular and planar cross-beds (Ghosh et al., 2014). Huge variation in thickness is observed in the BoS owing to depositional conditions. In the IFB, they form the high peak of Mt. Japfü (3015 m), southwest of Kohima (GSI, 2011). The Renji Formation overlies the younger Jenam gradationally, while they are unconformably overlain by the Surma Group of rocks. Sedimentary structure flaunted by the Jenam sandstone and shale include convolute bedding, flaser beds, lenticular bedding and asymmetric ripples (Chakradhar and Gaur, 1985).

The Tikak Parbat Formation comprises sand-shale alternations and thick coal seams (Mathur and Evans, 1964). The Tikak Parbat is a major source of coal in Nagaland. A reduction in the amount of sediment thickness is observed towards the southwest of Namsang-Chingchung villages, which may be due, either to the overlapping of the Tipam Sandstone or truncation of the Kongan Thrust (Mitra and Choudhary, 1970). The Tikak Parbat is further divided into three members, Lower, Middle and Upper, based on their lithological characteristics. The lower member is made up of grey shale, bluish grey clay, siltstone with a small amount of sandstone and coal seams. The middle member is composed of alternations of shale with sandstone while the upper member consists of massive sandstone and shale (Mitra and Choudhary, 1969, 1970).

#### *2.2.3 Surma Group*

The Surma Group of rocks has been assigned a Miocene age (Mathur and Evans, 1964). It lies unconformably over the Barail Group (Prasad and Sharma, 1983; Shitiri and Mishra, 1999). The rocks of this group include alternations of sandstone, shale and thin beds of conglomerate (Mathur and Evans, 1964; Prasad and Sharma, 1983). The Surma consist of two formations namely, the Bhuban and Boka Bil, based on their lithological composition.

### *2.2.3.1 Bhuban Formation*

Previously designated as the 'Bhuban stage', Evans (1932) designated the Bhuban after the Bhuban Range of Assam. The Bhuban Formation is composed of shale with few sandstone and siltstone (Shitiri, 2008; Ghosh et al., 2014). The Bhuban formation is again categorized into three members namely, Lower, Middle and Upper members.

#### 2.2.3.1a Lower Bhuban

This is the oldest member of the Bhuban Formation and is made up of well bedded sandstone, shale, sandy shale and conglomerates (Mathur and Evans, 1964). The thickness of the sandstone varies from place to place.

#### 2.2.3.1b Middle Bhuban

Overlying the lower member is the Middle Bhuban Member, also consisting of alternation of sandstone, sandy shale and shale (Mathur and Evans, 1964). The amount of sandstone fluctuates at different horizons (Chakradhar et al., 1986). Sedimentary structures found in this formation include lenticular beds, flaser bedding, convolute bedding, parallel lamination and asymmetric ripples (Chakradhar et al., 1986).

#### 2.2.3.1c Upper Bhuban

Conformably overlying the Middle Bhuban is the Upper Bhuban Member by a transitional contact. It is dominantly arenaceous, being mainly composed of medium grained sandstone with minor shale and siltstone. Siltstones exhibit trough and wedge shaped, cross lamination, lenticular beds, flaser bedding and wavy bedding (Chakradhar et al., 1986).

### *2.2.3.2 Boka Bil Formation*

The Boka Bil Formation gradationally overlies the Upper Bhuban Member (Chakardhar and Gaur, 1985); it is composed of shale, sandy shale and ferruginous sandstone, and is dominantly argillaceous in some localities (Mathur and Evans, 1964). Thickly bedded sandstones are not encountered due to abundance of argillaceous matter at places, which is a distinguishing characteristic from the Bhuban Formation (Mathur and Evans, 1964). Sedimentary structures such as cross bedding,

flaser bedding, lenticular bedding, wave ripples and load cast are frequently observed (Chakradhar and Gaur, 1985; Ghosh et al., 2014).

#### 2.2.4 Tipam Group

The Tipam Group of rocks of Mio-Pliocene age consists of thickly-bedded, medium to coarse grained sandstone and subordinate shale and clay (Bezbaruah et al., 2016). It derives its name after the Tipam Hills of Assam (Mallet, 1876). It conformably overlies the Surma, without any perceptible break. The Tipam Group is subdivided, into two formations namely, Tipam Sandstone (lower sandy unit) and Girujan Clay (upper unit) formations, based on their arenaceous and argillaceous characteristics (Evans, 1932).

##### 2.2.4.1 *Tipam Sandstone Formation*

The Tipam Sandstone Formation is predominantly arenaceous. It is composed of grey to light greenish grey, medium to coarse-grained, massive sub-arkosic sandstone with alternations of subordinate claystone and mottled clay (GSI, 2011; Ghosh et al., 2014). The sandstones are arkosic to lithic arenites that are occasionally interbedded with shale and coal. The Tipam Sandstone Formation displays sedimentary features such as wedge and trough cross bedding, parallel lamination and bedding fissility (Chakradhar and Gaur, 1985; Chakradhar et al., 1986).

##### 2.2.4.2 *Girujan Clay Formation*

Conformably overlying the Tipam Sandstone is the Girujan Clay Formation, named after the Girujan River near Digboi. It is made up of thick amount of molted clay with minor argillaceous sandstone (Evans 1932). The sandstone in the Girujan Clay Formation are molted, friable and usually white to greyish-white in colour (Prasad and Sarma, 1983). It is best exposed along the Asian Highway (AH) 1, near Medziphema in Dimapur district. It occasionally contains coal fragments (Mathur and Evans, 1964). Common sedimentary structures noted in the Girujan Clay include current, cross and flaser beds, parallel laminations and trough and fill cross-stratification (Chakradhar and Gaur, 1985; Chakradhar et al., 1986; GSI, 2011).

### 2.2.5 Dupi Tila Group

The Namsang Beds of Mio-Pliocene age (Mathur and Evans, 1964), belonging to the Dupi Tila Group, unconformably overlies the Girujan Clay (Ghosh et al., 2014). The Namsang Formation, named after Namsang River, is made up of poorly consolidated sequences of mottled clay and sandstone, with pebbles, conglomerate, grit and interbeds of lignite seams (Mathur and Evans, 1964). Along the Kiker stream near Chumukedima, a conglomerate bed of about 7 m is seen (Chakradhar et al., 1986). The sediments are arenaceous with pebbles derived from the Barail and Surma sandstones (GSI, 2011).

### 2.2.6 Dihing Group

Mallet (1876) christened the Dihing Group after the Dihing River for those pebbles and cobbles of Barail sandstone embedded in a sand, silt and clay matrix. It also includes conglomerate, grit and sometimes lignite bands. This group of rocks, assigned a Plio-Pleistocene age (Ghosh et al., 2014), unconformably overlies the Namsang Beds (Mathur and Evans, 1964) and Girujan Clay (Chakradhar et al., 1986). The conglomerate beds are poorly bedded and ungraded. Tilting of this group of rocks mostly depends on the dip of underlying bedrocks (Chakradhar et al., 1986), indicating neotectonic events. In the BoS, the Dihing is mostly confined within intermontane basins and are overlain by the Late Pleistocene - Holocene Chathe Alluvium (Moiya et al., 2019).

## 2.3 Geology and structure of the study area

The present study has been carried out in the BoS in of parts Dimapur and Peren districts of Nagaland. The structural framework of the BoS originated during the Alpine-Himalayan movements (Roy and Kacker, 1982). The study area is affected by regional thrust systems, numerous faults and complicated folds (Moiya et al., 2019). The thrust systems of the BoS have a general NE-SW trend, which include sequences of thrust planes (Fig. 2.1).

### 2.3.1 Lithostratigraphy

The lithostratigraphy of the study area may be broadly classified as Palaeogene, Neogene and Quaternary of the Cenozoic Era (Table 2.2). The Palaeogene comprises

the Barail, while the Neogene consists of the Surma, Tipam and Namsang. The Quaternary includes the Dihing and Chathe Alluvium (Table 1.1, Fig. 2.1). These units range in age from Upper Eocene to Holocene (Moiya et al., 2019). The litho-units in the thrust belt are older towards the interior and younger towards the exterior (Ranga Rao and Samanta, 1987).

**Table 2.2:** Stratigraphic succession of the study area (after Moiya et al., 2019)

<b>Group</b>	<b>Formation Member</b>	<b>Age</b>	<b>Lithology</b>
Unclassified	Chathe Alluvium	Late Pleistocene to Holocene	Cobbles and pebbles in matrix of sand, silt and clay
	-----	Unconformity	-----
Unclassified	Dihing	Plio-Pleistocene	Pebble bed, soft sandy clay, clay, conglomerate, grit and sandstone
	-----	Unconformity	-----
Dupi Tila	Namsang Bed	Mio-Pliocene	Pebbles of sandstone, grit, conglomerate and mottled clay
	-----	Unconformity	-----
Tipam	Girujan Clay		Thick bedded clay
	Tipam Sandstone		Massive sandstone
Surma	Upper Bhuvan	Miocene	
	Middle Bhuvan		Sandstone, shaly sandstone, siltstone, shale
	Lower Bhuvan		
	-----	Unconformity	-----
Barail	Renji		
	Jenam	Oligocene	Thick sequences of sandstones with minor shale
	Laisong		
Disang	Upper	Upper Cretaceous to Eocene	
	Lower		Shale with thin flaggy sandstone

#### 2.3.1.1 *Chathe Alluvium*

Chathe Alluvium named after the Chathe River (formerly Diphupani River) where it is magnificently exposed, consists of cobbles and pebbles with matrix of sand, silt, clay and mud. It is assigned a Late Pleistocene - Holocene age based on optically stimulated luminescence dates. Strath terraces are observed in the Medziphema, Molvom, Razephema and Jalukie area consist of bedrocks of older formations that are overlain by the Chathe Alluvium. The Chathe Alluvium displays an angular unconformable relationship with the older rocks (Moiya et al., 2019).



## 2.3.2 Structure

### 2.3.2.1 Thrust

The BoS in Dimapur and Peren districts include four main thrust planes, viz., Naga Thrust, Sanis-Chongliymnsen Thrust, Piphema Thrust and Disang Thrust (Fig. 2.1). The Naga Thrust, the northeast continuation of the Haflong Thrust (Haflong-Naga Thrust), is the frontal thrust of the BoS.

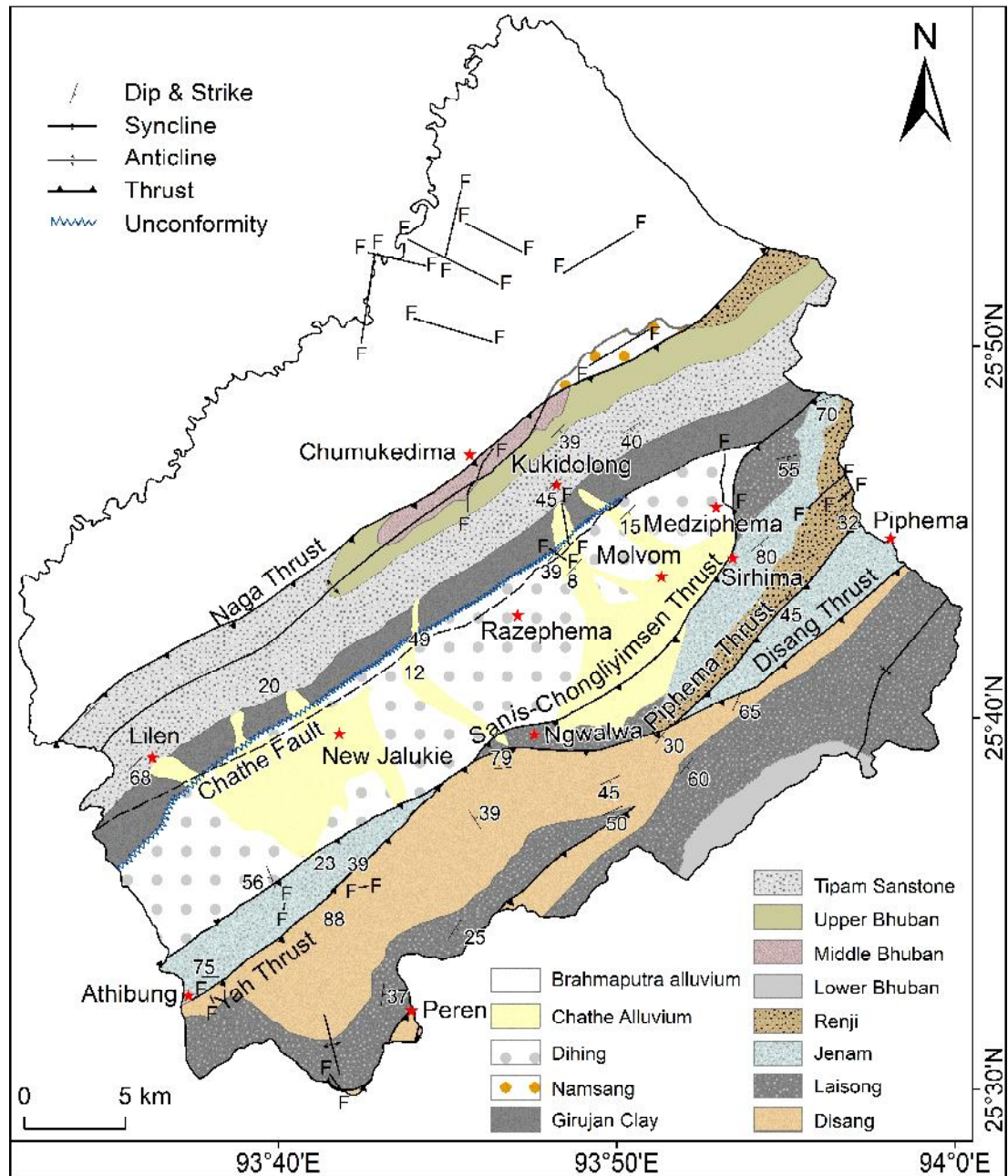


**Figure 2.1:** Geology of the study area (modified after Chakraborty and Sarma, 1982; Chakradhar and Gaur, 1985; Moiya et al., 2019)

The youngest emergent Naga Thrust delineates the BoS from the Brahmaputra alluvium on the northwest. The Sanis-Chongliyimsen Thrust separates the Palaeogene sediments from the younger Neogene-Quaternary sediments. The Piphema Thrust separates the Jenam Formation from the younger Renji Formation of the Barail Group (Moiya et al., 2019). The Disang Thrust acts as barrier between the BoS and the IFB towards the southeast.

The Yah Thrust, trending NE-SW, designated by the Assam Oil Company, is observed southwest of the BoS. The Jenam Formation is bounded between the Disang Thrust and Yah Thrust (Chakradhar and Gaur, 1985). The Yah Thrust may be considered as a splay of the Disang Thrust. Two sub-thrusts with NE-SW trends and analogous with the regional thrust system, are encountered towards the west and northeast of Peren. Along this thrust plane, Barail rocks are in contact with the underlying argillaceous Disang shale. This thrusts plane is considered to be the southwestern extension of the BoS (Chakraborty and Sarma, 1982).

#### *2.3.2.2 Fault*

The Chathe Fault, trending NE-SW (Fig. 2.1), corresponds to the thrusts system of the BoS was identified by Moiya et al. (2019). The Chathe Fault extends from the north of Medziphema town in Dimapur district to the northwest of Lilen village in Peren district (Fig. 2.1) and may continue beyond that. This fault is about 37 km long in the study area and is considered a reverse fault separating the Dihing and Chathe alluvium from the Girujan Clay. The Chathe Alluvium of Late Pleistocene-Holocene age is confined between the Chathe Fault and the Sanis-Chongliyimsen Thrust in the Dimapur district and Chathe Fault and Disang Thrust toward Peren district. Besides this, local faults are also observed in the study area.

#### *2.3.2.3 Anticline*

The Nichugard (old name of Chumukedima) anticline in the southwestern part of the BoS is a prominent NE-SW fold (Fig. 2.1). Late Alpine movements is considered key factor for its formation (Roy and Kacker, 1982). The northern limb of this anticline is truncated by the Naga Thrust towards the southwest of Chumukedima. The Tipam Sandstone Formation occupies the northern limb of this anticline while the Upper Bhuban Member lies in the core of this plunging anticline. The Tipam Sandstone is

largely exposed in this area of the BoS because this anticline plunges 5-10° towards SW (Chakradhar and Gaur, 1985). An anticline trending NNW-SSW is also observed southwest of Peren (Chakraborty and Sarma, 1982).

## **CHAPTER: 3**

### **METHODOLOGY**

The SoI topographic map nos. 83G/9, G/10, G/13, G/14 and 83K/2 on 1:50,000 scales (surveyed during 1974-75, 1974-76, 1971-72, 1973-74 and 1973-74, and published in 1979, 1981, 1974, 1975 and 1975 respectively) and 1:26,720 scale of 1944 (1921-23 survey) and map no. 83G/14 on 1:25,000 of 1986 (1982-83 survey) were used in conjunction with data of remote sensing processed on a GIS platform to carry out the present study. Satellite imagery of IRS-1D (PAN+LISS III merged), Google Earth and SRTM-DEM were used in ArcGIS 10.3, River Tools, Global Mapper 15 and RockWorks 16 software to carry out analysis of the various morphometric and morphotectonic features. A hand-held GPS was used in the field for mapping.

The topographic maps were georeferenced and digitized. The basin boundary, drainage networks, drainage order, contours, 20 sub-basins and 58 mini-basins were demarcated and digitally marked using topographic maps (1:50,000 scale) in ArcGIS. Drainage migrations were studied comparing the topographic maps of 1944 with that of 1986 and Google Earth imagery of 2017. Detection and analysis of active faults/lineaments and other morphotectonic features were delineated using satellite imagery. Lineaments and transverse topography symmetry factor orientations were plotted using RockWorks software while drainage order orientations were plotted using an ArcGIS extension.

#### **3.1 Morphometric analysis**

##### **3.1.1 Drainage analysis**

Drainage orders were marked from the 1<sup>st</sup> till the highest order by Strahler's (1952) method in which the unbranched fingertip-streams are assigned as first order streams. The merging or joining of two first order streams form the next higher order stream that is the second order streams and so on. During the merging of two streams of different orders, the streams are assigned the number of higher order stream. Drainage patterns were studied to decipher the influence of initial slope, structure, diastrophism and geomorphic history. Drainage density is an important element of landform in

stream-eroded topography (Horton, 1932). A drainage density map was constructed following Horton (1932) using the following equation:

$$Dd = L_u/A_u$$

where  $L_u$  is defined as the total length of the stream channels and  $A_u$  is the area of the basin in  $\text{km}^2$ .

### 3.1.2 Longitudinal profile

The slope of a river profile is inversely proportional to the amount of discharge (Gilbert, 1877). Increase in the amount of discharge will give a concave up profile curve (Chorley, 1969). A longitudinal profile is indicative of perturbations in a river course (Keller and Pinter 1996). Abrupt changes in river profile slope due to knickpoints are attributed to sudden break by faults, thrusts or lithological variation. Examining these knickpoints helps decipher the role of active tectonism. The longitudinal profile is a plotted elevation against the distance.

### 3.1.3 Stream length gradient index

Stream length gradient index (SL) is derived following the mathematical equation of Hack (1973), which is expressed as

$$SL = (\Delta H/\Delta L) L$$

where,  $\Delta H$  is considered as the elevation change of the reach,  $\Delta L$  denotes horizontal length of the reach and  $L$  as the total length of the river channel (upstream) to the particular end of interest. A high value of SL is attributed to a river flowing over a region experiencing tectonic uplift, while a low SL value usually occurs when a river channel flows over a stable area (Keller and Pinter, 2002; El Hamdouni et al., 2008).

### 3.1.4 Steepness index

The steepness index is based on the equation of Flint (1974) to determine the relative gradient of the channel in response to differential uplift and channel incision (Kirby and Whipple, 2003). It is expressed as

$$S = k_s A^{-\theta}$$

where,  $k_s$  is the steepness index,  $S$  signifies channel slope,  $A$  indicate area occupied by the drainage and  $\theta$  denote concavity (Hack, 1957; Flint, 1974; Snyder et al., 2000). The steepness index has been widely used to determine uplift rates and tectonic activity through knickpoints (Whipple and Tucker, 1999; Snyder et al., 2000; Kirby and Whipple, 2001; Whipple, 2004).

### 3.1.5 Asymmetry factor

Asymmetry factor (AF) determines whether the river basin is undergoing tectonic activity, on the basis of presence or absence of tilt (Hare and Gardner, 1985; Cox, 1994; Keller and Pinter, 1996). It is based on the mathematical equation

$$AF = 100(A_r/A_t)$$

where,  $A_r$  denotes the basin area towards the right of the main trunk of the river channel and  $A_t$  signifies the whole drainage basin area. AF values greater or lesser than 50 indicates tilt. Value greater than 50 suggests tilt to the left side of the drainage basin while values below 50 indicate tilt towards the right. A value of 50 indicates a stable setting.

### 3.1.6 Transverse topographic symmetry factor

Transverse topographic symmetry factor (T) was proposed by Cox (1994) to detect areas undergoing lateral tilting. It is based on the following equation:

$$T = D_a/D_d$$

$D_a$  indicates the distance calculated from the point of drainage basin midline till the present river channel while  $D_d$  is the distance measured from the basin midline till the river basin boundary. Values of  $T$  fall in between 0 to 1. A zero value of  $T$  indicates a symmetric basin while values greater than zero indicate point to an asymmetric basin.

### 3.1.7 Basin elongation ratio

Basin elongation ratio ( $R_e$ ) is the ratio of diameter of a circle and length of the basin (Schumm, 1956). The basin elongation ratio could denote tectonism (Bull and McFadden, 1977; Bhatt et al., 2007). It determines the tectonic activity according to

the shape of the watershed (Parveen et al., 2012). It is expressed by the following formula:

$$R_e = (2\sqrt{A:\sqrt{\pi}})L$$

A implies total drainage basin area and L signifies the length of the river basin. A  $R_e$  value of less than 0.05 implies a basin to be tectonically very active; values from 0.05-0.75 signify basin that are slightly active while values more than 0.75 depict river basin to be inactive.

### 3.1.8 Channel sinuosity

Channel sinuosity (S) can help in identifying the consequence of tectonism on river courses (Mueller, 1968). Meandering, sinuous and straight courses are types of patterns displayed by rivers. Mueller (1968) proposed the following formula:

$$S = SL/VL$$

SL denotes the length of a stream channel and VL depicts length of a river valley. The river follows a straight path when the value is 1, sinuous path when the value is between 1-1.5 and a meandering path when the value is  $>1.5$ . High S values indicate the influence of active deformation in an area (Burbank and Anderson, 2001).

### 3.1.9 Mountain front sinuosity

Mountain-front sinuosity ( $S_{mf}$ ) determines the balance between erosion and tectonics. Mountain fronts that are sinuous are results of erosion while straight mountain fronts are considered to be the products of tectonic process (Bull and McFadden, 1977; Keller and Pinter, 1996; Tsodoulos et al., 2008).

$$S_{mf} = L_{mf}/L_s$$

where,  $L_{mf}$  implies the distance of mountain front and  $L_s$  signifies distance measured in a straight line of the same mountain front.  $S_{mf}$  values of less than 1.4 symbolize tectonically active areas and values ranging from 1.4-3 indicate slight activity; values of more than 3 point toward an inactive mountain front (Bull and McFadden, 1977; Rockwell et al., 1984; Bhatt et al., 2007; El Hamdouni et al., 2008).

### 3.1.10 Valley floor width to valley height ratio

The ratio of valley floor width to valley height ( $V_f$ ) quantifies the valley incision in an uplifted area (Bull and McFadden, 1977).

$$V_f = 2V_{fw}/[(E_{ld}-E_{sc})+(E_{rd}-E_{sc})]$$

where,  $V_{fw}$  indicates width of the valley floor,  $E_{ld}$  and  $E_{rd}$  imply the elevations of valley divides (left and right) and  $E_{sc}$  denotes the elevation of the valley floor. Low values of  $V_f$  indicate river with active incision with high uplift rate associated with tectonic activity thus giving rise to deep or V-shaped valleys. High values of  $V_f$  depict a less active river due to low uplift, thus resulting in a broad or U-shaped valley. The  $V_f$  may be categorized as class 1 (value  $<1.8$ ) associated with tectonically active terrains, class 2 (value between 1.8-3.4) for slightly active terrain and class 3 (value  $>3.4$ ) for inactive terrains (Bull and McFadden, 1977).

### 3.1.11 Hypsometric curve and hypsometric integral

Strahler (1952) proposed the hypsometric curve (HC) and hypsometric integral (HI). The hypsometric curve signifies the relative area of a watershed under a given altitude (Schumm, 1956; Pérez-Peña et al., 2009). The area under the hypsometric curve is the hypsometric integral (Keller and Pinter, 1996; Pérez-Peña et al., 2009). The hypsometric curve can be obtained on plotting the relative basin area against basin height (Keller and Pinter, 1996). The hypsometric integral is calculated from the equation of Pike and Wilson (1971) using elevation parameters from a drainage basin.

$$HI = (Elev_{mean} - Elev_{min}) / (Elev_{max} - Elev_{min})$$

where,  $Elev_{mean}$  is the mean basin elevation,  $Elev_{min}$  and  $Elev_{max}$  are the minimum and maximum basin elevations. HI values  $<0.4$  show concave curves, depicting old stage. Values between 0.4-0.5 give a concave-convex or straight curve, indicating mature age. Value  $>0.5$  show convex curves, pointing to youthful age (El Hamdouni et al., 2008).



## 3.2 Optical Chronology

### 3.2.1 Fieldwork

A total of 11 samples were collected in the field for chronology dating. Samples were collected from the valleys of Chathe and Bara Manglu rivers. Samples for palaeodose were collected by driving 25×2.5 cm metal pipes horizontally into freshly cleaned terrace exposures. The samples collected were covered with opaque materials in order to avoid exposure to light. The samples were packed and assigned numbers.

### 3.2.2 Laboratory work

Under red or orange light conditions, about 1.5 cm material from both ends of the metal pipe was discarded to avoid possible contamination due to exposure to light during sample collection. The discarded materials were used for determining dose rates. The samples for palaeodose were washed with 1N HCl to eradicate carbonates and then with 30% H<sub>2</sub>O<sub>2</sub> to eliminate organic matter. This was followed by thoroughly cleaning with distilled water after which the samples were dried. Quartz grains of about 90-150 µm were isolated from the fraction of the dried samples and placed on a Frantz Magnetic Separator for eliminating the contamination of magnetic. The grains obtained were then etched with HF (40%) and concentrated HCl for 80 and 30 minutes to remove contamination by feldspar and fluorides respectively, all the while using a magnetic stirrer to ensure that the quartz grains were continuously exposed to the acids. Silicon oil was used to mount the uncontaminated quartz grains as monolayers on stainless steel plates. The quartz grains were tested for purity to avoid any contamination by feldspar samples through infrared stimulated luminescence (IRSL). The measurement of luminescence proceeded with RISOE TL/OSL Reader TA-15 for dose rates and blue light stimulation sources (LEDs of wavelength 470±30 nm), blue light stimulated photons (PMT (EMI 9235 QA) for optical stimulation of quartz and a detection unit (optical filter U-340) for OSL signals (Moiya et al., 2019). The equivalent dose ( $D_e$ ) was measured following the Murray and Wintle, (2000) techniques, using a single aliquot regeneration (SAR) dose protocol. The dose response curves were constructed with a single saturating exponential function to calculate the burial dose ( $D_e$ ) by interpolation. Interpolation of burial dose was carried out following the procedure of Bailey and Arnold (2006) to

calculate the kurtosis, skewness, relative standard deviation and over-dispersion from the dose distribution.

Since the samples were subjected to heterogeneous bleach before their deposition therefore, the mean age, minimum age parameter (MAM) and centralized age models (CAM) have been considered (Galbraith et al., 1999; Moiya et al., 2019). Heterogeneous bleaching is visible in the dose over-dispersion distribution with 64% and 65.8% for samples JNM-3 and JNM-4 respectively. X-ray Fluorescence (XRF) was used for calculating the concentration of potassium and radioactive minerals such as uranium and thorium. Systematic errors and statistical uncertainties are <5%. The average water content of about  $10\pm 5\%$  (mass percentage) was utilized. The cosmic radiation input to the total dose rate was estimated following Prescott and Stephan (1982).

## CHAPTER: 4

### **MORPHOMETRIC ANALYSIS**

Morphometric analysis has been considered a significant tool that provides quantitative information of fluvial landforms (Keller and Pinter, 1996; Kulkarni, 2015). It was first proposed by Horton (1945) and has been functional in a broad range of studies. This approach is significant for geomorphological studies, which emphasizes on the quantification of details of lithology, structure and tectonics that affects landforms through different parameters and indices (Leopold et al., 1964; Sulaksana, 2017). Quantitative analysis encompasses various parameters along with implication of data from topographic maps, satellite imagery and field evidences.

Active tectonics implies ongoing tectonic movements since Late Pleistocene to the Holocene period (Burbank and Anderson, 2001; Elias, 2013). Geomorphic indices of active tectonics are quantitative measurements of landforms of suspected terrains that are undergoing tectonic deformations and are used as a reconnaissance tool to investigate areas experiencing active deformation (Keller and Pinter, 1996; Burbank and Anderson, 2001). These tools have proven to be of immense use to study the level of tectonic movements in large active regions (Bull, 1977; Keller and Pinter, 1996). Geomorphic indices can detect anomalies arising from disturbances related to tectonism in the fluvial system, mountain front, valleys, etc. (El Hamdouni et al., 2008). In a region where surface exposure is limited due to thick vegetation cover, geomorphic indices have proven to be a constructive method to identify active tectonics (Chen et al., 2003; Troiani and Della Seta, 2008).

Therefore, studies have been carried out using drainage, longitudinal profile, stream length gradient index, steepness index, asymmetry factor, transverse topography symmetry factor, basin elongation ratio, channel sinuosity, mountain front sinuosity index, valley floor width to valley height ratio and hypsometric curve and hypsometric integral to study the function of tectonics in origin of landforms.

## **4.1 Drainage Analysis**

### **4.1.1 Drainage Pattern**

The development of drainage patterns is influenced by tectonic activity as well as river anomaly (Valdiya and Narayana, 2007), which could be a source to infer tectonic events on regional or local scales (Mathew, 2016). Drainage patterns are sensitive to tectonic movements as well as lithology (Schumm et al., 2000). Drainage pattern analysis is considered to be useful for investigation of tectonic activity (Radaideh et al., 2016). As drainage pattern has a tendency to reflect the influencing factors, it can thus provide information about the underlying structure such as, faults and folds (Jackson et al., 1998). Drainage patterns such as parallel, rectangular and trellis are often related with structurally induced, faulted bedrock terrain (Slattery, 2011). The drainage network displayed in the study area includes dendritic, trellis, parallel and rectangular patterns. The dendritic pattern is most commonly displayed in the study area, as it mostly originates in horizontal sedimentary rocks. Structural controls over the drainage pattern are recognized in the present area in the presence of trellis, parallel and rectangular patterns. Trellis patterns indicate the alignment of stream along the strike of rock formations while parallel patterns usually depict structural control or presence of prominent slopes.

Trellis pattern is observed along the Der Ker stream, a tributary of the Chathe River towards SW of New Chumukedima. Parallel drainage patterns are observed in the sub-tributaries of the Chathe River and Khova River towards Razhephema. Most of the parallel drainage patterns are observed between the Chathe Fault and Disang Thrust towards Jalukie and Chathe Fault and Sanis-Chongliymesen Thrust towards Dimapur. Rectangular patterns are indicative of stream following distinct joints, faults or other lineaments. A few tributaries of the Jharnapani and Kukipani rivers display rectangular pattern towards NW and NNW of Piphema; these are bounded by the Sanis-Chongliymesen Thrust and Piphema Thrust. From the patterns observed in the study area, the drainage network seems to be extremely controlled by structures (Fig. 4.1a1, 2, 3, 4).

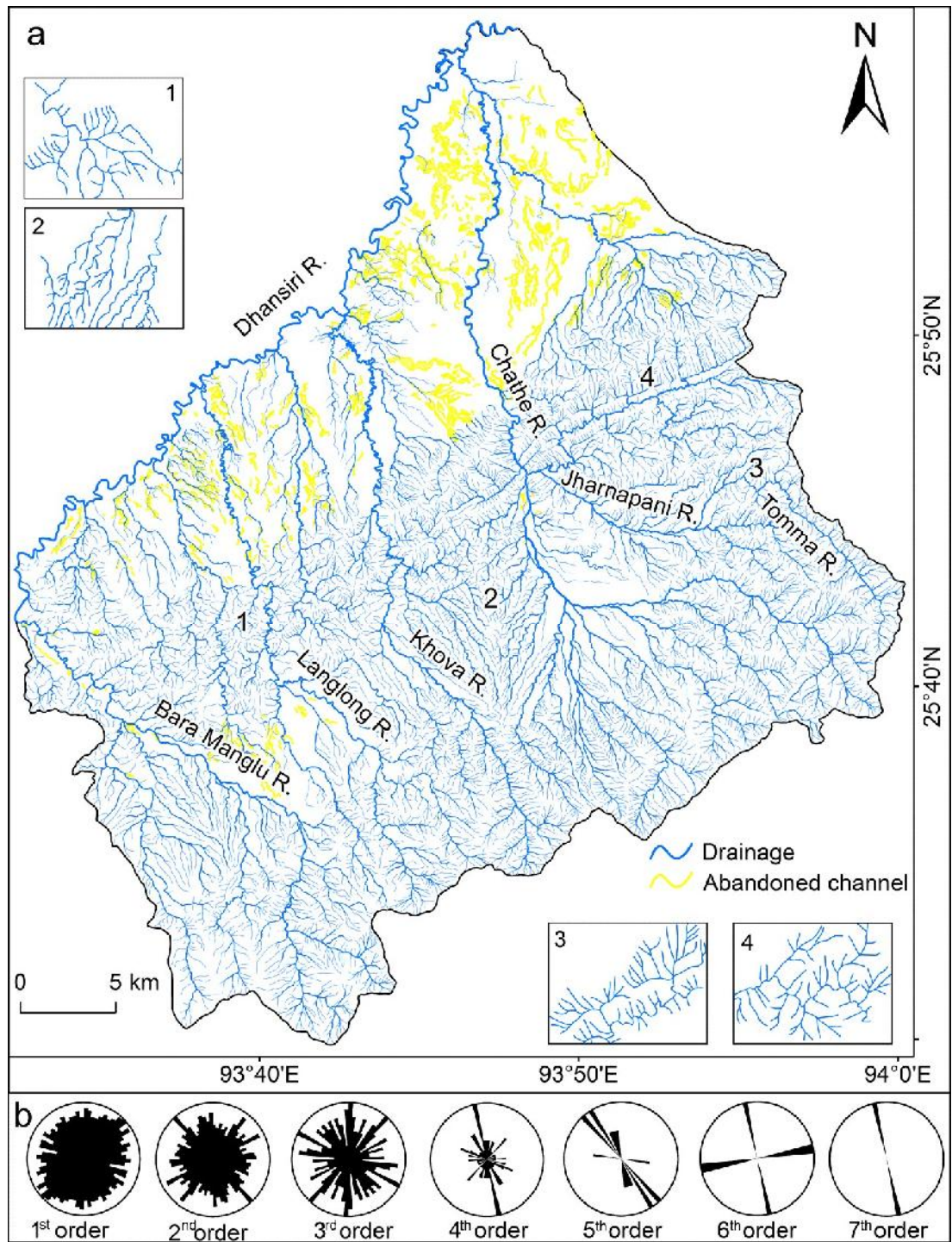


**Figure 4.1:** (a) Drainage map of the study area (modified after Moiya et al., 2019) (a1) Dendritic pattern, (a2) Parallel pattern, (a3) Trellis pattern, (a4) Rectangular pattern, (b) Drainage orientation of the various drainage orders

#### 4.1.2 Drainage order and orientation

The drainage networks are well developed till the 7<sup>th</sup> order stream. The orientations of the 1<sup>st</sup> order streams are WNW-ESE and NE-SW, the 2<sup>nd</sup> order streams are NW-SE, NE-SW, N-S and ENE-WSW, while the 3<sup>rd</sup> order streams are NE-SW, WNW-SSE

and N-S. The 4<sup>th</sup> order streams display NNW-SSE while the 5<sup>th</sup> order streams show NW-SE directions. The 6<sup>th</sup> order streams have WNW-ESE and NNW-SSE orientations while the highest order streams are oriented NNW-SSE.

The direction displayed by the 1<sup>st</sup> order streams indicates control by joints and normal faults. The 2<sup>nd</sup> order streams are dominantly controlled by normal faults and thrusts, while the 3<sup>rd</sup> order streams are mostly by thrusts. The 4<sup>th</sup>, 6<sup>th</sup> and 7<sup>th</sup> order streams are influenced by strike-slip faults. The 5<sup>th</sup> order streams are generally controlled by normal faults (Fig. 4.1b). Here orientation of the drainage orders suggests major influence of structures in the study area.

#### 4.1.3 Drainage density ( $D_d$ )

Drainage density values are highly influenced by lithology, climate and tectonic activity (Gregory and Gardiner, 1975; Tucker et al., 2001; Garrote et al., 2008; Faghih et al., 2015). High drainage density is ascribed to rejuvenation of a region (Faghih et al., 2015) and uplift along active fault zones (Han et al., 2003; Hou and Han, 1997).

The values range from 0.1 to 6.1. The computed values of more than 3.6 are confined to the Naga and Disang thrusts of the BoS. The high values are mostly seen along the thrust zone area of the BoS while the low values are mostly confined to the Dimapur plains (Fig. 4.2). High values of drainage density depend on the frequency of structures such as thrust, faults and fracture zones. The high value of drainage density towards the thrust zones may be attributed to tectonic structures.

The drainage analysis of the study area includes drainage pattern, drainage order orientations and drainage density. Analyses show high structural control within the thrust belts due to the effects of joints, normal faults and strike-slip faults, which point to high tectonic activity in the region.



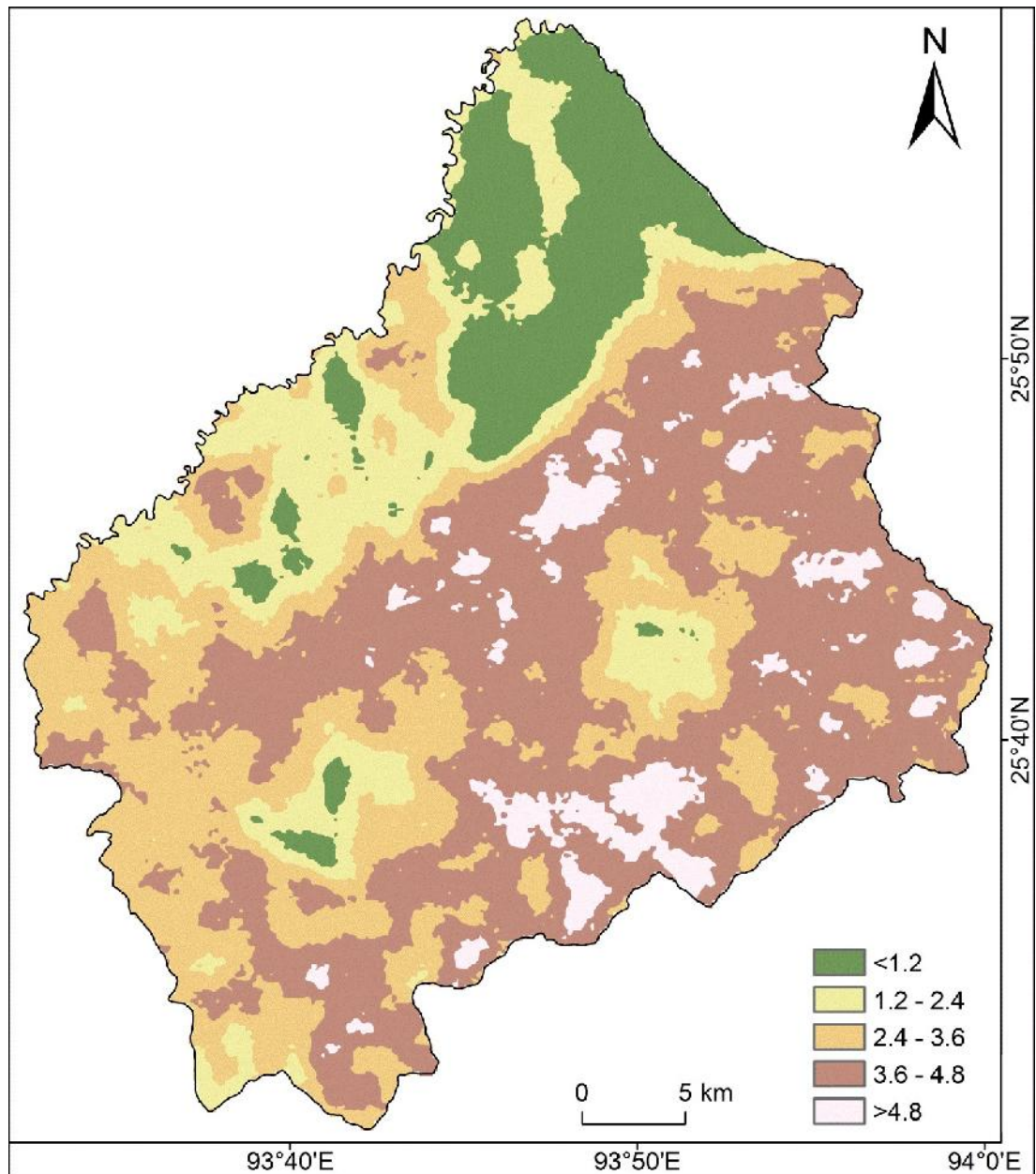


**Figure 4.2:** Drainage density map showing high values within the Belt of Schuppen (modified after Moiya et al., 2019)

## 4.2 Geomorphic indices

### 4.2.1 Longitudinal profile

The longitudinal river profile is used for topographic interpretations in relation to tectonics (Whipple and Tucker, 1999). The longitudinal profile represented by an erosional curve helps recognize the history behind the surface and valley development (Pareta and Pareta, 2011). Hack (1957) states that a graded stream is represented by a concave-upward shape while a stage of disequilibrium is characterized by a convex-

upward shape. Longitudinal profiles with convex curves and knickpoints provide a platform to decipher past tectonic activity (Figueroa and Knott, 2010). The longitudinal profile can detect slight disturbances in a river course; therefore, tectonic interruptions through location of knickpoints can be inferred (Keller and Pinter, 1996; Figueroa and Knott, 2010).

The longitudinal profile of the Bara Manglu River, ~38 km in length, displays several knickpoints. From the upstream, the first knickpoint is observed ~12 km upstream at the Yah Thrust, the second knickpoint ~16 km upstream at Disang Thrust, the third knickpoint ~21 km at the Chathe Fault and final knickpoint at a growing anticline ~28 km downstream. The longitudinal profile of the Langlong River, which is ~49 km long, knickpoints are observed ~7 km from the upstream at the Yah Thrust, ~10 km at the Disang Thrust, ~20 km at the Chathe Fault, ~25 km at the anticline and ~32 km at the Naga Thrust. The longitudinal profile of the Khova River, which is ~50 km long, knickpoints are observed at ~9 km at the Disang Thrust around, ~11 km at the Sanis-Chongliyimsen Thrust, ~18 km at the Chathe Fault and ~25 km at the anticline. The Chathe River longitudinal profile of ~45 km shows knickpoints at the Disang Thrust, Sanis-Chongliyimsen Thrust, Chathe Fault and the anticline about ~9 km, ~11 km, ~17 km and ~24 km from the upstream. In the Jharnapani River longitudinal profile of ~50 km length, knickpoints are observed at the Disang Thrust (~7 km), at a local fault (~13 km) and at the Sanis-Chongliyimsen Thrust (~17 km) (Fig. 4.3).

#### 4.2.2 Stream length gradient index

The diastrophic forces that shaped the area are indicated by the stream length gradient index (Hack, 1973). SL is receptive to change in relation to slope, lithology and uplift. As such, this provides a platform for evaluating stream response to uplift and displacement related to active tectonics (Hack, 1973; Keller and Pinter, 1996; Burbank and Anderson, 2001; Azor et al., 2002; Chen et al., 2003; Pérez-Peña et al., 2008; Tsodoulos et al., 2008).

SL calculations from the 5 rivers show spike along the river profile (Fig. 4.3). The Bara Manglu River profile of ~38 km length displays several SL spikes. From ~12 km upstream, the first SL spike is observed at the Yah Thrust with a value of 304. About 16 km downstream, a sharp SL spike with the highest SL value of 557, is



observed at the Disang Thrust. The Chathe Fault displays a SL spike at ~21 km with a SL value of 328. At ~28 km, at the anticline, a knickpoint with a SL value of 402 is noted. Along the Langlong River profile of ~49 km length, a SL value of 191 is observed at the Yah Thrust, ~7 km from the upstream. A SL value of 324 is observed at the Disang Thrust ~10 km downstream. A SL value of 179 is observed ~20 km at the Chathe Fault. A SL spike with value of 225 is observed ~25 km, in the growing anticline. The highest SL spike at ~32 km, with a value of 524, is observed at the Naga Thrust. In the Khova River profile of ~50 km length, a SL value of 287 is observed at the Disang Thrust, ~9 km downstream. A SL value of 271 is observed at a distance of 11 km at the Sanis-Chongliyimsen Thrust. A prominent spike with a SL value of 410 is observed at the Chathe Fault (~18 km downstream). A SL spike with SL value of 479 is observed ~25 km downstream, in the anticlinal structure. A SL spike of 426 value, ~20 km downstream, is observed at the lithological contact between the Tipam Sandstone and Girujan Clay formations. Here, the main trunk stream is aligned approximately NNE-SSW. A satellite image of IRS-1D (PAN+LISS III merged) reveals the presence of a lineament ~ 2 km in length. The high value of SL may either be due to the lineament, which appears to be a fault. The Chathe River profile of ~45 km length shows a high SL value of 961 at the Disang Thrust (~9 km downstream), 1426 at the Sanis-Chongliyimsen Thrust (~11 km) and 247 at the Chathe Fault (~17 km). A SL value of 1204, with a prominent SL spike is observed at the anticline (~24 km downstream). In the Jharnapani River profile, along a length of ~50 km, a SL value of 950 with a prominent spike is noted along the Disang Thrust (~7 km downstream). Further downstream at ~11 km, a SL value of 552 is observed at the Piphema Thrust. A SL value of 1536, with a prominent spike is seen at a local fault ~13 km downstream. The Sanis-Chongliyimsen Thrust shows a SL spike of value of 618 at ~17 km. About ~26 km downstream, at the Chathe Fault, a SL value of 618 is observed. A prominent SL spike with a value of 470 is observed between the Sanis-Chongliyimsen Thrust and Chathe Fault, where the main trunk of the Chathe River is affected by a lineament trending NE-SW.

#### 4.2.3 Steepness index

The steepness index is used for estimating rock upliftment (Snyder et al., 2000; Kirby and Whipple, 2001, 2003) as it is directly proportional to the uplift rates, which can help deduce the role of tectonics in a stream profile (Kirby and Whipple, 2001).

When the stream is in steady state condition, the  $k_s$  value remains constant as erosion is balanced by uplift. However, during differential uplift, changes in  $k_s$  values are observed from segment to segment (Snyder et al., 2000; Wobus et al., 2003; Whipple et al., 2013).

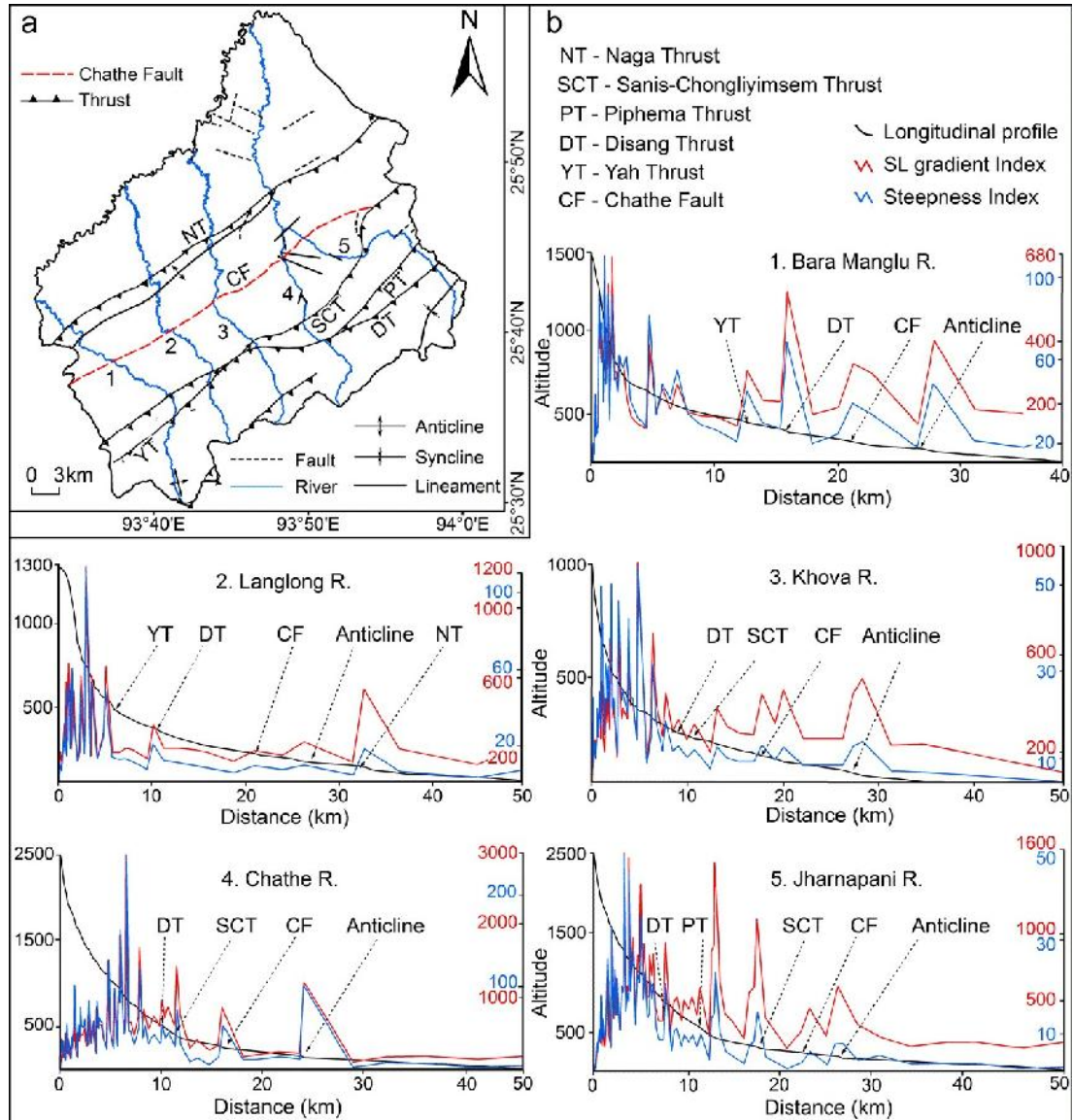


**Figure 4.3:** (a) Profiles of the Bara Manglu, Langlong, Khova, Chathe and Jharnapani rivers; (b) Knickpoints observed along the longitudinal profile, stream length gradient index and steepness index of the five major rivers of the study area.

Spikes of  $k_s$  are observed along ~38 km length of the Bara Manglu river profile (Fig. 4.3). The values of steepness index obtained are 43, 67, 38 and 47 from distances of ~12 km, ~16 km, ~21 km and ~28 km from the upstream, at the Yah Thrust, Disang Thrust, Chathe Fault and the anticline respectively. In the Langlong

River profile of ~49 km length, the  $k_s$  values obtained are 12, 20, 8, 9 and 17 at distances of about ~7 km, ~10 km, ~20 km, ~25 km and ~32 km downstream at the Yah Thrust, Disang Thrust, Chathe Fault, anticline and Naga Thrust respectively. Along the Khova River profile of ~50 km length, the steepness values obtained in the Disang Thrust, Sanis-Chongliymnsen Thrust, Chathe Fault, and anticline are 9, 8.5, 9.6 and 10 at ~9 km, ~11km, ~18 and ~28 km respectively. In the Chathe River profile of ~45 km length,  $k_s$  values are 44 at the Disang Thrust (~9 km), 74 at the Sanis-Chongliymnsen Thrust (~11 km), and 22 at the Chathe Fault (~ 17 km) and 16 at the anticline (~ 24 km). The Jharnapani River section of ~50 km length shows prominent  $k_s$  spikes at the Disang Thrust (~7 km), 10 at the Piphema Thrust (~11 km), and 14 at the Sanis-Chongliymnsen Thrust (~ 17 km) and 7.8 at the Chathe Fault (~ 26 km). Spikes of  $k_s$  are observed ~13 km and ~22 km with values of 23 and 6.16 respectively, which correspond with the SL spikes.

From the 5 river profile analyses, viz., longitudinal, stream length gradient index and steepness index, the knickpoints are developed along the thrusts, Chathe Fault and anticline. No prominent peaks are observed along the lithological contacts. The development of knickpoint along the longitudinal profile and high values with steep peaks of SL and  $K_s$  correspond with each other, suggesting the areas are highly influenced by tectonic activity.

#### 4.2.4 Asymmetry factor

Drainage basin analysis was carried out to elucidate the complex relationship that exists between the forms and processes for determining the role of tectonics. The asymmetry factor helps decipher tectonic activity based on tilt of river basins (Keller and Pinter, 1996). The trunk stream of a drainage basin will migrate in relation to tectonic tilting (Morrish, 2015). This tilting nature of AF perpendicular to the main tributary course helps unravel tectonic activity of a basin (Cox, 1994; Tsodoulos et al., 2008).

The computed values of asymmetry factor shows out of the 20 sub-watersheds analyzed, 11 sub-watersheds have values ranging from 20-49 indicating right tilt (NE) while the remaining 9 sub-watersheds tilt towards the left (SW), with values ranging from 52-67 (Table 4.1). All the sub-watersheds drained by the Bara Manglu River are tilted towards the left while the sub-watersheds drained by the Chathe, Langlong and

Khova rivers are right tilted, except for 1 each that tilt towards the left (Fig. 4.4). A maximum tilt of 30 is observed in sub-basin 5, while the least of 1 is observed in sub-basin 10. The average amount for basins tilting left is 7.7 while for those tilting right is 11.54. The maximum for sub-basins tilting left is 17 for sub-basin 14 while the least is 2 for sub-basin 8. The sub-basins have an average tilt amount of 9.62, which suggests that the migrations of streams are not much influenced by ground tilting of the area. However, the tilting nature of subwatersheds indicates basin to be active.

**Table 4.1:** Asymmetry factor

<b>Sub-basin</b>	<b>AF</b>	<b>Inference</b>	<b>Sub-basin</b>	<b>AF</b>	<b>Inference</b>
1	58	Left tilt	11	34	Right tilt
2	53	Left tilt	12	60	Left tilt
3	52	Left tilt	13	25	Right tilt
4	66	Left tilt	14	67	Left tilt
5	20	Right tilt	15	42	Right tilt
6	43	Right tilt	16	44	Right tilt
7	58	Left tilt	17	37	Right tilt
8	52	Left tilt	18	42	Right tilt
9	45	Right tilt	19	42	Right tilt
10	49	Right tilt	20	54	Left tilt

#### 4.2.5 Transverse topography symmetry factor

Transverse topography symmetry factor is a 2-D vector of magnitude and direction (Keller and Pinter, 1996). The numerical value indicates the asymmetry of the basin while the orientation gives the direction of asymmetry (Pinter, 2005). This index helps in determining the tilt direction of a river and magnitude in relation to active tectonics (Cox, 1994). A greater-than zero value is indicative of an asymmetric river basin (Keller and Pinter, 1996).

The average T-values calculated in the study area ranges from 0.0 to 0.59. A rose plot displays prominent ENE-WSW directions (Fig. 4.4). Maximum stream migration is observed in sub-basin 5 while the least migration is observed in sub-basin 8. The average T value for 20 sub-basins is 0.373, which indicates that the streams have not migrated much. Though the area is tectonically active it is not highlighted by ground tilting. From the 20 sub-basins, 827 T values have been computed; migration directions shown by the rose diagram are either NE or SW. However, most migration directions fall towards SE; this anomaly is due to averaging the T values (Table 4.2).

**Table 4.2:** Transverse topography symmetry factor

Sub-basin	T	T average bearing (°)	Sub-basin	T	T average bearing (°)
1	0.32	167	11	0.34	75
2	0.40	183	12	0.31	114
3	0.40	164	13	0.51	82
4	0.40	213	14	0.37	251
5	0.59	78	15	0.42	158
6	0.28	91	16	0.41	95
7	0.34	190	17	0.32	50
8	0.22	157	18	0.35	136
9	0.38	173	19	0.26	314
10	0.32	159	20	0.52	147

#### 4.2.6 Basin elongation ratio

Basin elongation ratio is a quantitative morphometric parameter that deals with the shape of a river basin (Bhattacharya et al., 2013). River basins that are undergoing active tectonism are elongated in shape (Burbank and Anderson, 2001), as an outcome of continuous faulting and thrusting (Sreedevi et al., 2005; Argyriou, 2012). A circular basin is indicative of an inactive setting; an oval basin depicts a slightly active basin, while an elongated basin indicates active tectonics (Bull and McFadden, 1977).

An analysis shows 15 sub-watersheds are tectonically active with values ranging from 0.21-0.47 while the remaining 5 sub-watersheds have values between 0.53-0.59, being slightly active (Table 4.3). The average value calculated for Re is 0.42, which is  $<0.5$ , pointing to a tectonically active basin. The basin elongation ratio suggests an active tectonic setting in the study area (Fig. 4.4).

**Table 4.3:** Basin elongation ratio

Sub-basin	Area (km <sup>2</sup> )	Length (km)	Re	Inference
1	58	20.31	0.39	Active
2	50	18.96	0.47	Active
3	24	15.72	0.38	Active
4	66	19.15	0.47	Active
5	40	12.32	0.56	Slightly active
6	71	25.44	0.35	Active
7	37	29.64	0.23	Active
8	93	19.29	0.57	Slightly active
9	62	22.64	0.39	Active
10	69	28.02	0.32	Active
11	59	22.42	0.40	Active

12	35	11.94	0.58	Slightly active
13	183	41.17	0.21	Active
14	26	14.53	0.41	Active
15	41	16.75	0.41	Active
16	48	15.06	0.53	Slightly active
17	64	19.53	0.46	Active
18	90	29.73	0.33	Active
19	73	22.10	0.45	Active
20	146	23.42	0.59	Slightly active

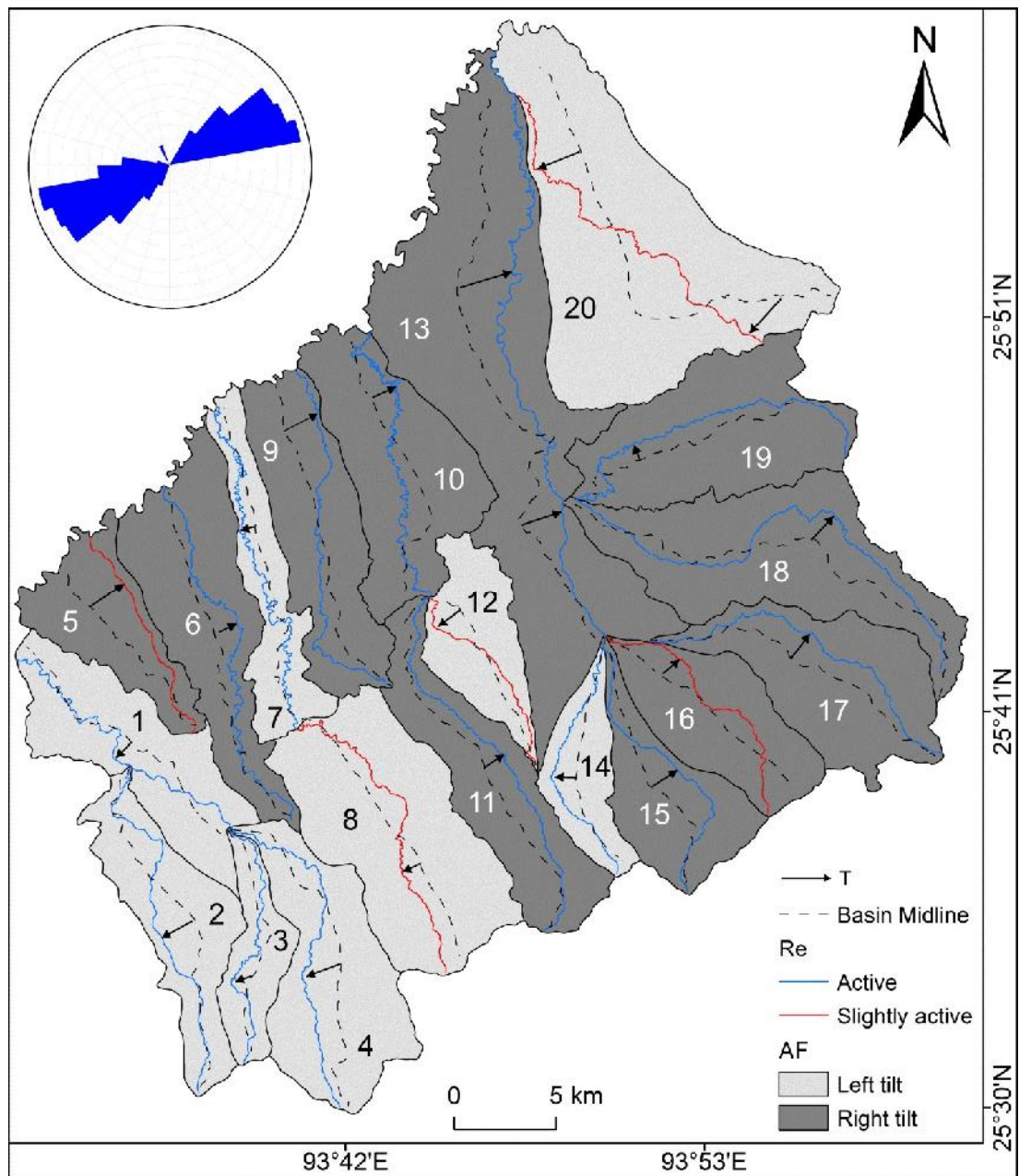


**Figure 4.4:** Asymmetry factor, transverse topography symmetry factor and basin elongation ratio map with T orientation showing a prominent NE-SW direction (modified after Moiya et al., 2019)

#### 4.2.7 Channel sinuosity

This qualitative index has been considerably applied for interpreting the evolution of landscapes through river courses (Pareta and Pareta, 2011). Factors such as hydraulic, climatic, lithologic or tectonic forces cause rivers to deviate from straight courses (Bhatt et al., 2007). Channel sinuosity values range from 1.05-3.52 (Table 4.4). Out of 65 segments computed, 22 segments show meandering courses while the remaining 43 shows sinuous courses. The channel sinuosity index indicates that the study area is deprived of straight courses, suggesting an outcome of tectonic activity (Fig. 4.5).

**Table 4.4:** Channel sinuosity

Segment	VL	S	Inference	Segment	VL	S	Inference
1	1.89	1.64	Meandering	34	3.05	1.64	Meandering
2	3.17	1.58	Meandering	35	3.84	1.30	Sinuuous
3	3.43	1.46	Sinuuous	36	4.31	1.16	Sinuuous
4	4.22	1.18	Sinuuous	37	4.46	1.12	Sinuuous
5	4.21	1.19	Sinuuous	38	4.04	1.24	Sinuuous
6	3.99	1.25	Sinuuous	39	3.33	1.50	Meandering
7	3.91	1.28	Sinuuous	40	3.31	1.51	Meandering
8	4.67	1.07	Sinuuous	41	3.13	1.60	Meandering
9	4.79	1.05	Sinuuous	42	4.46	1.12	Sinuuous
10	4.07	1.23	Sinuuous	43	3.50	1.12	Sinuuous
11	4.13	1.21	Sinuuous	44	4.54	1.10	Sinuuous
12	3.62	1.38	Sinuuous	45	4.48	1.12	Sinuuous
13	3.26	1.54	Meandering	46	4.15	1.20	Sinuuous
14	2.96	1.69	Meandering	47	4.43	1.13	Sinuuous
15	4.06	1.23	Sinuuous	48	4.24	1.18	Sinuuous
16	1.98	2.52	Meandering	49	4.39	1.14	Sinuuous
17	2.76	1.81	Meandering	50	3.81	1.31	Sinuuous
18	3.04	1.81	Meandering	51	4.42	1.13	Sinuuous
19	2.45	2.04	Meandering	52	4.68	1.07	Sinuuous
20	3.24	1.54	Meandering	53	4.43	1.10	Sinuuous
21	2.89	1.73	Meandering	54	4.48	1.12	Sinuuous
22	4.12	1.21	Sinuuous	55	4.11	1.21	Sinuuous
23	3.93	1.27	Sinuuous	56	3.28	1.53	Meandering
24	4.57	1.09	Sinuuous	57	4.72	1.06	Sinuuous
25	4.05	1.23	Sinuuous	58	4.40	1.14	Sinuuous
26	3.62	1.38	Sinuuous	59	2.60	1.92	Meandering
27	4.24	1.18	Sinuuous	60	4.16	1.20	Sinuuous
28	4.26	1.17	Sinuuous	61	4.27	1.17	Sinuuous
29	1.42	3.52	Meandering	62	3.92	1.27	Sinuuous
30	2.01	2.49	Meandering	63	3.40	1.47	Sinuuous
31	2.28	2.19	Meandering	64	3.33	1.50	Meandering
32	3.11	1.61	Meandering	65	4.45	1.12	Sinuuous
33	3.02	1.66	Meandering				



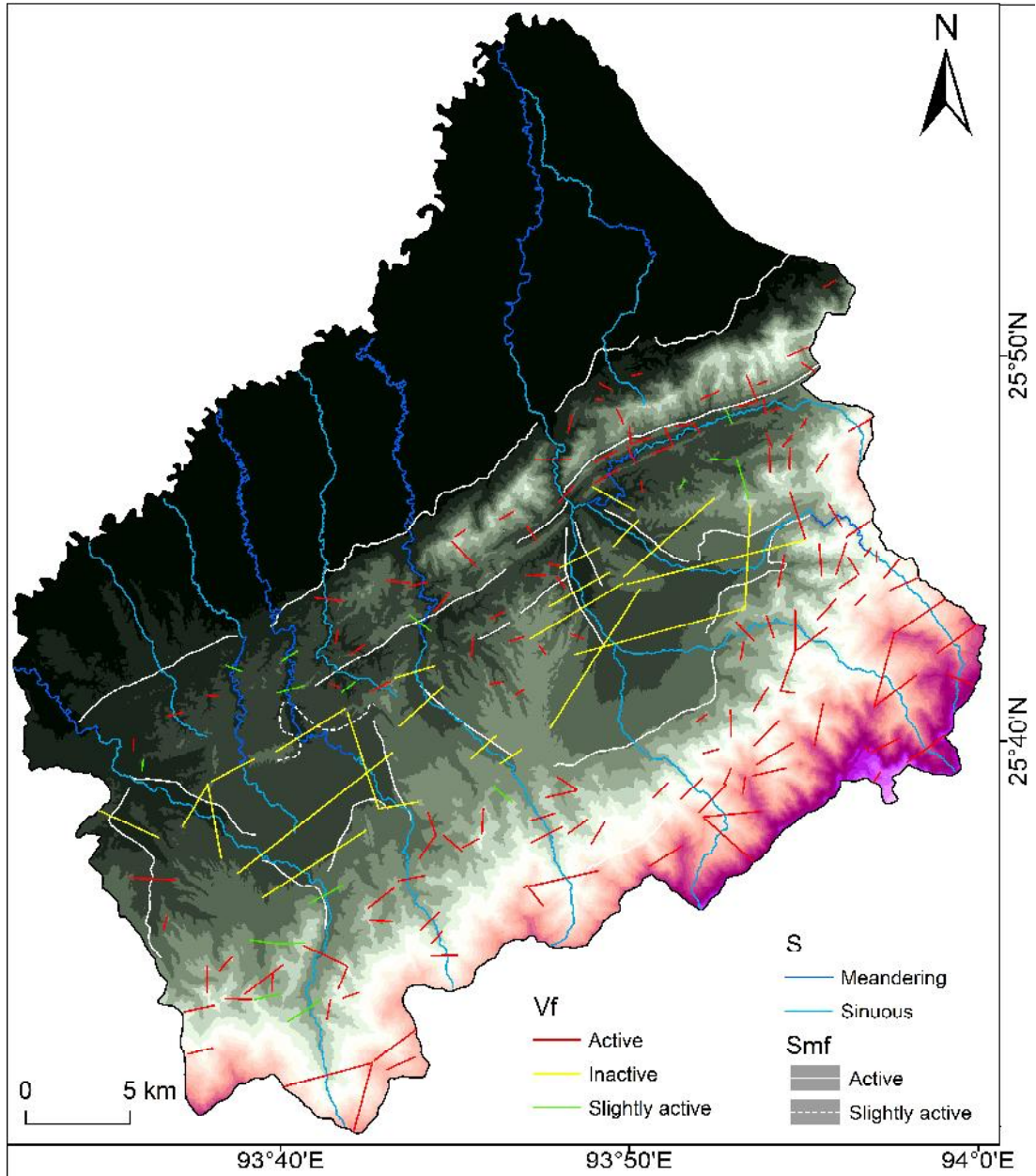


**Figure 4.5:** Channel sinuosity, mountain front sinuosity and valley floor width to valley height ratio map of the study area (modified after Moiya et al., 2019)

#### 4.2.8 Mountain front sinuosity

Active mountain fronts are usually straight, which help to distinguish areas undergoing tectonic activity. High values characterize mountain fronts that are associated with erosional processes, while low values depict mountain fronts with tectonic activity.

For the present study, 28 mountain front segments were considered. The  $S_{mf}$  values obtained range from 1-1.76 (Table 4.5). Values ranging from 1-1.32 are noted



in 27 segments, which are considered tectonically active terrains. A value of 1.72 is noted in 1 segment, which is slightly active (Fig. 4.5). The mountain front in this area is defined by the Naga Thrust. The nature of the mountain front points to tectonic activity of the Naga Thrust.

**Table 4.5:** Mountain front sinuosity

Segment	$L_{mf}$ (km)	$L_s$ (km)	$S_{mf}$ (km)	Inference
1	8.97	8.76	1.02	Active
2	18.11	16.14	1.12	Active
3	6.07	5.40	1.12	Active
4	8.96	7.58	1.18	Active
5	10.01	8.34	1.20	Active
6	7.13	6.72	1.06	Active
7	9.47	5.40	1.76	Slightly active
8	10.89	10.81	1.01	Active
9	3.18	3.12	1.02	Active
10	14.05	13.70	1.03	Active
11	1.77	1.76	1.00	Active
12	2.97	2.94	1.01	Active
13	6.11	5.92	1.03	Active
14	3.37	3.35	1.01	Active
15	4.85	4.77	1.02	Active
16	5.96	4.96	1.20	Active
17	5.16	4.48	1.15	Active
18	5.32	4.23	1.26	Active
19	5.15	5.06	1.02	Active
20	5.61	5.59	1.00	Active
21	9.99	7.54	1.33	Active
22	11.00	9.55	1.16	Active
23	6.06	5.82	1.04	Active
24	3.36	3.34	1.09	Active

#### 4.2.9 Valley floor width to valley height ratio

This index indicates landscapes experiencing high or low rates of uplift. Low values of  $V_f$  are linked with high incision and uplift rates, giving rise to deep valleys, while high values of  $V_f$  are related to low uplift, therefore with broad valleys (Bull and McFadden, 1977; Keller and Pinter, 1996). This index has proven to be an influential tool to establish the role of tectonism on the valley floor (Burbank and Anderson, 2001).

The  $V_f$  was considered for 179 segments with lengths from 0.2 km to 9.3 km. The  $V_f$  values range from 0.04 to 38.7 (Table 4.6). Out of 179 segments computed, 140 segments are of class 1, 16 segments fall in class 2 and the rest in class 3. The low values of Class 1 are restricted along the Naga-Patkai Hills, suggesting the region to be high in uplift and incision that resulted in giving rise to V-shaped valleys. The creation of V-shaped valleys with steep valley walls is attributed primarily to tectonic activity facilitated by the presence of soft sedimentary rocks. High values are mostly confined to the plains of Medziphema and Jalukie. The high values of  $V_f$  in these regions may be due to the broad intermontane valley surrounded by moderate and high structural hills (Fig. 4.5). The average value of  $V_f$  is 2.3, which points to narrow river valleys. This in turn gives an idea of tectonic activity taking place in the frontal part of the IMR. The low values of  $V_f$  suggest tectonic activity along the Naga Thrust. These values also corroborate data obtained from the computation of mountain front sinuosity index.

#### 4.2.10 Hypsometric curve and hypsometric integral

Hypsometric curves represent the phase of geomorphic maturity of a basin. Hypsometric curves that are convex are immature or at the youthful stage, the S-shaped characterizes mature stage and concave indicates old stage or stage of equilibrium (Strahler, 1952; Pérez-Peña et al., 2009). The area that exists beneath the hypsometric curve represents the hypsometric integral (Pérez-Peña et al., 2009). Hypsometric analysis deals with complex relationships between erosion and tectonics, which may be associated to uplift rates (Strahler, 1952; Schumm 1956). Hypsometric analysis has been widely used as a tool to infer tectonism in active regions (Keller and Pinter, 1996). Though it may not be directly linked with tectonic activity, the high values of hypsometric integral imply younger landscape, possibly the outcome of recent tectonics or high incision, while low values representing older landscape are presumably not much influenced by active tectonics (Chen et al., 2003; El Hamdouni et al., 2008). Hypsometric analysis was carried out for 58 mini-watersheds; 9 are straight while 13 are curved. The remaining 36 mini-watersheds are convex, pointing to a youthful stage (Fig. 4.6). The convex curves representing the youthful stage are mostly confined to the foot-and hanging wall blocks of the Naga Thrust zone, which is possibly associated with recent uplift.

**Table 4.6:** Valley floor width to valley height ratio

Sl. no.	Length (m)	Vf	Inference	Sl. no.	Length (m)	Vf	Inference	Sl. no.	Length (m)	Vf	Inference
1	1215	9.85	Inactive	31	711	0.95	Active	61	641	0.79	Active
2	3909	6.98	Inactive	32	1011	0.83	Active	62	673	1.07	Active
3	876	0.81	Active	33	1847	0.08	Active	63	496	0.64	Active
4	2853	7.51	Inactive	34	830	0.19	Active	64	978	1.11	Active
5	1572	0.61	Active	35	2012	0.09	Active	65	1077	0.42	Active
6	1115	0.52	Active	36	1758	0.3	Active	66	1299	2.56	Slightly active
7	1306	0.77	Active	37	2959	0.15	Active	67	1024	0.72	Active
8	616	0.78	Active	38	925	2.34	Slightly active	68	1200	0.48	Active
9	2416	0.29	Active	39	823	1.87	Slightly active	69	1242	0.47	Active
10	875	0.47	Active	40	635	0.57	Active	70	1151	1.92	Slightly active
11	1125	0.31	Active	41	514	1.11	Active	71	2272	1.15	Active
12	1853	0.04	Active	42	1265	0.54	Active	72	1277	0.5	Active
13	2545	0.15	Active	43	2505	0.15	Active	73	1063	1.38	Active
14	2076	0.08	Active	44	1123	0.83	Active	74	1287	1.37	Active
15	2204	0.1	Active	45	1504	0.89	Active	75	1321	0.36	Active
16	762	0.78	Active	46	3169	0.07	Active	76	1098	0.48	Active
17	1004	0.69	Active	47	2791	0.27	Active	77	1734	8.14	Inactive
18	1181	0.61	Active	48	873	0.83	Active	78	2118	6.68	Inactive
19	1699	0.52	Active	49	1371	0.65	Active	79	3135	17.87	Inactive
20	2293	5.05	Inactive	50	1177	1.33	Active	80	8815	11.91	Inactive
21	1157	0.19	Active	51	1177	1	Active	81	1122	0.44	Active
22	1335	0.2	Active	52	1285	0.42	Active	82	5863	26.75	Inactive
23	2394	0.82	Active	53	4427	0.12	Active	83	9374	38.75	Inactive
24	904	0.71	Active	54	648	1.43	Active	84	2266	12.55	Inactive
25	1008	1.75	Active	55	1203	0.97	Active	85	2327	7	Inactive
26	2217	1.42	Active	56	650	0.69	Active	86	1929	6.02	Inactive
27	1469	0.29	Active	57	2001	2.21	Slightly active	87	5172	3.56	Inactive
28	1286	2.04	Slightly active	58	1595	0.35	Active	88	5713	5.35	Inactive
29	1953	2.09	Slightly active	59	1522	0.19	Active	89	8378	17.23	Inactive
30	1223	0.77	Active	60	1226	1.04	Active	90	1614	6.62	Inactive

Sl. no.	Length (m)	Vf	Inference	Sl. no.	Length (m)	Vf	Inference	Sl. no.	Length (m)	Vf	Inference
91	4697	36.65	Inactive	121	831	0.66	Active	151	1255	2	Slightly active
92	3572	7.45	Inactive	122	717	0.58	Active	152	1238	0.25	Active
93	1576	1.72	Active	123	879	0.42	Active	153	904	0.56	Active
94	1272	0.31	Active	124	268	1.08	Active	154	1390	0.35	Active
95	1991	6.49	Inactive	125	604	0.46	Active	155	1949	0.62	Active
96	705	1.53	Active	126	480	1.35	Active	156	1659	0.19	Active
97	581	0.47	Active	127	654	1.12	Active	157	1095	0.23	Active
98	797	2.2	Slightly active	128	1346	0.17	Active	158	1374	0.3	Active
99	1318	2.33	Slightly active	129	1288	0.46	Active	159	689	1.54	Active
100	520	1.66	Active	130	402	0.47	Active	160	963	0.3	Active
101	492	2.61	Slightly active	131	764	0.53	Active	161	938	0.77	Active
102	485	2.08	Slightly active	132	3393	0.28	Active	162	849	1.34	Active
103	515	1.25	Active	133	1218	0.71	Active	163	1290	0.55	Active
104	421	0.85	Active	134	712	1.18	Active	164	993	2.63	Slightly active
105	1231	0.32	Active	135	1473	0.39	Active	165	716	1.98	Slightly active
106	795	0.8	Active	136	2293	1.35	Active	166	713	0.91	Active
107	831	0.62	Active	137	3642	0.11	Active	167	509	1.07	Active
108	1161	0.55	Active	138	681	0.52	Active	168	437	0.85	Active
109	870	1.78	Active	139	962	0.47	Active	169	1511	0.38	Active
110	494	0.66	Active	140	978	0.57	Active	170	1000	0.71	Active
111	753	0.66	Active	141	689	0.61	Active	171	916	0.48	Active
112	488	1.17	Active	142	2119	0.23	Active	172	683	0.77	Active
113	620	0.67	Active	143	797	0.68	Active	173	560	1.24	Active
114	754	1.33	Active	144	3686	0.25	Active	174	1512	0.11	Active
115	1601	0.19	Active	145	1645	0.34	Active	175	1585	0.22	Active
116	999	0.59	Active	146	805	0.96	Active	176	4940	7.82	Inactive
117	459	1.67	Active	147	968	0.56	Active	177	7912	28.51	Inactive
118	802	0.58	Active	148	1877	2.09	Slightly active	178	3326	6.58	Inactive
119	549	0.6	Active	149	1308	2.11	Slightly active	179	1233	0.36	Active
120	722	1.22	Active	150	864	0.58	Active				

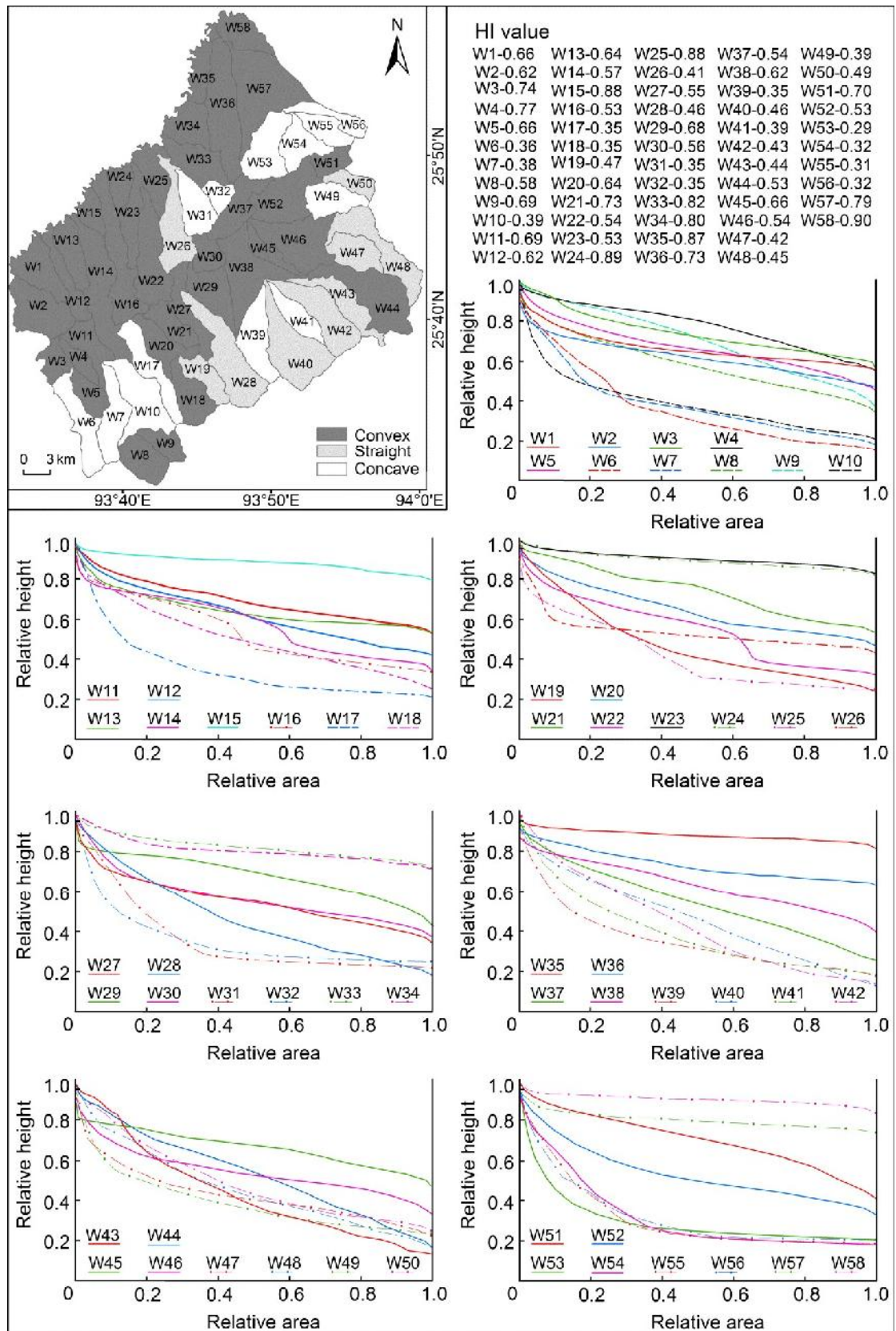


**Figure 4.6:** Hypsometric curves and hypsometric integral

## CHAPTER: 5

### **MORPHOTECTONICS**

Morphotectonics is an amalgamation of tectonics and geomorphology (Scheidegger, 2004). It is considered synonymous with tectonic geomorphology, which focuses on the relationship between tectonics and processes that are responsible for landscape shape in regions of active deformation (Burbank and Anderson, 2001). It aids in studying problems related to tectonics in a tectonically active region (Keller and Rockwell, 1984). Tectonic activity is responsible for evolution of ocean basins, continents, mountains and plateaus, along with structural characteristics such as fold, faults, joints and thrusts (Ollier, 1981; Keller and Pinter 1996; Burbank and Anderson, 2001). These landscapes are continuously modified by external and internal forces. The internal forces of tectonism cause uplift of the crust and movements or deformation to build the landscapes (Keller and Pinter, 2002).

The present study is an attempt to decipher the landforms associated with structures and the denudational and fluvial processes (Fig. 5.1). Structural landforms in the study area include fault scarps, ridges, strath terraces and broad intermontane valleys. Intermontane valleys are significant parts of mountainous landscapes developed in areas of climatic instability and tectonic activity (Sinha and Sinha, 2016). The intermontane basins of the study area are developed within the thrust-fault zones of the BoS (Aier et al., 2011). In tectonically active orogens, the synorogenic sediments of the intermontane basins provide information that could decipher the history behind the uplift (Burbank and Johnson, 1983; Streit et al., 2015). These sediments not only record the formation and evolution of basin but also tectonic processes involved (Zhu et al., 2006). Investigation of the structure, deformation and uplift of fluvial sediments could help in interpreting the role played by tectonic activity in development of the intermontane basins. Lineaments are associated with fractures and faults (Ni et al., 2016) as well as ridges, linear valleys and drainage features (Dalati, 2000) that could essentially provide information about the regional structure and tectonics (Bhatt et al., 2007). Faults in Quaternary fluvial sediments are indicators of neotectonic activity within the intermontane basin.



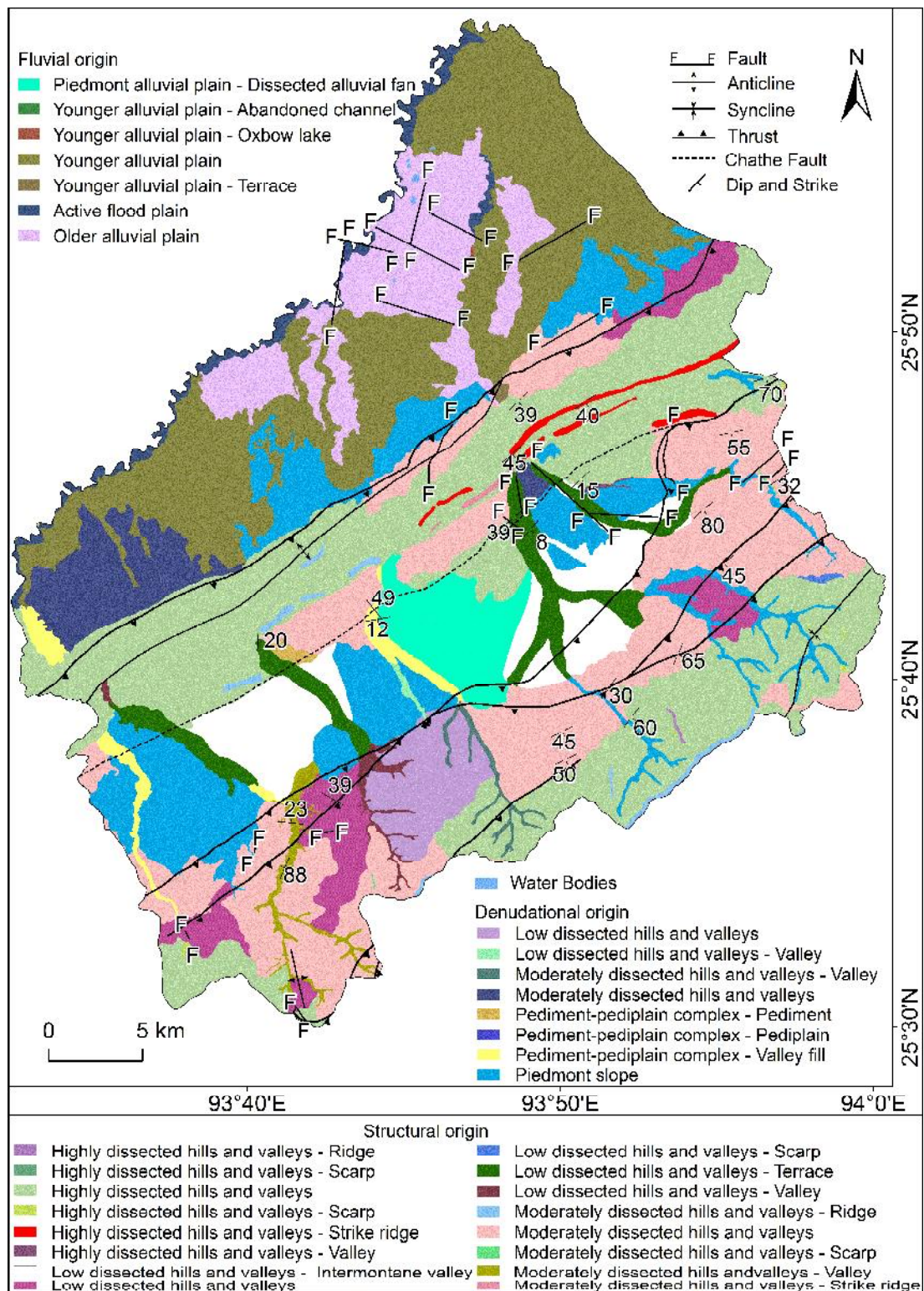


**Figure 5.1:** Tectonogeomorphic map of the study area (modified after NGISRSC, 2014)

Drainage features such as stream diversion, stream capture/piracy are investigated for the identification of neotectonic signatures because of their sensitivity to tectonic uplift owing to thrusting and faulting in regions of tectonically complicated

settings (Audemard, 1999; Perucca et al., 2013). Topographic profiles across and along the BoS were considered to decipher the relationship between thrusts, faults and drainage to established their role in the evolution of the intermontane basins in the study area.

### **5.1 Seismotectonics**

Northeast India is one of six of the world's active seismic regions (BIS, 2002), being subjected to two great earthquakes and 20 large earthquakes (Fig. 5.2) between 1897 and 2015 (Bora, 2016). Devi (2012) opines that a major earthquake is due in the region between the Shillong earthquake (1897) epicenter and Patkai Range and the Arunachal Pradesh earthquake (1950) epicenter based on seismological research and history of earthquakes. Talukdar and Barman (2012) conducted seismotectonic studies of the northeastern region and classified the tectonic blocks into different groups. The number of earthquake occurrences during 1964-2011 was higher in the IMR, which includes the Arakan-Yoma, Chin Hills, Sagaing Fault and the BoS than in the other tectonic blocks that include the Eastern Himalayan Ranges and Syntaxis Zone. Studies of earthquake depth also suggest that shallow to deep focus earthquakes are predominant in the IMR. The BoS is susceptible to shallow to intermediate earthquakes associated with the complex tectonic setting of the region. In particular, is the Naga Thrust, which is responsible for reactivating the residual strain in the BoS (Roy and Kacker, 1982) that BoS signifies a high stress accumulation area (Talukdar, 2013).

### **5.2 Lineaments**

Lineaments are straight or curvilinear forms resulting from tectonic stress and strain that are indicative of subsurface faults (Ni et al., 2016). Mapping and analysis of lineaments can help in identifying deformation related to late Quaternary tectonic movements (Radaideh et al., 2016). The direction of lineaments indicates fracture patterns of a rock associated with tectonic activity (Ni et al., 2016). High density zones of lineaments are representative of neotectonics (Kumanan, 2001). A total of 3,681 lineaments were extracted, with lengths ranging between 480 and 500 m. A rose diagram constructed of the lineaments displays two main trends, NW-SE and NE-SW (Fig. 5.3). The NE-SW trend is analogous to the fold and thrust systems while the NW-SE orientations are parallel to the regional compression. A number of the



lineaments trending NW-SE are recognized as normal faults. The high values of lineament density that are confined to the thrust zones of the BoS, are associated with the Naga Thrust and Disang Thrust, possibly an indication of tectonic movements.

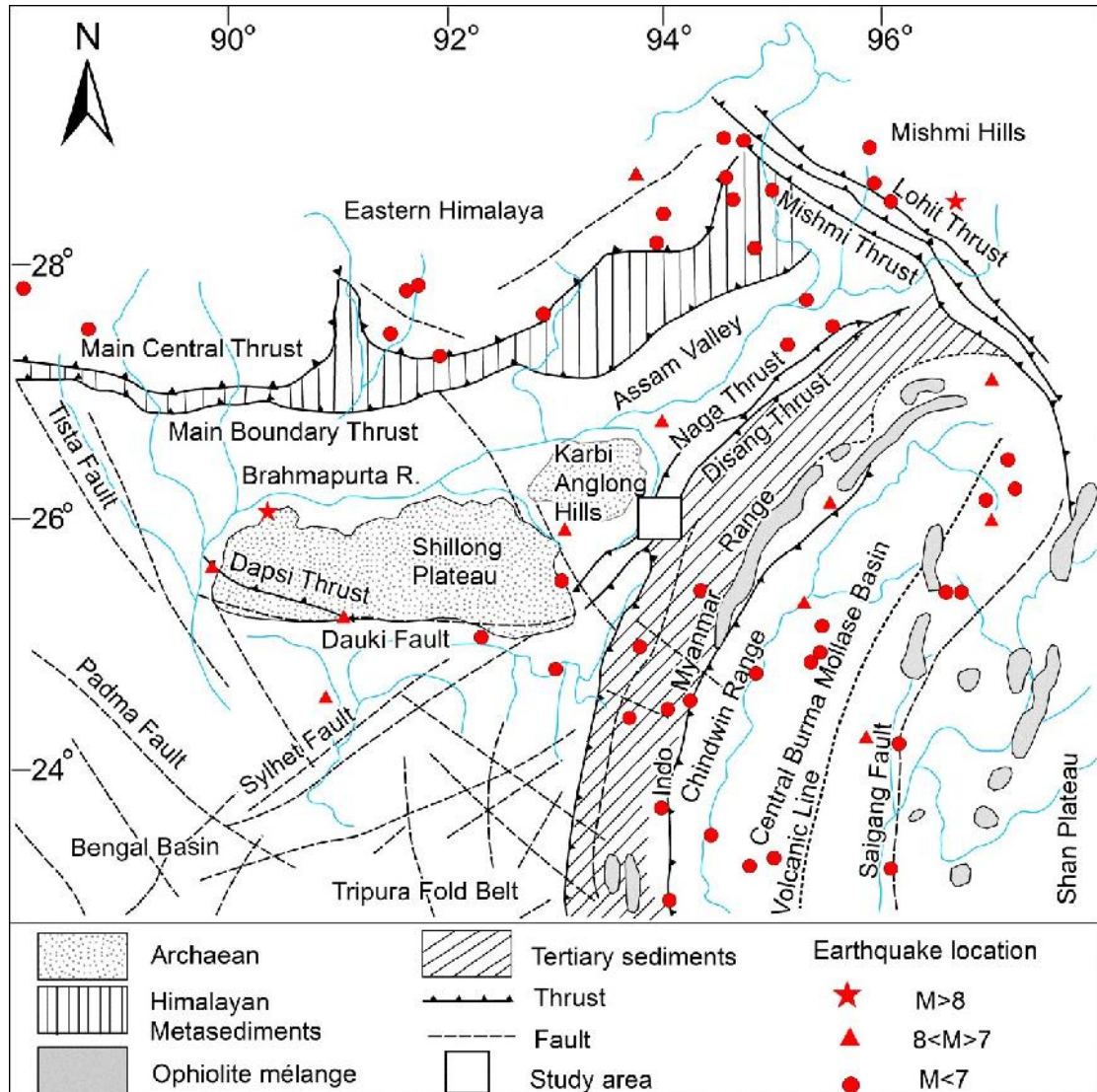


**Figure 5.2:** Seismotectonic map of NE India (after Nandy, 2000; earthquake epicenters - USGS, 1915-2016)

### 5.3 Faults

Faults are fracture planes resulting from earth movements. Prominent geomorphic signatures associated with faults are scarps, triangular facets, cones, structural control on drainage pattern, truncation of Quaternary landforms, linear traces of fault on landforms and uplifted terraces and fan deposits. The Chathe Fault (Fig. 5.4a) is characterized by NE-SW trending linear valleys.

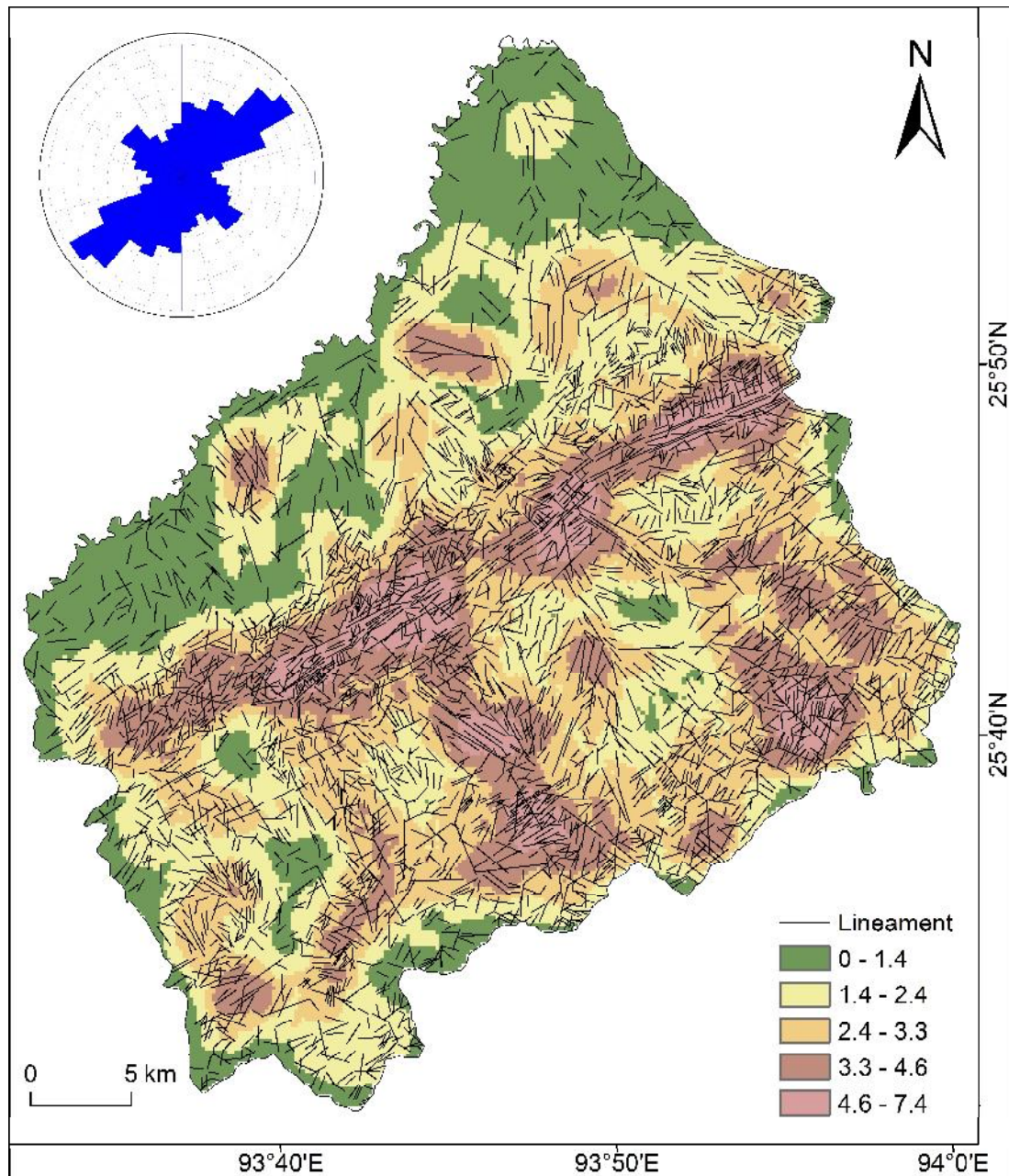


**Figure 5.3:** Lineament map of the study area showing prominent NE-SW and NW-SE trends; higher densities are noted in the thrust zones (modified after Moiya et al., 2019)

Along this fault a scarp, ~15-20 m in height, is observed. The Chathe Fault marks the boundary between the Quaternary Chathe alluvium and Dihing sediments at the north and the older Neogene rocks in the south. These Quaternary sediments have horizontal to sub-horizontal dips, which indicate that the Chathe Fault is a low angle, reverse fault. The Chathe Fault has affected the fluvial terraces as evident from field observations. This fault has truncated a strath terrace causing an elevation difference of about 10 m.



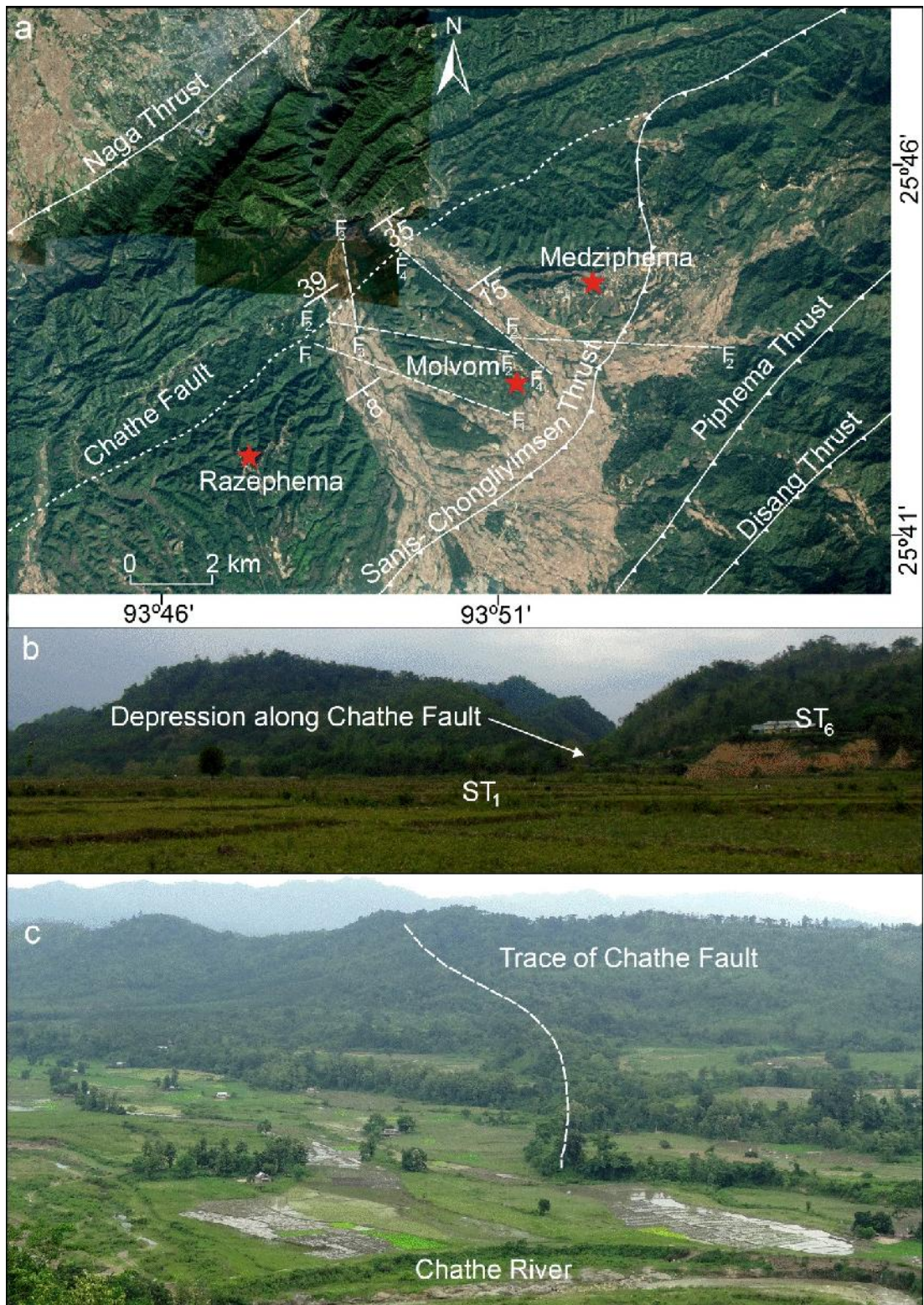


**Figure 5.4:** (a) Chathe Fault and local faults observed in the study area, (b) Depression along the Chathe Fault, (c) Trace of Chathe Fault (after Moiya et al., 2019)

Deformation due to normal faults is also observed within the Quaternary Chathe Alluvium. Besides, the Chathe Fault, four other local faults have been

identified from satellite imagery. These local faults designated F<sub>1</sub>, F<sub>2</sub>, F<sub>3</sub> and F<sub>4</sub>, trend NW-SE, WNW-ESE, N-S and NNW-SSW respectively (Fig. 5.4a). F<sub>1</sub> has caused an abrupt change in topography with the formation of steep fault scarps towards its southern extension (Fig. 5.4b, c). The development of a topographic high towards the north, a 10-m height difference between two levels of strath terraces, changes in the Chathe River course, presence of Chathe River palaeochannels along the downthrown block, and faulting of the bedrock and overlying sediments of the strath terraces are attributed to F<sub>1</sub> fault. F<sub>2</sub> has led to the development of a fault scarp, deformation of the Girujan bedrock due to faulting towards the western end of the fault, height difference of 9 m between the two levels of strath terraces and shift of the river course. The fault trace F<sub>3</sub> is ~2.3 km long with a 16-m fault scarp. It has affected the course of the Chathe River, as evident by the presence of N-S trending palaeochannels along the east of fault and forming the two levels of strath terraces. F<sub>4</sub> has caused the horizontal displacement of F<sub>2</sub> and a 23-m fault scarp, causing significant alteration in topography (Moiya et al., 2019).

#### **5.4 River anomalies**

Palaeochannels and abandoned channels are remnants of active stream channels that are indicative of fault movements associated with tectonics (Mathew, 2016). Abrupt change in flow direction, straightened river path, offset stream, river piracy/capture, etc. are anomalies that depict the control of structure and tectonics on drainage (Moiya et al., 2019).

About 4 km ENE of Razhephema, abandoned channels lying about 300-400 m SW of the present Chathe River, characterize the hanging valley (Fig. 5.5a). The development of such abandoned channels over the hanging valley is an outcome of terrain uplift related to tectonic movements. Two ephemeral streams east of the Chathe River, flow along a WNW direction (Fig. 5.5a). These ephemeral streams merge with the Chathe River further downstream. These streams are located on the broad intermontane valleys separated by three topographic highs (Fig. 5.5b). The topographic highs are enclosed by faults and linear structures. The sudden breaks in slope are due to down-cutting of the bedrock due to uplift of the intermontane basin (Fig. 5.5a, b). Normal faulting may be the reason for the breaks in the slopes. The valleys flanked by the highs are portrayed by single drainage order with high rate of



incision. The palaeochannels have migrated towards the southwest due to tilting of the terrain in recent times. The ongoing tectonic movements have rejuvenated these landforms (Moiya et al., 2019).

Towards the southwest of the Chathe River, two streams flowing towards the NNW and NNE (Fig. 5.5c) were demarcated from a topographic map of 1944 (surveyed 1921-23). These streams unite with the Chathe River further downstream. The SoI map of 1986 shows the southeastern NNW-flowing stream change course to merge directly with the Chathe River as result of stream capture. The Chathe River then shifts about 171 m towards the northeast (Fig. 5.5d). Stream piracy was caused by upliftment of the present topographic high near the western block of the NNW flowing river. From 1921 to 2017, there is a remarkable shift ranging from ~380 to 453 m along the flow path of the Chathe River (Moiya et al., 2019).

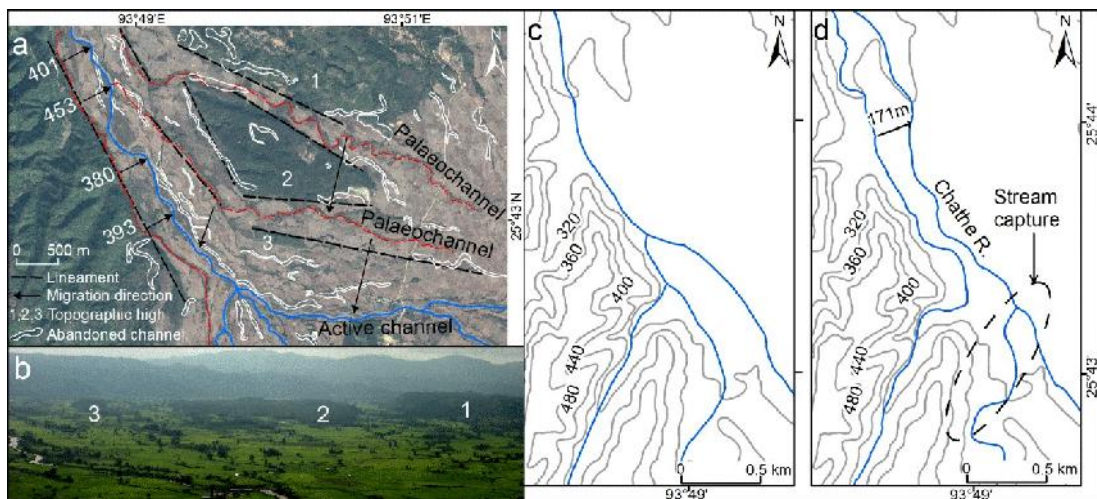


**Figure 5.5:** (a) Google Earth image showing palaeochannels, (b) Topographic highs - 1, 2, 3, (c) Chathe River course (1921-23), (d) Chathe River showing stream capture and migration (1982-83) (after Moiya et al., 2019)

## 5.5 Strath and valley-fill terraces

Valley-fill terraces and different levels of strath terraces are exposed within the Medziphema intermontane basin. The strath terraces are capped by the Chathe Alluvium. These terraces are good indicators of rivers being subjected to terrain uplift, which result in development of different levels of terraces. The displacement of sediments in the terraces that are affected by folding and faulting could act as a geomorphic marker to decipher neotectonic events (Molnar et al., 1994; Moiya et al., 2019).

### 5.5.1 Unpaired terraces

Location 1: In the Chathe River valley, six unpaired levels of strath terraces (Fig. 5.6a), ST<sub>1</sub> at 262 m, ST<sub>2</sub> at 263 m, ST<sub>4</sub> at 267 m and ST<sub>5</sub> at 278 m asl on the eastern bank (Fig. 5.6a1) and ST<sub>3</sub> at 266 m and ST<sub>6</sub> at 295 m asl on the western bank (Fig. 5.6a2) are observed. The present river channel has an elevation of 258 m asl. ST<sub>1</sub>, ST<sub>3</sub> and ST<sub>6</sub> are freshly exposed, consisting of Dihing bedrock which is overlain by the younger Chathe Alluvium. ST<sub>1</sub> is composed of 3.5-m-thick bedrock overlain by 1.5 m of Chathe Alluvium, ST<sub>3</sub> consists of 4.8-m-thick bedrock overlain by 3.2 m thick Chathe Alluvium, while ST<sub>6</sub> is about 35 m from the active river bed, consisting of Dihing bedrock overlain by 7.7 m thick Quaternary fluvial sediments. ST<sub>4</sub> and ST<sub>5</sub> are separated by 11 m steep scarp. Normal faults in the bedrock and the overlying sediments are observed in the freshly exposed ST<sub>6</sub> (Moiya et al., 2019).

Location 2: Unpaired strath terraces of six levels (Fig. 5.6b) are observed further downstream along the Chathe River valley. ST<sub>1</sub> at 256 m, ST<sub>2</sub> at 257 m, ST<sub>3</sub> at 258 m and ST<sub>5</sub> at 267 m asl along the eastern river bank (Fig. 5.6b1) and ST<sub>4</sub> at 261 m and ST<sub>6</sub> at 278 m asl along the western river bank (Fig. 5.6 b2) are seen, while the active channel bed is at 253 m asl. These strath terraces consist of Girujan bedrock that is capped by the Chathe Alluvium. ST<sub>1</sub> is about 3 m thick, being composed of bedrock of 2.3 m thickness and overlain by younger sediments of about 0.7 m in thickness. ST<sub>4</sub> of about 8.2 m consists of a 4.4-m- layer of bedrock capped by Chathe Alluvium of ~3.8 m thickness. ST<sub>6</sub> is about 24.4 m in height from the existing river bed and is composed of bedrock of thickness of ~16.6 m; this is overlain by a 7.8-m layer of fill sediments. ST<sub>3</sub> is separated from ST<sub>5</sub> by a sharp erosional scarp of ~9 m (Moiya et al., 2019).

Location 3: Two levels of unpaired strath terraces (Fig. 5.6c) ST<sub>1</sub> at 247 m asl along the western bank (Fig. 5.6c1) and ST<sub>2</sub> at 262 m asl on the east bank (Fig. 5.6c2) of the Chathe River are observed. The present river bed is at 246 m asl. In ST<sub>2</sub> the Tipam Sandstone of ~16 m thickness dips SE, which is overlain by the Chathe Alluvium of ~5.4 m thickness. Fault movement is obvious in the bedrock of ST<sub>2</sub>, (Fig. 5.6c3), where the eastern fault-block has moved upwards relative to the western downthrown block. Palaeochannel traces on ST<sub>2</sub>, along with N-S trending scarp, 2.4 km in length further adds evidences of fault movements (Moiya et al., 2019).

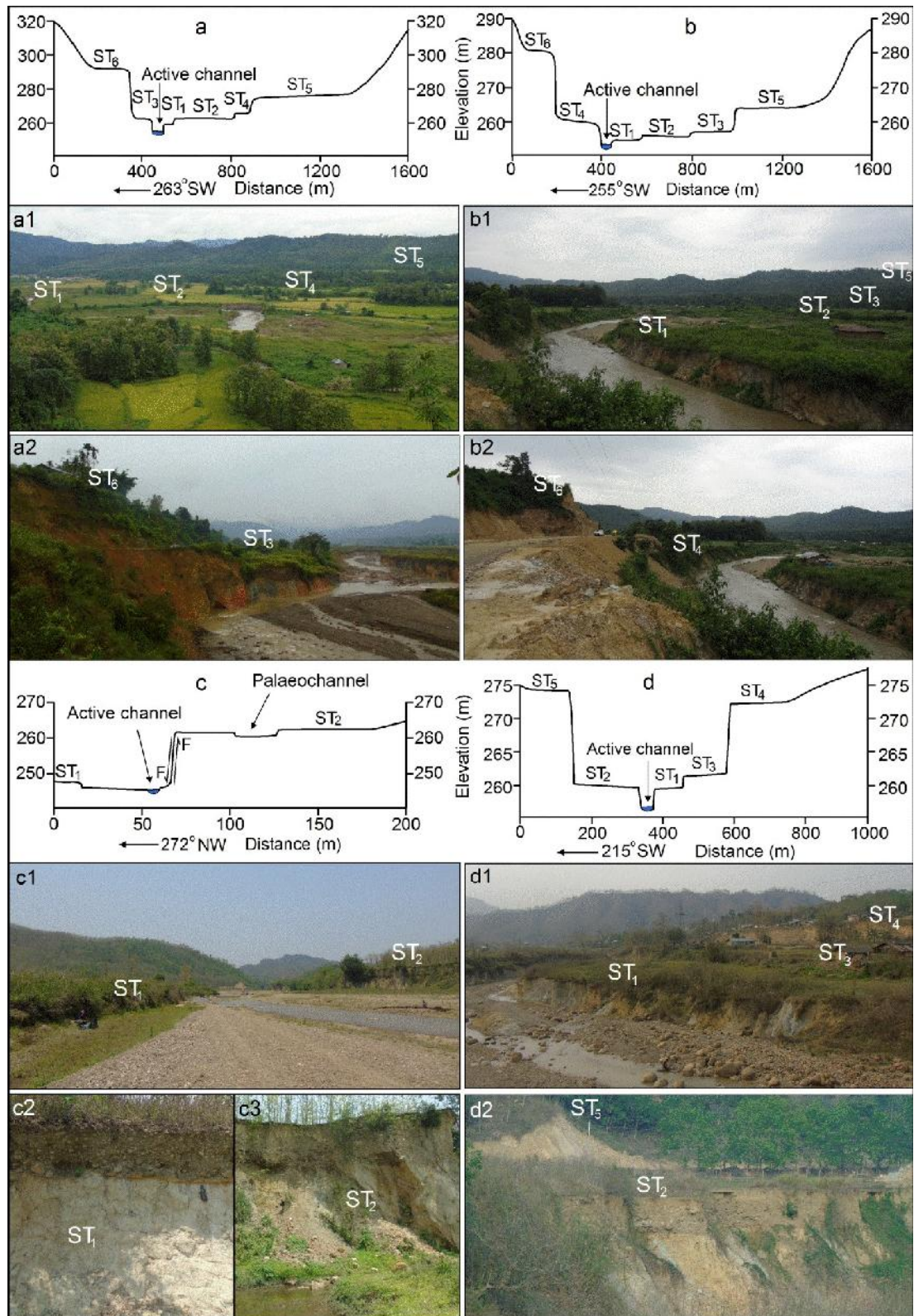


**Figure 5.6:** (a-d) Unpaired levels of strath terrace observed in the study area (modified after Moiya et al., 2019)

Location 4: Along the Jharnapani River valley, five unpaired levels of strath terraces are developed (Fig. 5.6d). The strath terraces composed of Girujan Clay Formation



bedrock with the younger Chathe Alluvium capping them. ST<sub>1</sub> at 258 m , ST<sub>3</sub> at 260 m and ST<sub>4</sub> at 270 m asl along the eastern bank (Fig. 5.6d1) and ST<sub>2</sub> at 259 m and ST<sub>5</sub> at 273 m asl along the western bank (Fig. 5.6d2) are observed. The active channel has an elevation of 252 m asl. In ST<sub>1</sub>, the bedrock is ~5.5 m, whereas the younger fluvial sediments are ~0.5 m. In ST<sub>2</sub>, ~7 m is made up of 5.5 m bedrock and 1.5 m of younger sediments. In ST<sub>4</sub>, ~18 m from the present river channel, the bedrock of the Girujan Formation displays an angular unconformity with the overlying fill sediments. The bedrock and the overlying fluvial sediments are affected by later phases of deformation, as evident from numerous faults in the bedrock and overlying sediments (Moiya et al., 2019).

### 5.5.2 Faulted terraces

Location 1: Along the Tomma stream near the Sanis-Chongliyimsen Thrust (25°44'30.13"N / 93°54'04.71"E), a terrace deposit, ~4 m thick, at an altitude of 385 m asl is observed northeast of Sirhima village. The terrace deposit is made up of gravel in a sand-mud matrix overlying the bedrock of Jenam sandstone. The bedrock is sheared and fractured, dipping 52° towards 112° SE. The Jenam sandstone and the overlying fluvial sediments are affected by normal faulting, which have been displaced ~2 m (Fig. 5.7) (Moiya et al., 2019)



**Figure 5.7:** Fault-displaced Quaternary sediments near Sanis-Chongliyimsen Thrust (after Moiya et al., 2019)



Location 2: At 25°44'28.76"N / 93°48'21.38"E, towards Razephema, bedrock of the Dihing Formation and overlying Quaternary sediments have been affected by numerous faults (Fig. 5.8a). The Dihing bedrock and overlying younger Chathe Alluvium composed of boulders, pebbles, sand and silt are dislocated by a normal fault (Fig. 5.8b, c). From the sense of movement, as observed at the outcrop, they are mainly normal faults (Fig. 5.8d). Imbricate pebbles within the Dihing bed dip 31° towards SW (Fig. 5.8e). At 25°44'28.66"N / 93°48'21.18"E, the Dihing bed and overlying sediments of the Chathe Alluvium are affected by a normal fault. The fault plane dips 63° toward SSW with a displacement of about 1.8 m (Moiya et al., 2019).

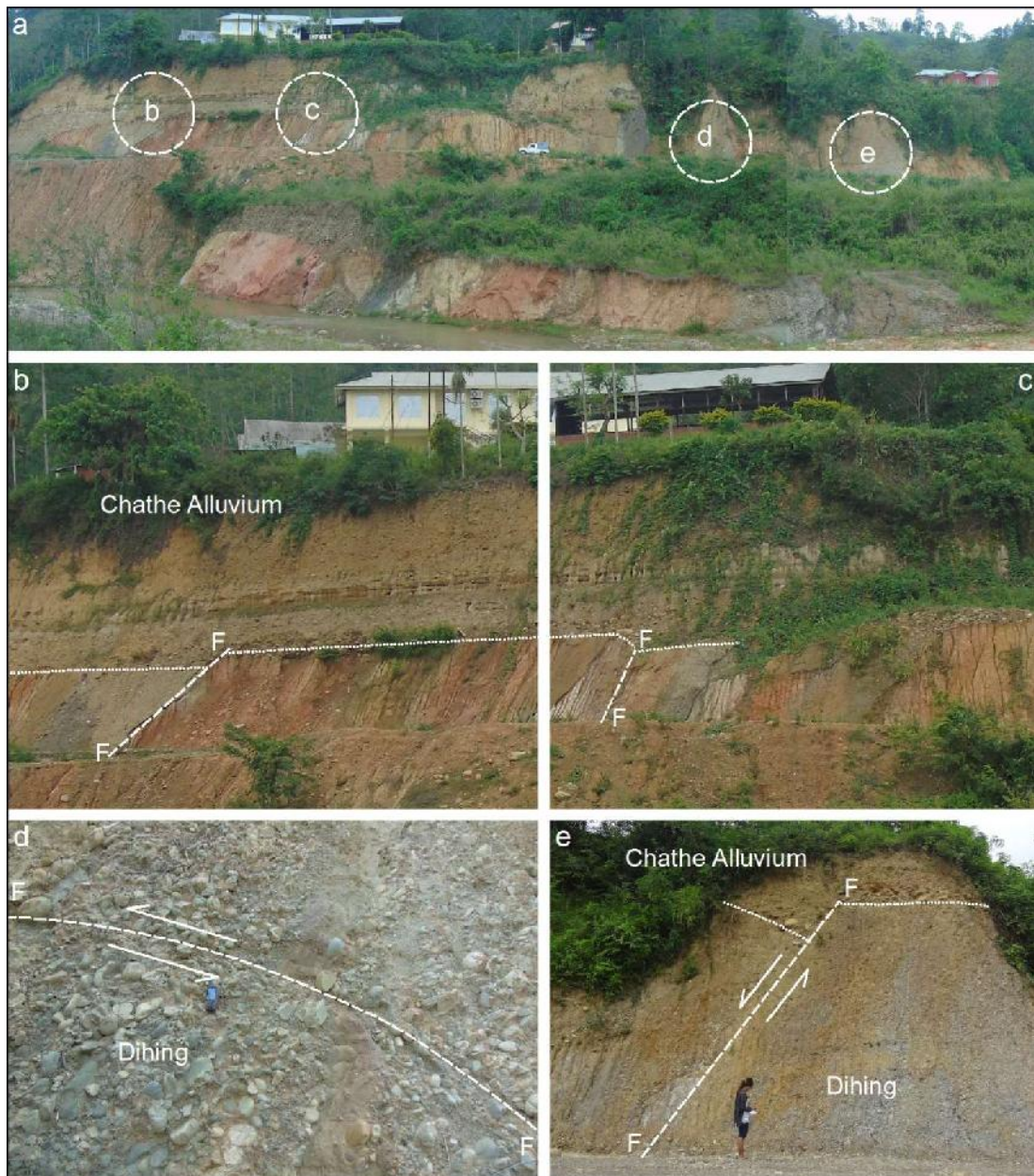


**Figure 5.8:** (a) Strath terraces along the Chathe River, (b, c) Chathe Alluvium and Dihing displaced by normal fault, (d) Faulting within Dihing, (e) Normal fault dislocating Dihing and overlying Chathe Alluvium (after Moiya et al., 2019)

Location 3: Evidences of fault movements are exposed at different outcrops (Fig. 5.9a) near Kukidolong. Girujan bedrock as well as Chathe Alluvium have been affected by a normal fault; the throw varies from 0.8 to >1 m (Fig. 5.9b, c) and dip ranges from 40°-45° towards the southeast. Chathe Alluvium, lying on the footwall block of these faults, is tilted 18°-20° towards SE (Fig. 5.9b, c) ) (Moiya et al., 2019).



**Figure 5.9:** (a) Displacements at various locations of the strath terrace along AH1 (b) Numerous faults dislocating the bedrock and younger sediments (c) Fault observed in the Girujan bedrock with displacement extending into the overlying Chathe Alluvium) (after Moiya et al., 2019)

Location 4: On the western bank of the Chathe River (25°45'18.8"N / 93°48'32.9"E), a terrace deposit, ~2 m thick, at an elevation of 254 m asl is observed. The terrace deposit includes boulders at the bottom followed upward by cobbles and pebbles in matrix of sand and silt; the upper layer is made up of intercalations of sand and silt measuring 5-15 cm (Moiya et al., 2019). The silty layers have been eroded to form small, horizontal caves due to differential erosion. A normal fault, about 45°, has dislocated the layers by about 1.3 m (Fig. 5.10).



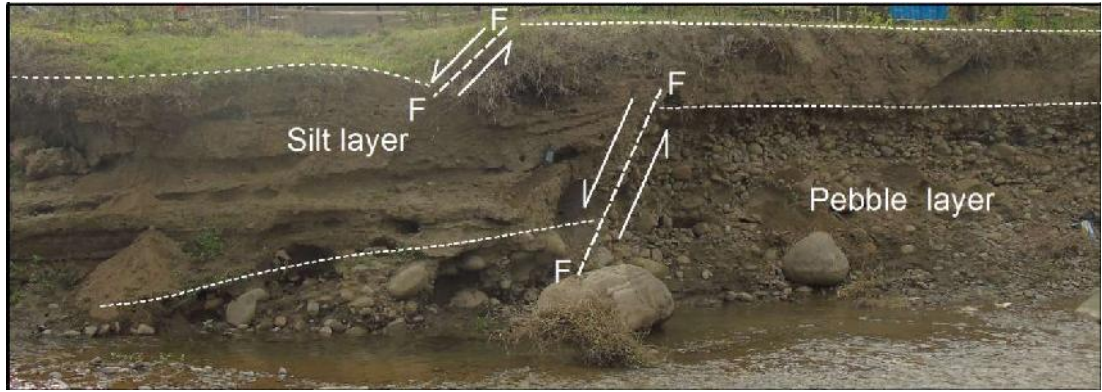


**Figure 5.10:** Fill terrace displaced by normal fault along the Chathe River (after Moiya et al., 2019)

Location 5: At the periphery of the Yah Thrust, along the Bara Manglu stream, bedrock of the Jenam Formation, ~3 m thick, are overlain by younger Quaternary fluvial sediments of ~3 m thickness. The Jenam bedrock is highly sheared and folded, dipping  $18^{\circ}$ - $41^{\circ}$  WNW. A normal fault has affected the Jenam bedrock, where the displacement is almost ~0.5 m (Fig. 5.11).



**Figure 5.11:** Displacement of Jenam bedrock and overlying fluvial deposits

### 5.5.3 Folded terraces

Location 1: Along western bank of the Bara Manglu stream, three levels of strath terraces are observed, with Jenam bedrock overlain by younger Quaternary sediments. Two phases of tectonic activity are discernable near the Yah Thrust zone, 6 km NW



of Peren (Fig. 5.12a). The morphotectonic features are evident from the presence of multiple levels of strath terraces; slickenside is noted on the bedrock. The first phase took place after deposition of a 2.5-m thick fluvial sediment layer (ST<sub>2</sub>) that was uplifted almost 2.5 m.

The second took place after deposition of ~0.5 m of fluvial sediments (ST<sub>1</sub>) and uplift of about 0.5 m. ST<sub>2</sub> is truncated at two levels as ST<sub>1a</sub> and ST<sub>1b</sub>. The Jenam bedrocks are intensely sheared in the fault zone (Fig. 5.12b). The presence of slickenside indicates the geometry of the fault. The fault appears to be a reverse fault (Fig. 5.12c).



**Figure 5.12:** (a) Three levels of strath terraces along the bank of Bara Manglu River, (b) Folded Jenam bedrock affected by normal fault, (c) Slickenside on bedrock

Location 2: Near the Naga Thrust zone, younger fluvial sediments consisting of a 3.5-m thick layer of gravel and sand overlies bedrock Surma. The bedrock and the sediments are folded. The limbs of the fold dip towards NW and SE, as a result of which the bedrock and gravel beds lean moderately towards the axial hinge of the fold (Moiya et al., 2019). The gravel is seen to be aligned toward the limbs but randomly



arranged along the hinge (Fig. 5.13a). Two conjugate shear planes observed along this section may be part of the Naga Thrust (Fig. 5.13b).

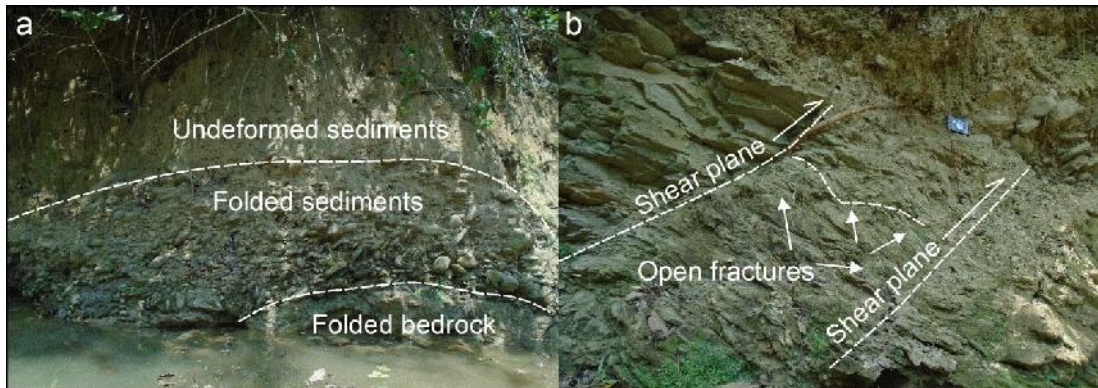


**Figure 5.13:** (a) Folded bedrock and sediments, (b) Sheared sandstone bed exposed near Naga Thrust zone (after Moiya et al., 2019)

#### 5.5.4 Tilted terraces

Location 1: At location 25°46'28.9" / 93°48'15", along the AH1, fluvial sediments are observed over the Tipam Sandstone at an altitude of 229 m asl. These sediments, made up of boulders, pebbles and layers of sand lens, are tilted 32° ESE (Fig. 5.14).



**Figure 5.14:** Tilted terrace observed along the AH1 (after Moiya et al., 2019)

Location 2: At 25°40'59.7" / 93°40'19.8", the Chathe Alluvium of ~3 m thick is seen along the Langlong River bank. The active river bed has an elevation of 238 m asl. Pebbles of the Chathe Alluvium are tilted 21° SW (Fig. 5.15).



**Figure 5.15:** Tilted sediments along Langlong River

## 5.6 Folded mountain front

The NE-SW mountain front, has taken a N-S bend near Hovishe, towards the northeast end of the present investigated area (Fig. 5.16a). As observed on LISS III and Google Earth images, and topographic map, this region is defined by a swing in the mountain front trend, in the form of localized syntaxial bend. This curved mountain front is probably a result of the subsurface indentation of the Mikir Hills obliquely into the Naga Hills. Moiya et al. (2019) have designated this feature the Yampha Bend. Such localized syntaxial bends are also developed in the mountain front of Tanakpur (Kumaun Himalaya) caused by displacement of the Moradabad Fault into the Himalaya (Luirei et al., 2017). A similar swing in strike of the mountain front is also observed at Laldhang, near Kodtwar in the sub-Himalaya; it is thought to be due to subsurface indentation of the basement ridge. This Yampha Bend has influenced the southwesterly-flowing Yampha River to flow northward; the hanging wall block of the Naga Thrust caused the Nra River to take a curved path. This phase of tectonic activity is younger than the initiation of the Naga Thrust and the other thrusts of the BoS (Moiya et al., 2019).

A terrace deposit composed of Quaternary fluvial sediments overlying the Upper Bhuban bedrock is observed in this area. The pebbles are tilted 28° SE. The bedrock dips 40°-46° SE. Two sets of joints are observed in the bedrock dipping 69°



towards 5° NNW and 4° toward 214°SW (Fig. 5.16b). The tilted terrace deposits indicate tectonic uplift along the Naga Thrust after the deposition of the fluvial fill terrace.

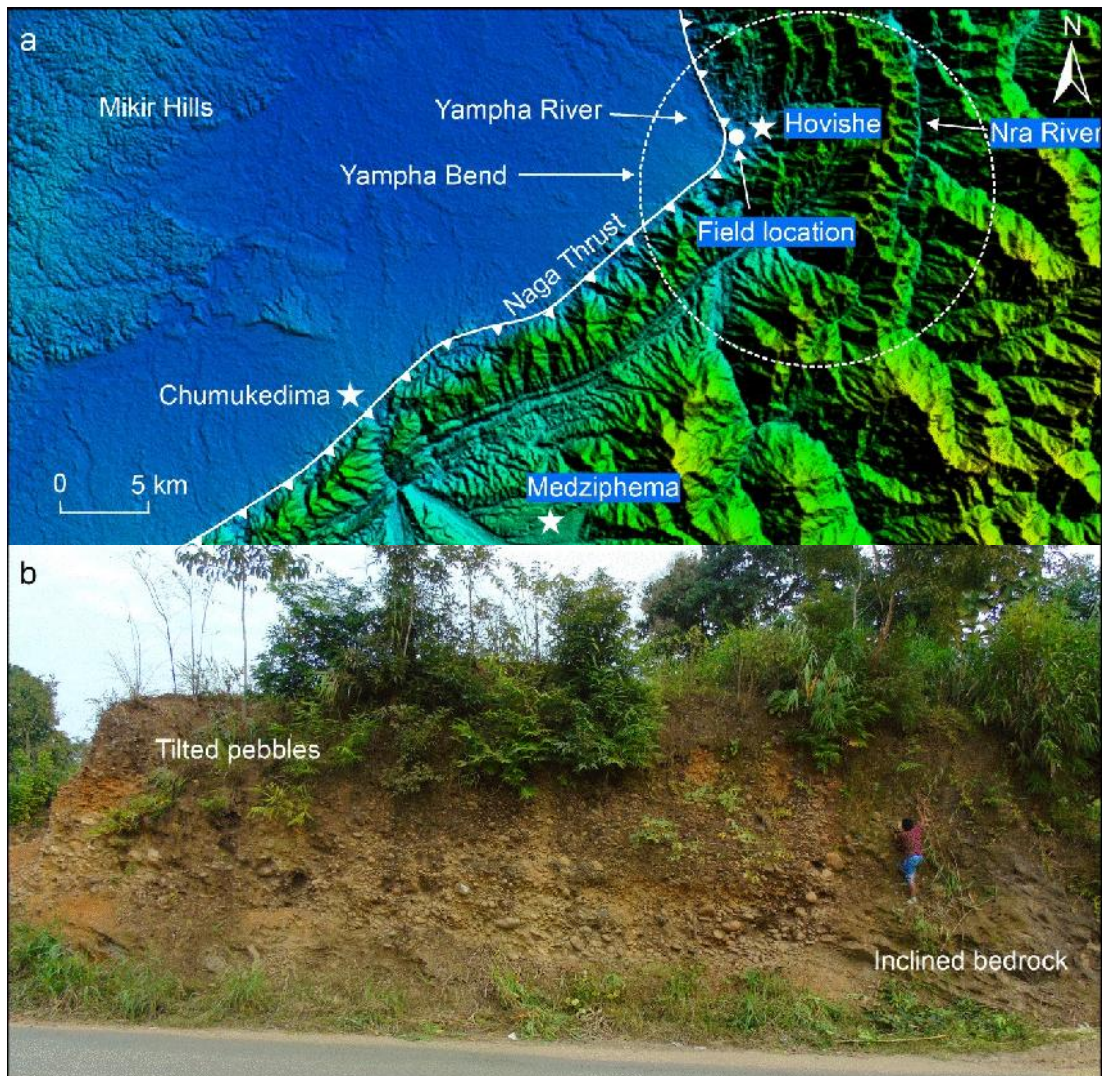


**Figure 5.16** (a) Folded mountain front) (b) Inclined Surma bedrock with tilted pebbles (modified after Moiya et al., 2019)

## 5.7 Topographic profiles

One longitudinal and four transverse topographic profiles have been prepared to decipher the evolution of intermontane basins formed as a result of uplift. The transverse profiles are oriented NW to SE while the single longitudinal profile is NE-SW.

The profile a-a' (Fig. 5.17a) along the thrusts of the study area shows the development of two depressions separated by the hills of Razephema (Fig. 5.17b).

The two depressions are designated the Jalukie intermontane basin and the Medziphema intermontane basin. The Jalukie intermontane basin is drained by the Bara Manglu (322 m asl) and Langlong (358 m asl) rivers while the Medziphema intermontane basin is drained by the Chathe (320 m asl) and Jharnapani rivers (400 m asl), respectively (Fig. 5.17c). In the profiles the intermontane basin valleys are defined by very broad depressions bounded by higher elevations on either side of the depressions.

Profile b-b' (Fig. 5.17a) shows an increase in elevation from 225 m to 317 m asl as it passes through the Naga Thrust at ~0.8 km. There is increase in elevation from 320 m to 387 m asl as it encounters an anticline ~1.74 km from the Naga Thrust. After ~4.42 km from the anticline, the elevation increases from 320 m to 420 m asl near the Chathe Fault. For about the next 5 km, the profile portrays a smooth topography with U-shaped valleys, which is the Jalukie intermontane basin at a maximum elevation of 380 m asl. As the profile nears the southern zone, the elevation rises up from 375 to more than 523 m asl as the Disang Thrust is encountered at ~6.3 km from the Chathe Fault (Fig. 5.17c).

Similarly, along profile c-c' (Fig. 5.17a) across the Jalukie intermontane basin, the elevation increases from 208 m to 280 m asl, as the Naga Thrust is encountered ~0.5 km from the north. The elevation drops to 260 m asl, but after ~2 km, as it encounters an anticline, the elevation increases from 260 m to nearly 380 m asl and thereafter drops to 320 m asl. After ~2.36 km, as it passes the Chathe Fault, the elevation abruptly increases from 320 m to 370 m asl. The intermontane basin is signified by broad topography, with elevations ranging from 320 m to 400 m asl. Towards the south, an altitude difference of more than 100 m is observed across the Disang Thrust, where the elevation increases from 400 m to 520 m asl. After ~0.73 km from the Disang Thrust, the Yah Thrust is encountered, where the elevation is above 599 m asl (Fig. 5.17c).

Profile d-d' (Fig. 5.17a) shows an abrupt elevation increase from 190 m to 260 m asl along the Naga Thrust at ~1.2 km. After ~0.98 km the elevation increases up to 760 m asl as it encounters the growing anticline. In the intermontane section the elevation drops down to nearly 260 m asl but again gain heights along the Chathe Fault at ~6.3 km from the Brahmaputra plain. The elevation of the Medziphema



intermontane basin is ~270 m asl, which increases after passing the Sanis-Chongliyimsen Thrust (Fig. 5.17c).

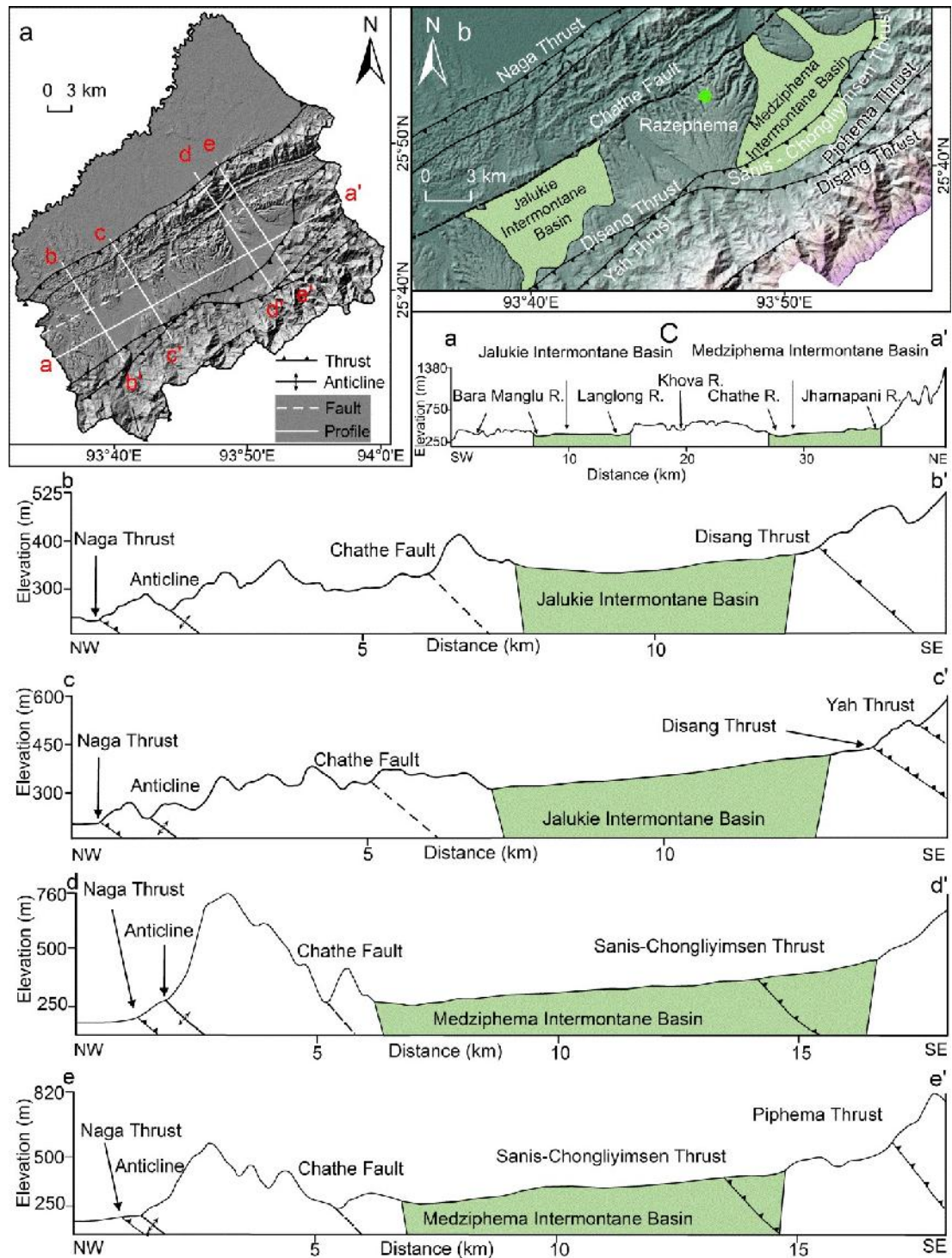


**Figure 5.17:** (a) Cross-sections, (b) Development of two intermontane basins within BoS, (c) Topographic profiles sections a-a', b-b', c-c', d-d' and e-e'

In profile e-e' (Fig. 5.17a), at ~0.5 km, it passes across the Naga Thrust where the elevation increases slightly from 181 m to 200 m asl; after ~0.15 km a V-shaped valley profile is observed as it passes the growing anticline where the elevation rises to more than 600 m asl and then drops down to 200 m asl. After a distance of ~6.2 km from the anticline, the elevation rises to about 300 m asl in the Chathe Fault zone. The profile section displays broad valleys representing the Medziphema intermontane basin with elevations between 300 and 400 m asl. The height slightly increases across the Sanis-Chongliyiimsen Thrust. The profile cuts across the Piphema Thrust at ~3.5 km from the Sanis-Chongliyiimsen Thrust where the elevation increases from 600 m to 800 m asl in the 17 km long profile (Fig. 5.17c).

The four transverse topographic profile sections show very slight increase in elevation near the Naga Thrust and but rise sharply on encountering the anticline and the Chathe Fault. This is similar to the longitudinal profile, stream length gradient index and steepness index of the Bara Manglu, Chathe and Jharnapani rivers, where prominent knickpoints and high value of  $k_s$  and SL with sharp peaks are observed. The low elevation in the Naga Thrust zone may be because this is a blind fault that is hidden below the surface. Even evidence of the Naga Thrust is not clear in the field. However, at the Langlong River, prominent knickpoints are noted in the Naga Thrust zone; the thrust may be exposed at the surface along this section.

## **5.8 Evolution of intermontane basins**

The Medziphema intermontane basin (Aier et al., 2011) and Jalukie intermontane basin (Jalukie intermountain valley of Madhav, 1989) are part of the BoS (Fig. 5.18). This region is considered to be part of a very complex structural setting that is affected by various tectonic phases associated with post-depositional tectogenesis (Roy and Kacker, 1982, 1986; Ranga Rao and Samanta, 1987). The sedimentary rocks have undergone vigorous tectonic deformations. The intermontane basins of the BoS owe their development to Pliocene-Quaternary movements. The Medziphema intermontane basin, with an area of ~55 km<sup>2</sup>, is ~14 km in length and ~9 km in width. It is bounded by high hills. Structurally, it is enclosed by the Naga Thrust in the northwest and Sanis-Chongliyiimsen in the southwest (Aier et al., 2011). The Jalukie intermontane basin is ~11 km in length and ~6.5 km in width, with an area of ~42 km<sup>2</sup>; it is surrounded by the Naga Thrust in the northwest and Disang Thrust in the

southeast (Fig. 5.18). Aier et al. (2011) compared the broad intermontane valleys of the BoS to the Doons of the Western Himalaya. In both cases, the valleys are bounded by regional thrust systems. The Disang Thrust, Sanis-Chongliyimsen Thrust and Naga Thrust surrounding the intermontane basins were propagated during Late Miocene-Pliocene (Roy and Kacker, 1982).

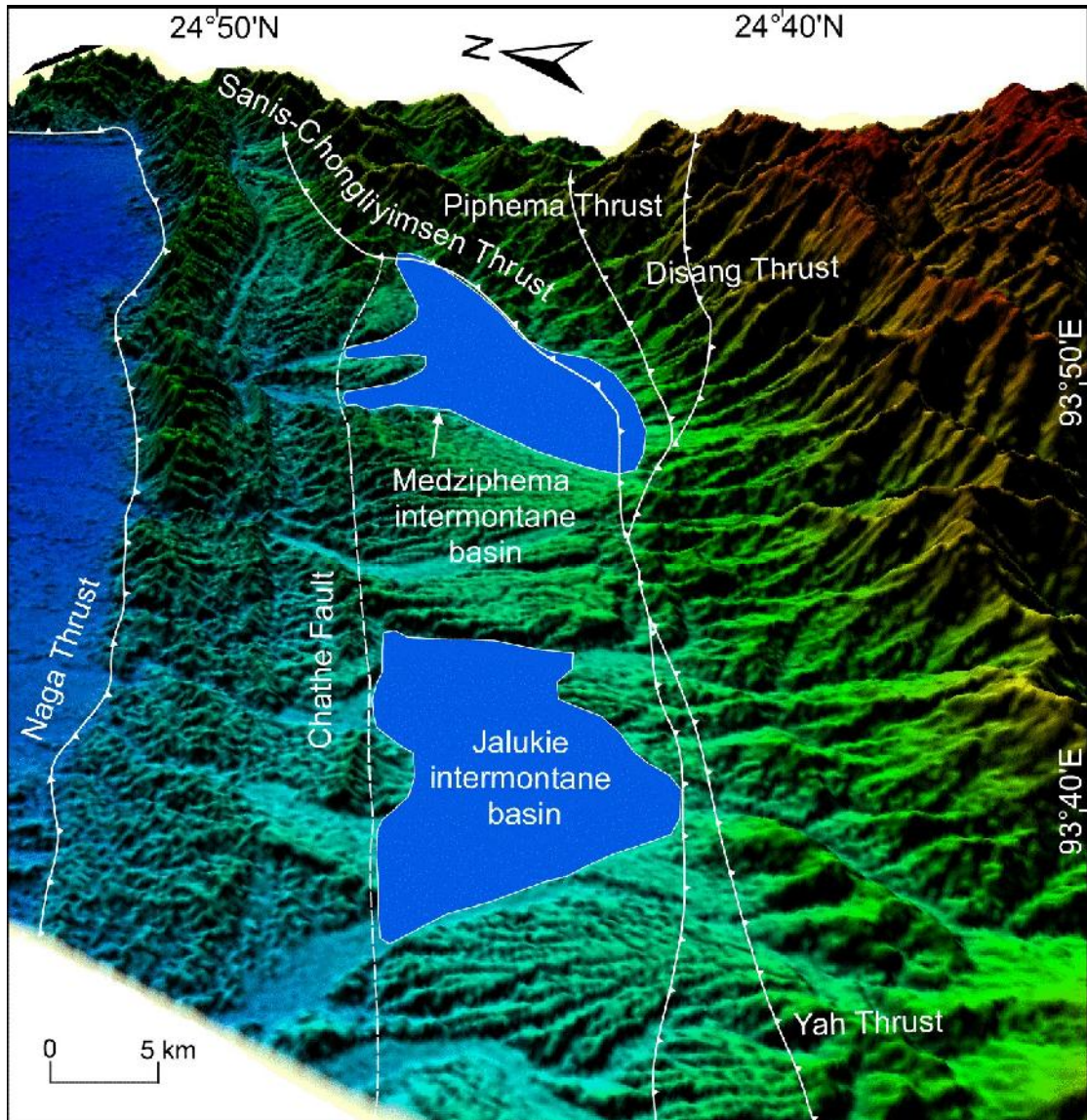


**Figure 5.18:** Development of Medziphema and Jalukie intermontane basins within the thrust plane of the BoS

The thrust planes surrounding the basins emerged during the later phase of collision between the Indian and Burma plates, when they were immensely uplifted (Roy and Kacker, 1982). The Naga Thrust, which represents the frontal thrust of the BoS, was subjected to three phases of deformations (Kent and Dasgupta 2004). Aier

et al. (2011) attribute the evolution of the intermontane basins to the third phase of deformation. Ranga Rao and Murthy (1980) opine that the Naga Thrust is a decollement plane, being deformed over several stages. During the Pliocene-Quaternary plate convergence, tensional and vertical movements occurred, creating several horst-and-graben structures in the Naga Hills (Roy and Kacker, 1982). Block faulting in the Medziphema intermontane basin is a result of Pliocene-Quaternary movements (Roy and Kacker, 1982). The basin, composed of Plio-Pleistocene and Holocene sediments, was formed with the Mio-Pliocene horst in the northwest and Upper Eocene-Oligocene horst in the south east. Tectonic modification is still continuing as the thrust planes of the BoS are being propagated towards the northwest, as evident from the development of the Jorhat Fault (Bezbarauh et al., 2016). In the Naga Thrust zone, folding and faulting of Quaternary sediments along with the bedrock, tilting of terrace sediments and realignment of Quaternary fluvial sediments by two shear planes confirms that the Naga Thrust is tectonically active. The sub-horizontal stratification of Quaternary sediments in the intermontane basin suggests vertical uplift, which is responsible for shaping the tectonic terrain. The intermontane basins in the study area are tectono-geomorphic landforms that have evolved from neotectonic activity as a result of uplift due to folding, faulting and thrusting. Similar Quaternary intermontane basins have evolved from different phases of tectonic movements in the Cassino intermontane basin in the Central Apennines of Italy (Saroli et al., 2019).



## CHAPTER: 6

### **OPTICAL CHRONOLOGY AND TIMING OF FLUVIAL AGGRADATION**

Luminescence dating is a tool of absolute chronology to find depositional ages of fine-grained sediments (Sohbati, 2013). Dating of sediments is considered to be an essential tool for active tectonics investigation. Absolute dating of sediments involved in active faulting and folding could establish a well defined chronology (Keller and Rockwell, 1984). Luminescence dating involves thermoluminescence and optical dating techniques. In thermoluminescence (TL) dating, the mineral grains are heated prior to measurements (Aitken, 1985) while optical dating involves exposing to a light source to eradicate charge from light sensitive charge (Huntley et al., 1985). For the present study, the OSL technique is utilized for dating of the samples to quantify the Quaternary neotectonic processes. Huntley et al. (1985) developed the OSL sediment dating technique owing to its extra sensitivity to light as compared to thermoluminescence signals (Wallinga et al., 2007). This method has been extensively used to date fluvial sediments with time of deposition ranging from a few tens to hundreds of years (Alappat, 2011). OSL dating has become the preferred technique in finding the burial age of sediments because of the abundance of quartz and feldspar in soft sedimentary terrain. Moreover, it provides accurate results (Murray and Olley, 2002; Wallinga et al., 2007).

The OSL dating method is quite similar to fission track dating of radioactive damage techniques, which includes four major procedures: a) elimination of charge trapped in the mineral grains through exposure to daylight during transfer, b) steady increase of charge as buried grains are exposed to natural radiations, c) gathering of samples and measuring the OSL the concentration of trapped charge and d) determining the dose rate inflicted on grains at the location of the sample. The method helps uncover the processes of the earth's surface. OSL is extraordinarily sensitive to conditions of the environment such as, signal deletion by natural light or heating from 200°C to 400°C. In addition, the minerals such as quartz and feldspar that are often used for OSL are abundant on the earth's surface. As long as the age varies between less than a century to more than a hundred thousand years and with indication that the

upper limit will extend by a certain order of magnitude, the method will help fill gaps between observational processes and events. This technique is preferred over dating methods such as radiocarbon, uranium series and cosmogenic nuclide.

Luminescence-dating consists of TL (Aitken, 1985), where grains are continuously heated during optical dating (Huntley et al. 1985; Aitken, 1998). Here, samples are exposed to intense light sources to remove charges from light-sensitive traps. The OSL signals of quartz (Smith et al., 1986) or feldspar (Godfrey-Smith et al. 1988) are utilised for optical dating or infrared stimulated luminescence of feldspar (Hütt et al., 1988). Using a variety of stimulation wavelengths, minerals, grain sizes and measurement procedures, the techniques can be puzzling. Nevertheless, one measurement protocol, known as the quartz OSL single aliquot regenerative dose (SAR) protocol of Murray and Wintle (2000, 2003) stands out due to its obvious accuracy and reliability (Murray and Olley, 2002; Rhodes et al., 2003).

Measuring the brightness of luminescence signals is considered for calculating the amount of radiation the sample was exposed to through the period of burial (Fig. 6.1). The age is calculated as follows:

Gray (Gy) is the SI unit of absorbed radiation. It measures the amount of energy absorbed by one kilogram of the sample and is expressed as joules per kilogram (Jkg<sup>-1</sup>).

## **6.1 Applications**

OSL has an extensive range spread over a few decades. Application began for archaeological and eolian problems (Rhodes, 1988; Smith et al., 1990) and was extended for the fluvial and glaciogenic environments (Perkins and Rhodes 1994; Owen et al., 1997). OSL applications cover a wide range of environments (Table 6.1). Positive reviews along with specific environments have been constructed for the fluvial environment and for neotectonism by Rittenour (2008) and for glaciogenic sediments (Fuchs and Owen, 2008). A resolution of  $\pm 5$  to 10% at  $1\sigma$ , with a range of 1 to ~200,000 years render OSL suitable for Holocene events on timescales of hundreds to thousands of years. The advantage of OSL dating of sediments over other techniques is that zeroing-in on to the target bears a direct relation with the depositional event as the material is the sediment itself.

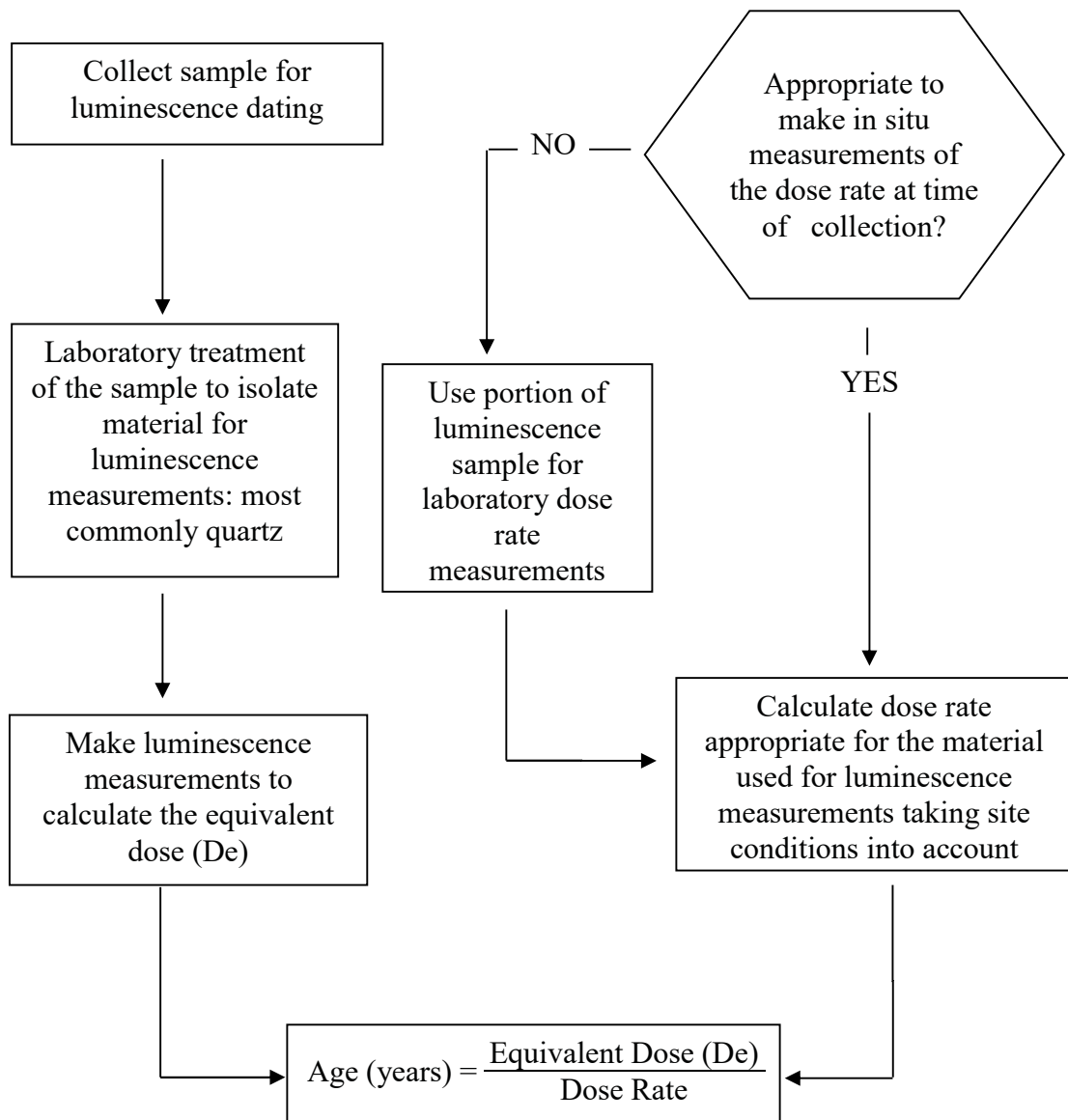


**Figure 6.1:** Flow chart for procedure to measure De (left) and the dose rate (right), are combined to calculate a luminescence age

**Table 6.1:** Application in sedimentary environments for OSL dating

Applications	Comment	Context
Tectonic and palaeoseismic	Relatively recently applied	Marine, fluvial, lacustrine, slope deposits
Palaeoclimatic and paleoenvironmental	Now widely used	Wide range of sediments
Geomorphic and Quaternary	Now widely used	Wide range of sediments
Environmental and process studies	Relatively recently applied	Soils, fluvial, potential for wider range
Archeological and paleoanthropological	Now widely used	Fluvial, colluvial, soils, heated/fired materials
Environments		
Eolian (wind transported)	Usually successful	Sand dunes, loess

Fluvial, alluvial, lacustrine (water lain)	Zeroing can be problematic	River terraces, alluvial fans, flood plains, lakes
Marine: coastal and offshore	Zeroing issue in deep water	Raised beaches, beach ridges, deep water
Glacigenic	Zeroing and characteristics can be problematic	Moraine and till, outwash, glacio-marine
Slope deposits	Zeroing and characteristics can be problematic	Colluvium, rockfall, debris flows
Caves (karstic)	Zeroing can be problematic	Shallow caves sediments, sands and silts
Anthropomorphic	Zeroing can be problematic	Artificial fill, anthropomorphic soils
Volcanic rocks, precipitation	Characteristics are often problematic	Opal, biogenic opal, phenocrysts, xenocrysts
Soils	Grain movement studies	Modern, compound and buried soils
Heated materials	Usually successful	Ceramics, wild fires, thermochronology
Strained and shocked materials	Little research to date	Impact craters, fault movement

## 6.2 Mechanism

OSL enables an inference of time elapsed from the time when the buried crystallized grains were previously exposed to natural light. This method involves utilization of optically and thermally sensitive light or luminescence signals trapped in mineral grains. Luminescence signals trapped within the grains are erased when exposed to light (Murray and Olley, 2002; Preusser et al., 2008). Once the grains are concealed from daylight and remain at normal temperatures, the luminescence signal begins to accumulate again due to presence of naturally occurring radionuclides in the deposits (Murray and Olley, 2002; Wallinga et al., 2007; Preusser et al., 2008).

## 6.3 Single aliquot regenerative dose

The palaeodose is determined using multiple aliquot (MA), single aliquot (SA) or single grain (SG) methods. The single aliquot regenerative dose (SAR) (Murray and Wintle (2000) has become a reliable method for heated and unheated quartz grains to determine the quartz equivalent dose, where luminescence-sensitive changes are examined and corrections made (Murray and Olley, 2002; Wintle and Murray, 2006; Wallinga et al., 2007; Duller, 2008). The SAR method involves quality control tests for obtaining accurate ages (Roy, 2013). The mineral-grain contaminations are further



checked for purity. Optical dating of feldspar known as IRSL (Wallinga et al., 2007) tends to stimulate luminescence in feldspars whereas quartz does not respond (Hütt and Jaek, 1989), which helps in separation of quartz from feldspar contamination (Preusser et al., 2008).

#### **6.4 Bleaching**

Bleaching, also known as zeroing of the trapped charged population is eliminated by light. This mechanism is important as sometimes samples are subjected to bedrock erosion or transportation, which exposes mineral grains to light. As a result, these grains get depleted of previously absorbed signals leading to extensive bleaching (Allapat, 2011). This phenomenon enabled Huntley et al. (1985) to develop optical dating techniques, a useful approach in the study of bleaching and depositional conditions of sediments. Bleaching is carried out by two methods. The first method involves isolation of most bleached parts in the luminescence signal to separate multiple components (Tsukamoto et al., 2003, Allapat, 2011) while the second method involves decreasing the number of grain in each aliquot (Olley et al., 1998) or by single grain techniques (Duller, 2008; Allapat, 2011). After completely bleaching the sediments, the OSL signal is calculated (Allapat, 2011).

#### **6.5 Measurement of equivalent dose**

Mineral grains acquired from the sample are exposed to photons of specific energy range to obtain decay curves of OSL or IRSL intensity versus stimulation time (Roy, 2013). The mineral-grain response to the artificially induced known dose (regenerative dose) is calculated. Thus, the total observed energy since burial (palaeodose) is estimated from these calculated measurements and natural signals of the mineral grain. Palaeodose estimation in the laboratory is known as equivalent dose (De), which generates identical amounts of natural OSL signals in the sample (Allapat, 2011).

#### **6.6 Determining the dose rate**

Dose rate of a sample consists of alpha, beta and gamma radiations and cosmic ray component. These radiations owe their origin to radioactive decay of uranium and thorium. These radionuclides are responsible for the naturally occurring radioactivity in samples (Allapat, 2011), which can be estimated by a different range of methods

such as, ICP-MS, XRF, NAA and high-resolution gamma-ray spectrometry (Wallinga et al., 2007). The radiations absorbed by mineral grains rely on the presence of water and organic substances as they draw radiations that decrease the effective dose rate (Aitken, 1985; Wallinga et al., 2007). A difference of 1% in water or organic contents causes an effect of ~1% on the natural dose rate of a sample, which will ultimately affect the luminescence age. Therefore, water or organic content should not go beyond 20% by weight, to acquire the luminescence age (Wallinga et al., 2007).

## 6.7 Dating results

OSL samples were collected within the intermontane basins of the BoS (Fig. 6.2). Eleven samples from the overlying fluvial terraces were dated; their ages and dosimetry data are shown in Table 6.2. The samples JNM-1 to JNM-7 were collected from distances of 16, 13.7, 1, 0.8, 26.6, 7.2, and 0.3 m respectively above the active river bed, while samples JNM-9, JNM-10, JNM-13 and JNM-14 were obtained from 1.92, 0.97, 21.4 and 7.42 m respectively above the present river bed. OSL ages obtained from samples JNM-1 to JNM-7 are  $7\pm0.7$  ka,  $11\pm1.2$  ka,  $3.4\pm0.6$  ka,  $2.9\pm0.3$  ka,  $9.3\pm0.7$  ka,  $1.8\pm0.2$  ka and  $20\pm1.5$  ka respectively, while samples JNM-9, JNM-10, JNM-13 and JNM-14 yielded ages of  $20\pm1.7$  ka,  $21.1\pm1.8$  ka,  $5.8\pm0.4$  ka and  $6.5\pm0.6$  ka respectively.

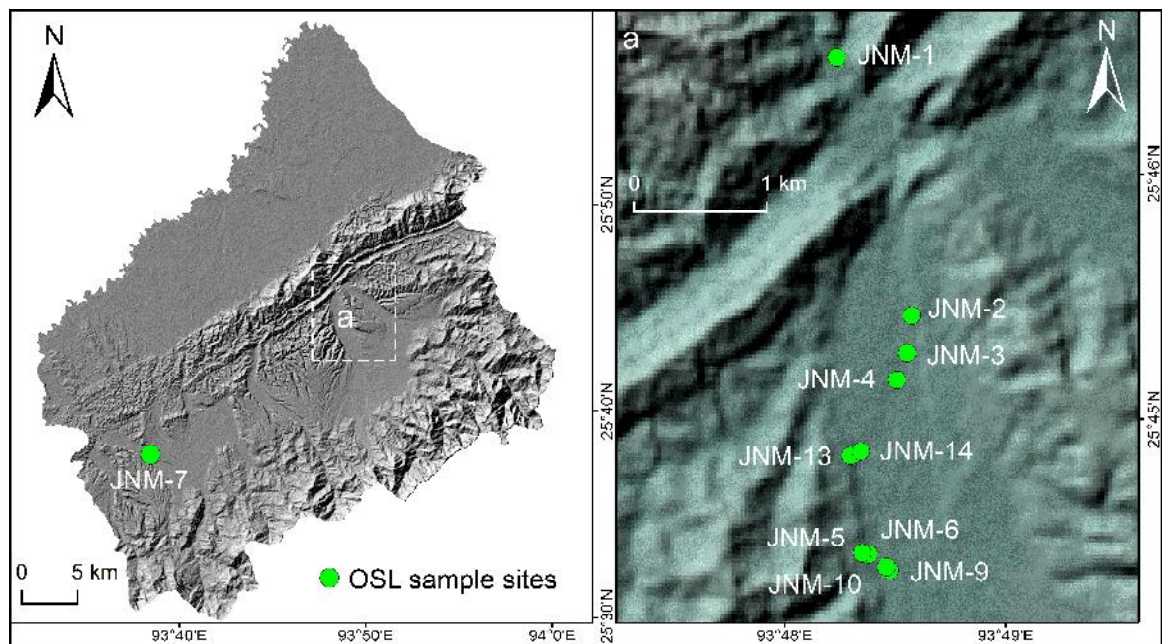


**Figure 6.2:** OSL sample sites of the study area (modified after Moiya et al., 2019)

## 6.8 Timing of deformation

In the present study, fluvial sediments are exposed within the intermontane basins bounded by thrusts of the BoS towards the northeast and southwest. The sediments are allocated a Pleistocene-Holocene age (GSI, 2011). The Chathe Alluvium is a newly designated fluvial sedimentary formation with horizontal to gentle dips. It often occurs as an alluvial cover above bedrock. It is composed of cobbles and pebbles in a sand-silt-clay matrix, which lie unconformably over the older bedrock. The bedrock and fluvial sediments have been variously deformed. Some are evidenced as growing anticlinal structures (Moiya et al., 2019).

The fluvial terraces provide information on uplift and incision rates of the bedrock. Therefore, these sediments overlying the older bedrock were analysed to establish their chronological ages (Moiya et al., 2019). From the dated sediments of the Quaternary fluvial terraces, the uplift rate is calculated by considering the geometry and elevation of the river to be stable throughout the downcutting process (Kothyari and Luirei, 2016). Elevation of the terraces is measured with respect to the present river channel (Lave and Avouac, 2000). The total incision rate  $\Delta H$  in mm/yr and expressed as  $\Delta H/\text{time}$ , (Pazzaglia et al., 1998; Kumar et al., 2010; Kothyari and Luirei, 2016) is thus obtained by subtraction of the total height of fill sediments determined from river channel ( $H_1$  in m) and the fill sediment height estimated from the bedrock ( $H_2$  in m).

The ages determined for the sediments indicate 21 and 1.8 ka for the oldest and youngest sediments of the area. On the basis of chronological data and sedimentation pattern, it is postulated that the terrace sediments underwent three major aggradational phases. The first phase took place around 21 ka, the second phase between 11-7 ka, while the last phase between 3.5-1 ka. Tilted terraces are indicative of uplift, faulting or thrusting due to ongoing tectonic activity. Samples collected from sand lens of tilted strath terraces along the hanging-wall of the Naga Thrust zone exposed between Kukidolong and Chumukedima suggest tectonic events after 7 ka. Near the Chathe Fault, the chronological ages of the fluvial sediments suggest that tilting began immediately after sediment deposition at 21 ka. This is probably due to the tectonic modification of the Chathe Fault (Moiya et al., 2019).

During the Plio-Pleistocene, fluvial sediments were deposited, followed by a phase of extreme tectonic activity, which uplifted and tilted the terraces. The bedrock, uplifted between 11-1.8 ka, was closely followed by increased incision rate due to over-steepening of the gradient of the river channels. During this phase of uplift, alluvium was deposited on the bedrock in the intermontane valleys. Bull (1990) and Starkel (2003) opine that strath terraces of thick bedrock overlain by thin alluvial cover result due to rapid uplift. The chronological dating of such strath terraces is therefore utilized to determine the rate of bedrock uplift and incision. From chronological data, five major phases is estimated. These took place at around 20 ka at 0.13 mm/year, 11 ka at 0.92 mm/year, 9 ka at 2.29 mm/year, 6 ka at 0.67 mm/year, and 1.8 ka at 2.6 mm/year, which indicate that the present study area were subjected to tectonic activity throughout the Late Pleistocene to early Holocene (Moiya et al., 2019).

Table 6.2 OSL Chronology (Institute of Seismological Research, Raisan Gandhinagar) (Modified after Moiya et al., 2019)

Sample	U	Th	K%	OD (%)	Dose rate (Gy/ka)	Palaeodose (Gray)			Ages (ka)			Final Age (ka)
						<i>ED (GY)</i> <i>WM</i>	<i>ED (GY)</i> <i>(MAM-3)</i>	<i>ED (GY)</i> <i>(CAM)</i>	<i>WM</i>	<i>MAM</i>	<i>CAM</i>	
JNM-1	5.6±0.28	22.6±1.13	1.45±0.07	37±1.4	4.1±0.3	24±0.5	29.08±2.37	31.50±1.77	5.8±0.4	7±0.7	7.6±0.7	7±0.7
JNM-2	4.6±0.23	17.5±0.87	1.64±0.08	35.6±0.2	3.7±0.2	44±0.9	41.26±3.47	67.36±4.81	11.8±0.8	11±1.2	18±1.8	11±1.2
JNM-3	2.8±1.4	13.7±0.68	1.51±0.07	64.9±2.6	2.9±0.3	12±0.2	10.18±1.58	16.2±1.32	4±0.5	3.4±0.6	5.4±0.8	3.4±0.6
JNM-4	4.0±0.2	16.8±0.84	1.42±0.07	66.8±2.5	3.3±0.2	9±0.1	9.78±1.03	17.46±1.38	2.6±1.9	2.9±0.3	5.1±0.5	2.9±0.3
JNM-5	5.6±0.28	21±1.05	1.05±0.05	17.4±0.6	3.6±0.2	34±0.4	33.78±1.98	36.60±0.93	9.3±0.7	9.2±0.8	10±0.7	9.3±0.7
JNM-6	3.9±0.19	15.40.77	1.27±0.06	47.9±1.5	3.1±0.2	5±0.1	5.64±0.58	3.25±0.17	1.6±0.1	1.8±0.2	1±0.09	1.8±0.2
JNM-7	3.7±0.18	16.6±0.83	1.56±0.07	38.3±1.6	3.4±0.2	69±1.2	82±7.1	89.1±4.3	20±1.5	24±2.7	26.1±2.2	20±1.5
JNM-9	2.3±0.11	14.2±0.71	1.17±0.05	43.7±2.6	2.6±0.1	53±2.4	93±9	100±6.9	20±1.7	35.6±4.2	38.3±3.8	20±1.7
JNM-10	3.1±0.15	14.5±0.72	1.05±0.05	41.1±2.8	2.6±0.1	57±2.6	94±9	102±6	21.1±1.8	34.9±4.1	37.8±3.5	21.1±1.8
JNM-13	1.8±0.09	30±1.5	1.8±0.09	21.7±0.7	4.1±0.3	24±0.2	24.29±0.99	26.31±0.74	5.8±0.4	5.9±0.5	6.4±0.5	5.8±0.4
JNM-14	1.3±0.06	11.1±0.55	1.3±0.06	33±1.2	2.3±0.1	19±0.4	15.18±0.89	20.49±0.84	8.2±0.6	6.5±0.6	8.8±0.7	6.5±0.6

1. OD → Over Dispersion (quantification of the spread in the Palaeodose data)
2. Grain size used: 90-150 µm
3. Age model used: MAM , WM and CAM
4. Water content (error 10%)

## CHAPTER: 7

### SUMMARY AND CONCLUSIONS

#### 7.1 Summary

Morphometric parameters were computed for the study area. Drainage patterns, including rectangular, parallel and trellis, are common in the study area, which are indicative of structural control. The drainage is developed up to the 7<sup>th</sup> order stream. Drainage orientation is dominantly controlled by various faults, thrusts and numerous joints. High drainage densities towards the thrust zones are due to the structures. River profile analyses such as, longitudinal profile, stream length gradient index and steepness index show prominent knickpoints at the thrusts, faults and an anticline in the study area; these are ascribed to ongoing tectonism. Along the Bara Manglu, Langlong, Khova, Chathe and Jharnapani rivers, prominent knickpoints with high values of steepness index and stream length gradient index are observed along the thrusts, faults and the growing anticline, suggesting the response of rivers to uplift. The asymmetry factor indicates that the whole watershed is tilted because of tectonic influence on the river basins. The T value indicates movement of the major trunk stream towards NE and SW. The basin elongation ratio indicates that all the basins are either tectonically active or slightly active. Channel sinuosity shows the absence of straight river courses, an indication that tectonic activity has caused their deviation from a straight path. The mountain front sinuosity index suggests that the mountain front of the thrust zone, particularly the frontal Naga Thrust, is tectonically active. The valley floor width to valley height ratios indicate that the valleys near the Naga Thrust and Disang Thrust are V-shaped with steep valley walls primarily due to ongoing tectonism. The hypsometric curve and hypsometric integral indicate high values with convex curves towards the Naga Thrust, suggesting young, active tectonics.

Lineament orientations show dominant NW-SE and NE-SW directions that correspond with the normal faults and fold and thrust systems of the region. The high lineament density near the thrust zones in the BoS is attributed to active tectonics. Some of the lineaments mapped are recognized as faults. The Chathe Fault and four

other local faults have affected river courses and outcrops of strath terraces. These faults have dislocated the bedrock and overlying Quaternary sediments and caused an elevation difference of up to ~10 m of two levels of strath terraces in portions of the Medziphema intermontane basin. The development of a 16-m fault scarp is attributed to uplift due to tectonism.

Palaeochannels are commonly observed in the intermontane basin. They owe their origin to piracy and river migration. Traces of palaeochannels over strath terraces with scarps of up to ~16 m height and ~2.3 km length in part of the Medziphema intermontane basin are strong indications of fault movements. The trends of these palaeochannels suggest south-westward migration of the main river channels (Moiya et al., 2019). The shift in the course of the Chathe River by more than 400 m in 96 years (1921-23 surveyed topographic map and Google earth image of 2017) suggests uplift of the terrain has caused the river to migrate.

Strath terraces are geomorphic markers that provide information about bedrock erosion, climatic factors and tectonic regime. Roy and Kacker (1982) opine that river terraces have been uplifted in parts of the Naga Hills during Pliocene-Quaternary block movements. The presence of strath terraces along the Chathe Fault and the Naga Thrust (hanging wall) are evidences of tectonic origin. Different levels of unpaired strath terraces, and folded, faulted and tilted terraces also indicate neotectonic events. In the Medziphema intermontane valley, strath terraces are unpaired and up to six levels. The strath terraces are affected by folds, fractures and faults. Deformations, including displacements, are observed, in the bedrock and in the younger Quaternary sediments, which point to rejuvenation of the region during Late Quaternary.

Near the Sanis-Chongliymesen Thrust zone at Sirhima, Quaternary fluvial sediments are downthrown with regard to the Jenam bedrock by a normal fault. The younger sediments are displaced by more than ~2 m by normal faults. Along the Chathe Fault, towards Razephema, normal faults have dislocated the Dihing bedrock and Chathe Alluvium by up to 1.8 m at various outcrops. Girujan bedrock and Chathe Alluvium have been displaced by normal faults, from 0.8 m to more than 1 m along various sections near Kukidolong. In the Chathe River section, two layers of fill terraces are dislocated by ~1.3 m by a normal fault. Normal faults have also displaced

bedrock and overlying sediments near the Bara Manglu stream by about ~0.5 m. All these displacements by normal faulting point to neotectonic movements.

Three levels of strath terraces developed in the Bara Manglu stream NW of Peren provides evidence of two phases of tectonic activity. The folded and highly sheared bedrock bearing slickenside indicates the presence of a reverse fault. The reactivation of the Naga Thrust has resulted in folding and realignment of the younger fluvial sediments along the thrust zone (Moiya et al., 2019). Rejuvenation of the Naga Thrust is also obvious from the thrusting of older Neogene rocks over the younger Quaternary sediments (Aier et al., 2019). Tilted sediments of fluvial terraces near the AH1 and Langlong River also indicate ongoing tectonic movements.

The subsurface extension of the Karbi Anglong Hills has caused an oblique indentation of the Naga Hills. This bend has been named the Yampha Bend (Moiya et al., 2019). The indentation has caused the SW-flowing Yampha River to take a swing and flow towards the north. The hanging wall of the rising Naga Thrust has also influenced the flow of the Nra River. These features suggest recent tectonic activity. Field evidences also indicate the uplift of the Naga Thrust after deposition of the Quaternary sediments.

OSL data of sediments from strath terraces provide incision/uplift rates. OSL dates of the tilted terraces signify very recent movements, after 7 ka. Five phases of bedrock uplift/incision are recorded during 20 ka, 11 ka, 9 ka, 6 ka and 1.8 ka, at rates of 0.13, 0.92, 2.29, 0.67 and 2.6 mm/year respectively. They point to ongoing tectonic activity from the Late Pleistocene to early Holocene in the present study area (Moiya et al., 2019).

The topographic profiles plotted across the BoS show uplift of the landscape towards the north, from the Naga Thrust and Chathe Fault, and towards the south from the Piphema, Disang and Yah thrusts, where intermontane basin development is confined between the thrust belts.

During late Mio-Pliocene, compressional forces produced asymmetrical, open folds and thrust planes in the BoS of the study area (Roy and Kacker, 1982). The later phase of the Pliocene-Quaternary convergence caused the formation of cross folds,



strike-slip faults and oblique-slip faults that are adjusted along the BoS (Roy and Kacker, 1986).

The origin of the BoS is ascribed to tremendous tectonic stresses of the Himalayan orogenesis (Roy and Kacker, 1982). The Disang Thrust started evolving during Late Miocene (Aier et al, 2011); prolonged tectonic movements are manifested in the occurrence of the Upper Bhuban rocks near the Nichuguard anticline (Ranga Rao and Samanta, 1987). Renewal of compressional forces caused the Sanis-Chongliymisen and Naga thrusts to emerge during Late Pliocene. Movements progressed further into the Pleistocene along the Sanis-Chongliymisen Thrust, which is evident from the deposition of Dihing sediments in front of the Sanis-Chongliymisen Thrust (Ranga Rao and Samanta, 1987). According to Kent and Dasgupta (2004), three phases of movements took place along the Naga Thrust. The first two displacements occurred during Mid-Pleistocene to form the two unconformities, while the third displacement caused the intervening of Neogene rocks over alluvium during the Holocene. However, the gentle dip of the Dihing sediments suggests that the commencement of the Naga Thrust began earlier (Aier et al., 2011).

The phase of Pliocene-Quaternary plate convergence is also responsible for major uplift in the IMR (Roy and Kacker, 1982). This phase affected the thrust planes, with NW-SE trending folds accounting for the double plunging nature of the BoS (Roy and Kacker, 1986) and development of horst-and-graben structures (Roy and Kacker, 1982). Block faulting in the Medziphema intermontane basin is perhaps associated with Pliocene-Quaternary movements (Roy and Kacker, 1982). The Medziphema and Jalukie intermontane basins are tectono-geomorphic landforms that have resulted from neotectonic activity, as a result of thrusting and uplift. The folding and faulting of the Quaternary sediments of the intermontane basin and the Naga Thrust zone indicate continuous tectonic modification, which suggests that the thrust planes of the BoS are still propagating.

## **7.2 Conclusions**

On the basis of studies carried out, the following conclusions are made.

7.2.1. The drainage network and patterns of the study area are structurally controlled. The various drainage orders are mostly controlled by joints, normal and strike-slip faults and thrusts. High drainage density is mostly confined within the BoS.

7.2.2. The lineaments prominently trend NW-SE and NE-SW, indicating the dominant control of regional thrusts and normal faults. Some of the NW-SE trending linear features mapped are normal faults. These are responsible for displacement of Quaternary fluvial sediments, river migration and development of fault scarps.

7.2.3. River piracy and migration are indicative of differential movements along faults as a result of ongoing tectonism that tilted the river basins. The remnants of older channels on the strath terraces, at much higher elevations than the present active channels are indicative of down-cutting induced by faulting.

7.2.4. Development of knickpoints along the longitudinal profiles and prominent SL and  $k_s$  peaks along the thrust zones indicate tectonic activity. Values of AF suggest tilting of the basins. A rose diagram for T values of the study area indicate migration towards NE and SW. Low values of  $R_e$  and high value of  $S_{mf}$  indicate active tectonism. High to moderate S values of the study area indicate active to slightly active deformation respectively. The high HI values of the study area and the convex hypsometric curves indicate probable active tectonism and high incision rates.

7.2.5. Low  $V_f$  values point to development of V-shaped valleys due to high uplift and incision rates and high tectonic activity along the thrust zones. High  $V_f$  values are related to low uplift and development of U-shaped valleys in the broad intermontane basins.

7.2.6. The Yampha Bend, a localized curved mountain front, is developed at the northeastern extremity of the study area. This syntaxial bend is due to indentation of the Karbi Anglong Hills in the subsurface, which has caused the NE-SW trending mountain front of the Naga Hills to align N-S.

7.2.7. The presence of geomorphic markers such as many levels of unpaired strath terraces, faulted, folded and tilted terraces in the study area suggest river adjustment to uplift. Development of five to six levels of unpaired river terraces, tilting and displacement of the Quaternary beds and bedrock caused by folding and faulting indicates recent tectonic activity. Evidence of folding of fluvial sediments and

bedrock, as well as realignment of fluvial sediments by shear planes suggests neotectonic activity.

7.2.8. OSL chronology of the fluvial terraces indicate five phases of deformation that occurred during 20 ka at 0.13 mm/y, 11 ka at 0.92 mm/y, 9 ka at 2.29 mm/y, 6 ka at 0.67 mm/y and 1.8 ka at 2.6 mm/y. They suggest tectonic activity throughout the Late Pleistocene to early Holocene. The tilt in terrace sediments indicates active tectonism after 7 ka.

7.2.9. Two post-collisional phases are accountable for the development of tectonically complicated structures in the area of study. The first phase may be linked to the origin of the thrust planes of the BoS along with asymmetrical open folds, while the second phase caused major uplift within the BoS.

7.2.10. Based on the above-mentioned geomorphic and tectonic setting, the evolution of the Medziphema and Jalukie intermontane basins is proposed. Neotectonic movements caused major uplift in the IMR, which has led to the development of horst-and-graben structures within the BoS. This tectonic phase is attributed to the evolution of the Medziphema and Jalukie intermontane basins of the BoS.

## REFERENCES

- Acharyya, S.K., 1986. Cenozoic Plate Motions creating the eastern Himalayas and Indo-Burmese Range around the north-east corner of India. In: Ophiolite and Indian Plate Margin: (Eds. N.C. Ghose and S. Varadrajana), 143-161.
- Acharyya, S.K., Roy, D.K. and Mitra, N.D., 1986. Stratigraphy and palaeontology of the Naga Hills Ophiolite Belt. Geological Survey of India, memoirs, 119, 64-74.
- Acharyya, S.K., Ray, K.K. and Sengupta, S., 1990. Tectonics of Ophiolite Belt from Naga Hills and Andaman Islands, India. In: Naha, K., Ghosh, S.K., Mukhopadhyay, D. (Eds.), Structure and Tectonics: The Indian Scene. National Academy of Science India (Earth and Planetary Sciences), 187-199.
- Agrawal, O.P. and Ghose, N.C., 1986. Geology and stratigraphy of the Naga Hills Ophiolite between Meluri and Awankhoo, Phek district Nagaland, India. In: N.C. Ghose and S. Varadarajan (Eds.), Ophiolite and Indian plate margin. Sumna Publication, Patna, 163-195.
- Agrawal, O.P. and Kacker, R.N., 1980. Nagaland ophiolites, India: A subduction zone ophiolite complex in a Tethyan orogenic belt. International Ophiolite Symposium, Cyprus, 454-461.
- Aier, I., Luirei, K., Bhakuni, S.S., Thong, G.T. and Kothiyari, G.C., 2011. Geomorphic evolution of Medziphema intermontane basin and Quaternary deformation in the Schuppen Belt, Nagaland, NE: India. Zeitschrift für Geomorphologie, 55, 247-265.
- Aitken, M.J., 1985. Thermoluminescence dating. Academic Press, London.
- Aitken, M.J., 1998. An introduction to optical dating. Oxford University Press.
- Alappat, L., 2011. Application of OSL dating on coastal sediments – Case studies from shallow marine sediments of Southern North Sea, Germany, and coastal sub-surface and surface sediments from south India. Ph. D., thesis, Freien Universität, Berlin.
- Argyriou, A., 2012. A Methodology for the Rapid Identification of Neotectonic Features using Geographical Information Systems and Remote Sensing: A Case Study from Western Crete, Greece. Ph.D., thesis, University of Portsmouth, United Kingdom.
- Audemard, F., 1999. Morpho-structural expression of active thrust fault systems in the humid tropical foothills of Colombia and Venezuela. Zeitschrift für Geomorphologie, 118, 1-18.
- Azor, A., Keller, E.A. and Yeats, R.S., 2002. Geomorphic indicators of active fold growth: South Mountain-Oak Ridge Ventura basin, Southern California. Geological Society of America Bulletin, 114, 745-753.
- Bailey, R.M. and Arnold, L.J., 2006. Statistical modeling of single grain quartz De distributions and an assessment of procedures for estimating burial dose. Quaternary Science Review, 25, 2475-2502.

- Banerjee, R.K. 1979. Disang Shale, its stratigraphy, sedimentation history and basin configuration in Northeastern India and Burma. *Quarterly Journal of the Geological, Mining and Metallurgical Society of India*, 51, 144-152.
- Bezbaruah, D., Kashyap, K. and Boruah, M.P., 2016. Field geology and morphometric evidences supporting active tectonics of Amguri-Tuli-Merangkong area in the Assam-Nagaland border, India. *South East Asian Journal of Sedimentary Basin Research*, 37-46.
- Bhatt, C.M., Chopra, R. and Sharma, P.K., 2007. Morphotectonic analysis in Anandpur Sahib area, Punjab (India) using remote sensing and GIS approach. *Journal of the Indian Society of Remote Sensing*, 35 (2), 129-139.
- Bhattacharjee, C.C., 1991. The ophiolites of Northeast India: A subduction zone Ophiolite Complex of Indo-Burman Orogenic Belt. *Tectonophysics*, 191, 213-222.
- Bhattacharjee, C.C., 1997. Tectonism and Sedimentation in the Indo-Burman Sedimentary Basin. *Journal of Geoscience*, 2, 1-8.
- Bhattacharya, F., Rastogi, B.K. and Kothiyari, G.C., 2013. Morphometric evidence of seismicity around Wagad and Gedi faults, eastern Kachchh, Gujarat. *Journal of the Geological Society of India*, 81, 113-121.
- Bhattacharyya, S. and Sanwal, R., 1985. Systematic geological mapping around Fakimile-Thanameir Saramati, district Tuensang, Nagaland. *Geological Survey of India, Progress report for the field season 1984-1985*.
- Bhatia, S.C., Ravi Kumar, M. and Gupta, H.K., 1999. A probabilistic seismic hazard map of India and adjoining regions. *Annali Di Geofisica*, 42, 1153-1166.
- Bora, D.K., Baruah, S., Biswas, R. and Gogoi, N.K., 2013. Estimation of source parameters of local earthquakes originated in Shillong-Mikir Plateau and its adjoining region of Northeastern India. *Bulletin of the Seismological Society of America*, 103 (1), 437-446.
- Bora, D.K., 2016. Scaling relations of moment magnitude, local magnitude, and duration magnitude for earthquakes originated in northeast India. *Earth Science*, 29(3), 153-164.
- Brunnschweiler, R.O., 1966. On the geology of Indo-Burman Ranges. *Journal of the Geological Society*, 13, 137-195.
- Bull, W.B., 1977. Tectonic geomorphology of the Mojave Desert. *U.S Geological Survey, contract report no. 14-08-001-G-394*.
- Bull, W.B., 1990. Stream-terrace genesis: implications for soil development. In: P. L. K. Knuepfer, & L. D. McFadden (Eds.), *Soils and Landscape Evolution. Geomorphology*, 3, 351-367.
- Bull, W.B. and McFadden, L.D., 1977. Tectonic geomorphology north and south of the Garlock Fault, California. In: *Geomorphology in Arid Regions, Proceedings of the 8th Annual Geomorphology symposium*. State University of NY, Binghamton, 115-138.
- Burbank, D.W. and Anderson, R.S., 2001. *Tectonic geomorphology*. Blackwell Scientific, Oxford.

- Burbank, D.W. and Johnson, G.D., 1983. The Late Cenozoic chronologic and stratigraphic development of the Kashmir intermontane basin, northwestern Himalaya. *Palaeogeography, Palaeoclimatology, Palaeoecology*, 43, 205-235.
- Bureau of Indian Standards, 2002. Indian standard criteria for earthquake resistant design of structures: general provisions and buildings. Bureau of Indian Standards, New Delhi (Part 1).
- Chakradhar, M. and Gaur, M.P., 1985. Systematic geological mapping around Jaluke, Kohima district, Nagaland. Geological Survey of India, Progress report for the field season 1984-85.
- Chakradhar, M., Naik, K.K. and Jayaraman, V., 1986. Systematic geological mapping in a part of Kohima district, Nagaland. Geological Survey of India, Progress report for the field season 1985-86.
- Chakraborty, S. and Sarma, H., 1982. Systematic geological mapping of Peren-Puilwa-Tesangki area, Kohima district Nagaland. Geological Survey of India, Progress report for the field season 1979-1980.
- Chattopadhyay, B., Venkataramana, P., Roy, D.K., Bhattacharya, S. and Ghosh, S., 1983. Geology of Naga Hills Ophiolite. Geological Survey of India, 2, 59-115.
- Chen, Y., Sung, Q. and Cheng, K., 2003. Along-strike variations of morphometric features in the western foothills of Taiwan: tectonic implications based on stream gradient and hypsometric analysis. *Geomorphology*, 56, 109-137.
- Chorley, R.J., 1969. The drainage basin as the fundamental geomorphic unit. In: R.J. Chorley (Ed.), *Introduction to physical hydrology*, Methuen, London.
- Chrucinska, A., Lankauf, K.R., Luc, M., Oczkowski, H.L., Przegietka, K.R. and Szmanda, J.B., 2004. Evolution of St. Laurent mountain near Chelmno based on luminescence dating. *Geochronometria*, 23, 27-32.
- Cox, R.T., 1994. Analysis of drainage basin asymmetry as a rapid technique to identify areas of possible Quaternary tilt-block tectonics: an example from the Mississippi Embayment. *Geological Society of America Bulletin*, 106, 571-581.
- Dalati, M., 2000. Lineaments on landsat images detection mapping and tectonic significance in north-western depressions of Syria. *International Archives of Photogrammetry and Remote Sensing*, Amsterdam, XXXIII (B7), 301-305.
- Devdas, V. and Gandhi, P., 1986. Systematic geological mapping in Maromi-Akuluto-Suruhuto areas, Zunheboto district, Nagaland. Geological Survey of India, Progress report for the field season 1985-1986.
- Devi, T. K., 2012. Seismic hazard and its mitigation in northeast, India. *International Journal of Science and Engineering Applications*, 1 (1), 79-84.
- Directorate of Geology and Mining, Nagaland, 1978. Miscellaneous Publication, no.1.
- Duller, G.A.T., 2008. Luminescence dating: guidelines on using luminescence dating in archaeology, Swindon: English Heritage.
- Evans, P., 1932. Tertiary succession in Assam. *Transaction of Mining and Geological Institute of India*, 27, 155-260.
- Evans, P., 1964. The tectonic framework of Assam. *Journal of Geological Society of India*, 5, 80-96.

- El Hamdouni, R., Irigaray, C., Fernandez, T., Chacon, J. and Keller, E.A., 2008. Assessment of relative active tectonics, southwest border of the Sierra Nevada (southern Spain). *Geomorphology*, 96, 150-173.
- Elias, Z., 2013. Quantitative Geomorphology of analyzing tectonic activity in the Roczek and Shwork rivers valley in the Zagros Mountains (Iraqi Kurdistan). *International Journal of Enhanced Research Science in Technology and Engineering*, 2(11), 22-34.
- Faghih, A., Nourbakhsh, A. and Kusky, T.M., 2015. GIS- based analysis of relative tectonic activity along the Kazerun Fault zone, Zangros mountains, Iran: Insights from Data Mining of Geomorphic Data. *Journal of Earth Science*, 26 (5), 712-723.
- Fareeduddin and Dilek, Y., 2015. Structure and petrology of the Nagaland-Manipur Hill Ophiolitic Mélange zone, NE India: A Fossil Tethyan Subduction Channel at the India -Burma Plate Boundary. *Episodes*, 38 (4), 298-314.
- Figueroa, M. and Knott, J.R., 2010. Tectonic geomorphology of the southern Sierra Nevada Mountains (California): Evidence for uplift and basin formation. *Geomorphology*, 123, 34-45.
- Flint, J.J., 1974. Stream gradient as a function of order, magnitude and discharge. *Water Resource Research*, 10, 969-973.
- Fuchs, M. and Owen, L.A., 2008. Luminescence dating of glacial and associated sediments: review, recommendations and future directions. *Boreas*, 37(4), 636-659.
- Galbraith, R.F., Roberts, R.G., Laslett, G.M., Yoshida, H. and Olley, J.M., 1999. Optical dating of single and multiple grains of quartz from Jinmium Rock Shelter, northern Australia: Part 1, experimental design and statistical models. *Archaeometry*, 41, 339-364.
- Garrote, J., Heydt, G.G., and Cox, R.T., 2008, Multi-stream order analyses in basin asymmetry: A tool to discriminate the influence of neotectonics in fluvial landscape development. *Geomorphology*, 102(1), 130-144.
- Geological Survey of India, 2011. Geology and mineral resources of Manipur, Mizoram, Nagaland and Tripura. Miscellaneous Publication no. 30, part IV, 1(2).
- Ghose, N.C. and Agrawal, O.P., 1989. Geological framework of the central part of the Naga Hills Ophiolite, Nagaland. *Phanerozoic Ophiolite of India* (eds.) N.C. Ghose, Sumna Publication, Patna, 165-188.
- Ghose, N.C., Agrawal, O.P. and Srivastava, S.C., 1987. Metamorphism of the ophiolite belt of Nagaland, NE India. *Proceeding National Seminar Tertiary Orogeny*, 189-213.
- Ghose, N.C., Agrawal, O.P. and Chatterjee, N., 2010. Geological and mineralogical study of eclogite and glaucophane schists in the Naga Hill Ophiolite, Northeast India. *Island Arc*, 19, 336-356.
- Ghosh, T., Basu, S. and Hazra, S., 2014. Geological mapping of the Schuppen Belt of north-east India using geospatial technology. *Journal of Asian Earth Sciences*, 79, 97-111.
- Gilbert, G.K., 1877. Report on the geology of the Henry Mountains, US Government



- Printing Office, Washington, D. C.
- Godfrey-Smith, D.I., Huntley, D.J. and Chen, W.H., 1988. Optical Dating Studies of Quartz and Feldspar Sediment Extracts. *Quaternary Science Reviews*, 7, 373-380
- Gregory, K.J. and Gardiner, V., 1975. Drainage density and climate. *Zeitschrift for Geomorphology*, 19, 287-298.
- Hack, J.T., 1957. Studies of longitudinal stream profiles in Virginia and Maryland. U.S. Geological Survey, Professional Paper, 294 (B), 45-97.
- Hack, J.T., 1973. Stream profile analysis and stream-gradient index. *U.S. Geological Survey Journal of Research*, 1(4), 421-429.
- Han, Z., Wu, L., and Ran, Y., 2003. The concealed active tectonics and their characteristic as revealed by drainage density in the North China Plain (NCP). *Journal of Asian Earth Sciences*, 21(9), 989-998.
- Hare, P.W. and Gardner, T.W., 1985. Geomorphic indicators of vertical neotectonism along converging plate margins, Nicoya Peninsula, Costa Rica. In: Morisawa, M, Hack, JT (Eds.). *Tectonic Geomorphology. Proceedings of the 15th Annual Binghamton Geomorphology Symposium* Allen and Unwin, Boston, MA, 123-134.
- Horton, R.E., 1932. Drainage basin characteristics. *Eos, Transactions American Geophysical Union*, 13(1), 350-361.
- Horton, R.E., 1945. Erosional development of streams and their drainage basins: Hydro-physical approach to quantitative morphology. *Geological Society of America Bulletin*, 56, 275-370.
- Htay, H., 2016. Tectonic Setting of Ophiolite Belts in Myanmar Search and Discovery Article #30452.
- Huntley, D.J., Godfrey-Smith, D.I. and Thewalt, M.L.W., 1985. Optical dating of sediments. *Nature*, 313, 105-107.
- Hou, J. and Han, M., 1997. A morphometric method to determine neotectonic activity of the Weihe Basin in Northwestern China. *Episodes*, 20(2), 429-432.
- Hütt, G., Jaek, I. and Tchonka, J., 1988. Optical dating K-feldspars optical-response stimulation spectra. *Quaternary Science Reviews*, 7, 381-385.
- Hütt, G. and Jaek, J., 1989. Infrared stimulated photoluminescence dating of sediments. *Ancient TL*, 7, 48-51.
- Imchen, W., Thong, G.T. and Pongen, T., 2014. Provenance, tectonic setting and age of the sediments of the Upper Disang Formation in the Phek district, Nagaland. *Journal of Asian Earth Sciences*, 88, 11-27
- Jackson, J., Van Dissen, R. and Berryman, K., 1998. Tilting of active faults and folds in the Manawatu Region, New Zealand: evidence from surface drainage patterns, *Journal of Geology and Geophysics*, 41, 377-385.
- Jain, A.K. and Bhowmik, S.K., 2016. Tectonics and Evolution of the Trans Himalayan Mountains and Nagaland Ophiolite Belt. *Proceedings of Indian National Science Academy*, 82(3), 617-624.
- Keller, E.A., 1986. Investigation of active tectonics: use of surficial earth processes. In: Wallace, R. E. (Ed.), *Active Tectonics*. National Academy Press, Washington DC, 136-147.

- Keller, E.A. and Pinter, N., 1996. *Active Tectonics: Earthquakes, Uplift and Landscapes* Prentice Hall, New Jersey.
- Keller, E.A. and Pinter, N., 2002. *Active Tectonics: Earthquakes, Uplift and Landscape* (2<sup>nd</sup> Ed.). Prentice Hall, Englewood Cliffs, New Jersey.
- Keller, E.A. and Rockwell, T.K., 1984. Tectonic Geomorphology, Quaternary Chronology and Paleoseismicity. Development and applications of Geomorphology.
- Kent, W.N. and Dasgupta, U., 2004. Structural evolution in response to fold and thrust belt tectonics in northern Assam. A key to hydrocarbon exploration in the Jaipur anticline area. *Marine and Petroleum Geology*, 21, 785-803.
- Kirby, E., and Whipple, K., 2001. Quantifying differential rock-uplift rates via stream profile analysis. *Geology*, 29(5), 415-418.
- Kirby, E. and Whipple, K.X., 2003. Distribution of active rock uplift along the eastern margin of the Tibetan Plateau: Inferences from bedrock channel longitudinal profiles. *Journal of Geophysical Research*, [https://doi: 10.1029/2001JB000861](https://doi.org/10.1029/2001JB000861).
- Kothyari, G.C. and Luirei, K., 2016. Late Quaternary tectonic landforms and fluvial aggradation in the Saryu River valley: Central Kumaun Himalaya. *Geomorphology*, 268, 159-176.
- Kulkarni, M.D., 2015. The basic concept to study morphometric analysis of the river drainage basin: A review. *International Journal of Scientific Research*, 4(7), 2277-2280.
- Kumanan, C.J., 2001. Remote sensing revealed morphotectonic anomalies as a tool to neotectonic mapping-experience from South India. Paper presented at the 22nd Asian Conference on Remote Sensing, 5 - 9 November 2001, Singapore. Copyright (c) 2001 Centre for Remote Imaging, Sensing and Processing, National University of Singapore; Singapore Institute of Surveyors and Valuers; Asian Association on Remote Sensing.
- Kumar, S., Wesnousky, S.G., Jayangondaperumal, R., Nakata, T., Kumahara, Y. and Singh, V., 2010. Paleoseismological evidence of surface faulting along the northeastern Himalayan front, India: Timing, size, and spatial extent of great earthquakes. *Journal of Geophysical Research*, 115, 1-20.
- Lavé, J. and Avouac, J.P., 2000. Active folding of fluvial terraces across the Siwaliks Hills, Himalayas of central Nepal. *Journal of Geophysical Research*, 105, 5735-5770.
- Leopold, B., Wolman, G. and Miller, J.P., 1964. *Fluvial processes in Geomorphology*. W.H. Freeman & Co., San Francisco, London.
- Longkumer, L., Luirei, K., Moiya, J.N. and Thong, G.T., 2019. Morphotectonics and neotectonic activity of the Schuppen Belt of Mokokchung. *Journal of Asian Earth Sciences*, 170, 138-154.
- Luirei, K., Bhakuni, S.S. and Negi, S.S., 2017. Landforms along transverse faults parallel to axial zone of folded mountain front, north-eastern Kumaun Sub-Himalaya, India. *Journal of Earth System Science*, <https://doi.org/10.1007/s12040-016-0789-4>.

- Madhav, C., 1989. Quaternary Geology and Geomorphology in parts of Kohima, Wokha, Mokokchung and Mon districts of Nagaland. Geological Survey of India, Progress report for the field season 1988 -1989.
- Mallet, F.R., 1876. On the coalfields of Naga Hills bordering Lakhimpur and Sibsagar districts, Assam. Geological Survey of India, memoirs, 12.
- Mathew, M.J., 2016. Geomorphology and morphotectonic analysis of north Borneo. Ph. D., thesis, Universite Bretagne Loire, Rennes, France.
- Mathur, L.P., and Evans, P., 1964. Oil in India. Proceedings of 22<sup>nd</sup> session of International Geological Congress, New Delhi.
- Mitchell, A.H.G., and Mckerrow, W.S., 1975. Analogous evolution of the Burma orogen and the Scottish Caledonides. Geological Society of America Bulletin, 86, 305-315.
- Mitra, N.D. and Choudhary, A., 1969. Geology and coal resources of the Nazira coalfield (north of the Dikhu River), Tuensang district, Nagaland. Geological Survey of India, Progress report.
- Mitra, N.D. and Choudhary, A., 1970. Geology and coal resources of the Jhanzl Disai valley coalfield around chanki and Chongliyiemsan area, Mokokchung district, Nagaland. Geological Survey of India, Progress report for the field season 1969-1970.
- Moiya, J.N., Luirei, K., Longkumer, L., Kothiyari, G.C. and Thong, G.T., 2019. Late Quaternary deformation in parts of the Belt of Schuppen of Dimapur and Peren districts, Nagaland, NE India. Geological Journal, <https://doi.org/10.1002/gj.3413>.
- Molnar, P. and Tapponnier, P., 1975. Cenozoic tectonics of Asia: Effects of a continental collision. Science, 189, 419-425.
- Molnar, P., Erik Thorson, B., Burchfiel, B.C., Deng, Q., Feng, X., Li, J., Raisbeck, G. M., Shi, J., Zhangming, W., Yiou, F. and You, H., 1994. Quaternary climate change and the formation of river terraces across growing anticlines on the north flank of the Tien Shan, China. Journal of Geology, 102, 583-602.
- Morrish, S.C., 2015. Characterization and digital morphotectonic analysis of drainage basins in a deforming forearc, Nicoya Peninsula, Costa Rica. M. Sc, thesis, California State Polytechnic University, Pomona.
- Mueller, J.E., 1968. An introduction to the hydraulic and topographic sinuosity indexes. Annals of the American Association of Geographers, 58, 371-385.
- Murray, A.S. and Olley, J.M., 2002. Precision and accuracy in the optically stimulated luminescence dating of sedimentary quartz: a status review. Geochronometria, 21, 1-16.
- Murray, A.S. and Wintle, A.G., 2000. Luminescence dating of quartz using an improved single-aliquot regenerative-dose protocol. Radiation Measurements, 32, 57-73.
- Murray, A.S. and Wintle, A.G., 2003. The single aliquot regenerative dose protocol: potential for improvements in reliability. Radiation Measurements, 37, 377-381.
- Nagaland GIS and Remote Sensing Centre, 2014. Geomorphology and Lineament mapping: Nagaland. A report on national Geomorphology and lineament mapping: Nagaland chapter.

- Naik, G.C., 1998. Tectonostratigraphic evolution and palaeogeographic reconstruction of Northeast India. Proceedings of Indo-German Workshop on Border Strandology magnetostratigraphy pilot project, Calcutta.
- Najman, Y., Sobel, E., Millar, I., Stockli, D., Govin, G., Lisker, F., Garzanti, E., Limonta, M., Vezzoli, G., Szymanski, E. and Kahn, A., 2019. The uplift of the Indo-Burman Ranges, Myanmar. *Geophysical Research Abstracts*, 21, 2019-2959.
- Nandy, D.R., 2000. Geodynamics of North-eastern India and the adjoining region. ACB Publications, Kolkata.
- Ni, C., Zhang, S., Liu, C., Yan, Y. and Li, Y., 2016. Lineament Length and Density Analyses Based on the Segment Tracing Algorithm: A Case Study of the Gaosong Field in Gejiu Tin Mine, China. Hindawi Publishing Corporation Mathematical Problems in Engineering. <http://dx.doi.org/10.1155/2016/5392453>.
- Ollier, C., 1981. Tectonics and landforms. *Geomorphology texts*, Longman Group Limited, New York.
- Olley, J.M., Caitcheon, G.G. and Murray, A.S., 1998. The distribution of apparent dose as determined by optically-stimulated luminescence in small aliquots of fluvial quartz: Implications for dating young samples. *Quaternary Science Reviews (Quaternary Geochronology)*, 17, 1033-1040.
- Olympa, B. and Kumar, A., 2015. A review on the tectonic setting and seismic activity of the Shillong plateau in the light of past studies. *Disaster Advances*, 8(7), 34-45.
- Owen, L.A., Mitchell, W., Bailey, R.M., Coxon, P. and Rhodes, E., 1997. Style and timing of Glaciation in the Lahul, Himalaya, northern India: a framework for reconstructing late Quaternary palaeoclimatic change in the western Himalayas. *Journal of Quaternary Research*, 12 (2), 83-109.
- Pareta, K. and Pareta, U., 2011. Quantitative morphometric analysis of a watershed of Yamuna basin, India using ASTER (DEM) data and GIS. *International Journal of Geomatics and Geosciences*, 2 (1), 248-269.
- Parveen, R., Kumar, U. and Singh, V.K., 2012. Geomorphometric Characterization of Upper South Koel Basin, Jharkhand: A Remote Sensing & GIS Approach. *Journal of Water Resource and Protection*, 4, 1042-1050.
- Pazzaglia, F.J., Gardner, T.W. and Merritts, D.J., 1998. Bedrock fluvial incision and longitudinal profile development over geologic time scales determined by fluvial terraces, in Tinkler, K., and Wohl, E., eds., *Rivers over rock: Fluvial processes in bedrock channels: Geophysical Monograph Series*, America Geophysical Union, Washington DC, 107, 207-235.
- Pérez-Peña, J.V., Azañón, J.M., Azor, A., Delgado, J. and González-Lodeiro, F., 2008. Spatial analysis of stream power using GIS: SLK anomaly maps. *Earth Surface Processes and Landforms*, 34, 16-25.
- Pérez-Peña, J.V., Azañón, J.M. and Azor, A., 2009. CalHypso: An ArcGIS extension to calculate hypsometric curves and their statistical moments. Applications to drainage basin analysis in SE Spain. *Computers and Geosciences*, 35, 1214-1223.
- Perkins, N.K. and Rhodes, E.J. (1994): Optical dating of fluvial sediments from Tattershall, U.K. *Quaternary Science Reviews*, 13, 517-520.

- Perucca, L.P., Rothlis, M. and Vargas, H.N., 2013. Morphotectonic and neotectonic control on river pattern in the Siera de la Cantera piedmont, central Precordillera, province of San Juan, Argentina, <http://doi:10.1016/j.geomorph.2013.09.014>.
- Pike, R.J. and Wilson, S.E., 1971. Elevation-relief ratio, hypsometric integral and geomorphic area-altitude analysis. U.S Geological Survey, 345, 1079-1083.
- Pinter, N., 2005. Application of tectonic geomorphology for deciphering active deformation in the Pannonian Basin, Hungary. In: Fodor L, Brezsynyansky K (eds) Proceedings of the workshop on “Application of GPS in Plate Tectonics in Research on Fossil Energy Resources and in Earthquake Hazard Assessment”, occasional papers of the Geological Institute of Hungary, 204, 25-51.
- Prasad, K.R.K. and Sarma, H., 1981. Systematic geological mapping around Tening Impai-Intuma area, Kohima district, Nagaland. Geological Survey of India, Progress report for the field season 1980-81.
- Prasad, K.R.K. and Sarma, H., 1983. Systematic geological mapping of Medziphema-Khonoma-Pulomi area, Kohima district, Nagaland. Geological Survey of India, Progress report for the field season 1981-82.
- Prescott, J.R. and Stephan, L.G., 1982. The contribution of cosmic radiation to the environmental dose for thermoluminescence dating - latitude, altitude and depth dependences. *Pact*, 6, 17-25.
- Preusser, F., Degering, D., Fuchs, M., Hilgers, A., Kadereit, A., Klasen, N., Krbetschek, M., Richter, D. and Spencer, J.Q.G., 2008. Luminescence dating: basics, methods and applications. *Quaternary Science Journal*, 57, 94-149.
- Radaideh, O.M.A., Grasemann, B., Melichar, Rostislav and Mosar, J., 2016. Detection and analysis of morphotectonic features utilizing satellite remote sensing and GIS: An example in SW Jordan. *Geomorphology*, 275, 58-79.
- Ranga Rao, A., 1983. Geology and hydrocarbon potential of a part of Assam Arakan basin and its adjacent regions. In: L.L. Bhandari (Ed.), *Journal of Petroleum Asia*, 127-158.
- Ranga Rao, A. and Murthy, K.N., 1980. The origin of Naga Thrust, Naga Hills, Assam. *ONGC Bulletin*, 17 (2).
- Ranga Rao, A. and Samanta, M.K., 1987. Structural style of the Naga Overthrust Belt and implications on exploration. *ONGC Bulletin*, 24 (1).
- Rastogi, B.K., Singh, J. and Verma, R.K., 1973. Earthquake mechanisms and tectonics in the Assam-Burma region. *Tectonophysics*, 18, 355-366.
- Rhodes, E.J., 1988. Methodological considerations in the optical dating of quartz. *Quaternary Science Reviews*, 7, 395-400.
- Rhodes EJ, Bronk-Ramsey C, Outram Z, Batt C, Willis L., 2003. Bayesian methods applied to the interpretation of multiple OSL dates: high precision sediment age estimates from Old Scatness Broch excavations, Shetland Isles. *Quaternary Science Reviews*, 22(12), 31-44.
- Rittenour, T.M., 2008. Luminescence dating of fluvial deposits: applications to geomorphic, palaeoseismic and archaeological research. *Boreas*, 37(4), 613-635.
- Rockwell, T.K., Keller, E.A. and Johnson, D.L., 1984. Tectonic geomorphology of alluvial fans and mountain fronts near Ventura, California. In: Morisawa, M.,

- Hack. T.J. (Eds.), Tectonic Geomorphology. Publ. in Geomorphology, State University of New York, Binghamton, 183-207.
- Roy, D.B., 2013. A study on OSL dating of sediments and its characteristic using SAR protocol. Summer internship report, Wadia Institute of Himalayan Geology, Dehradun.
- Roy, R.K. and Kacker, R.N., 1982. Tectonic analysis of Naga Hills Orogenic Belt along the eastern peri-Indian suture. *Himalayan Geology*, 10, 374-402.
- Roy, R.K. and Kacker, R.N., 1986. Cenozoic deformation pattern and mechanism in the Belt of Schuppen and their role in hydrocarbon accumulation: further exploratory concepts for Assam-Arakan basin. *Ophiolites and Indian Plate Margin* (eds), N.C. Ghose and S. Varadarajan, 197-221.
- Saha, D., 2011. Integrated analysis of Gravity and Magnetic data in the Upper Assam shelf and adjoining schuppen belt area-A critical review. The 2<sup>nd</sup> South Asian Geoscience Conference and Exhibition, GEO India.
- Sahu, N.K. and Venkataswamy, 1989. Report on systematic geological mapping around Chiephobozou and Tukuleqa areas of Kohima and Zunheboto districts, Nagaland. Geological Survey of India, Progress report for the field season 1988-1989.
- Sarma, H. and Bharatiya, S.P., 1978. Systematic geological mapping around Tuli, Merangkong and Changtongya area, Mokokchung district, Nagaland. Geological Survey of India, Progress report for the field season 1977-1978.
- Sarma, H. and Chakraborty, S.N., 1981. Systematic geological mapping of Peren-Pedi-Benreu area, Peren subdivision, Kohima district, Nagaland. Geological Survey of India, Progress report for the field season 1978-79.
- Saroli, M., Lancia, M. and Petitta, M., 2019. The geology and hydrogeology of the Cassino plain (central Apennines, Italy): redefining the regional groundwater balance. *Hydrogeology Journal*, <https://doi.org/10.1007/s10040-019-01953-w>.
- Schumm, S., 1956. Evolution of drainage systems and slopes in badland at Perth Amboy, New Jersey. *Geological Society of America Bulletin*, 67, 597-646.
- Schumm, S.A., Dumont, J.F. and Holbrook, J.M., 2000. Active tectonics and alluvial rivers. Cambridge University Press, Cambridge.
- Scheidegger, A., 2004. *Morphotectonics*, Springer, Amsterdam.
- Sen, K.K. and Krishna, T., 1975. Geological mapping in Naganimora-Tamlu areas of Mon, Tuensang and Mokokchung districts, Nagaland. Geological Survey of India, Progress report for the field season 1974-75.
- Shitiri, T.L., 2008. Report on systematic geological mapping in Dzuku valley, Kohima district and Tening subdivision, Peren district, Nagaland and its adjoining areas of Senapati and Tamenglong districts, Manipur. Geological Survey of India, Progress report for the field season 2006-2007 and 2007-2008.
- Shitiri, T.L. and Mishra, M.N., 1999. A report on photo-interpreted geological mapping in parts of Kohima, Mokokchung, Tuensang, Zunheboto and Phek districts, Nagaland. Geological Survey of India, Progress report for the field season 1998-99.

- Singh, L.S., 2017. Geodynamics and seismo-tectonics of Northeast India: A Review. *International Journal on Engineering Technology Sciences and Research*, 4(9), 700-703.
- Singh, S.K., Vidhyadharan, K.T. and Ray, S.B., 1983. Systematic geological mapping of Naga Hill ophiolites in the Phek district, Nagaland. Geological Survey of India, Progress report for the field season 1981-1982.
- Sinha, S. and Sinha, R., 2016. Geomorphic evolution of Dehra Dun, NW Himalaya: Tectonics and climatic coupling. *Geomorphology*, 266, 20-32.
- Slattery, S., 2011. Neotectonic Features and Landforms Assessment. Alberta Geological Survey report no. NWMODGR-TR-2011-19.
- Smith, G.I., Benson, L. and Currey, D.R., 1989. Quaternary Geology of the Great Basin 28<sup>th</sup> International Geological Congress Field Trip Guidebook T117, American Geophysical Union, Washington, DC.
- Smith, B.W., Rhodes, E.J., Stokes, S., Spooner, N.A. and Aitken, M.J., 1990. Optical dating of sediments - Initial quartz results from Oxford. *Archaeometry*, 32, 19-30.
- Snyder, N.P., Whipple, K.X., Tucker, G.E. and Merritts, D.J., 2000. Landscape response to tectonic forcing: Digital elevation model analysis of stream profiles in the Mendocino triple junction region, northern California: *Geological Society of America Bulletin*, 112 (8), 1250-1263.
- Sohbati, R., 2013. Luminescence rock surfaces. *Encyclopedia of Scientific Dating Methods*, 1-7, [https://doi.10.1007/978-94-007-6326-5\\_83-4](https://doi.10.1007/978-94-007-6326-5_83-4).
- Sreedevi, P.D., Subrahmanyam, K. and Shakeel, A., 2005. The significance of morphometric analysis for obtaining groundwater potential zones in a structural controlled terrain. *Environmental Geology*, 47 (3), 412-420.
- Starkel, L., 2003. Climatically controlled terraces in uplifting mountain areas. *Quaternary Science Reviews*, 22, 2189-2198.
- Strahler, A.N., 1952. Hypsometric (area-altitude) analysis of erosional topography. *Geological Society of America Bulletin*, 63, 1117-1142.
- Streit, R.L., Burbank, D.W., Strecker, M.R., Alonso, R.N., Cottle, J.M. and Kylander-Clark, A.R.C., 2015. Controls on intermontane basin filling, isolation and incision on the margin of the Puna Plateau, NW Argentina (~23°S). *Basin Research*, 1-25.
- Srinivasan, V., 2007. Regional structural configuration and seismic pattern of 'Belt of Schuppen' in Northeast India. *Journal of Geological Society of India*, 70, 801-814.
- Suess, E., 1904. The face of the earth. Oxford University Press.
- Sulaksana, N., Supriyadi, Ismawan, Rendra, P.P.R. and Sulastri, M., 2017. Active fault analysis through quantitative assessment method in Cikapundung Subwatershed. *International Journal of Scientific Research in Science and Technology*, 3(6), 147-153.
- Talukdar, P., 2013. Seismic study and spatial variation of b-value in Northeast India. *IOSR Journal of Applied Physics Japan*, 4(3), 31-40.



- Talukdar, P. and Barman, N.C., 2012. Seismic activity and seismotectonic correlation with reference to Northeast India. *IOSR Journal of Applied Physics Japan*, 2(1), 24-29.
- Troiani, F. and Della Seta, M., 2008. The use of the stream length gradient index in morphotectonic analysis of small catchments: A case study from Central Italy. *Geomorphology*, 102, 159-168.
- Tsodoulos, I.M., Koukouvelas, I.K. and Pavlides, S., 2008. Tectonic geomorphology of the easternmost extension of the Gulf of Corinth (Beotia, Central Greece). *Tectonophysics*, 453, 211-232.
- Tsukamoto, S., Rink, W.J. and Watanuki, T., 2003. OSL of tephric loess and volcanic quartz in Japan and an alternative procedure for estimation  $D_e$  from a fast component. *Radiation Measurements*, 23, 593-600.
- Tucker, G.E., Catani, F., Rinaldo, A. and Bras, R.L., 2001. Statistically analysis of drainage density from digital terrain data. *Geomorphology*, 36, 187-202.
- US Geological Survey. Earthquake epicenters from 1915 to 2016.
- Valdiya, K.S. and Narayana, A.C., 2007. River response to neotectonic activity: Example from Kerala, India. *Journal of Geological Society of India*, 70, 427-443.
- Verma, R.G., 1989. Photogeological mapping in parts of Kohima district, Nagaland. Geological Survey of India, Progress report for the field season 1988-1989.
- Vidyatharan, K.T., Srivastava, R.K., Bhattacharyya, S., Joshi, A. and Jena, S.K., 1986. Distribution and description of major rock types. Geological Survey of India, memoirs, 119, 18-27.
- Wallinga, J., Davids, F. and Dijkmans, J.W.A., 2007. Luminescence dating of Netherlands' sediments. *Netherlands Journal of Geosciences-Geologie en Mijnbouw*, 86 (3), 179 -196.
- Watitemsu, 2013. Paleomagnetic, petrographic and geochemical studies of the rocks of parts of central and eastern Nagaland. Ph.D., thesis, Nagaland University.
- Whipple, K.X., 2004. Bedrock rivers and the geomorphology of active orogens, *Annual Review of Earth and Planetary Sciences*, 32(1), 151-185.
- Whipple, K.X. and Tucker, G.E., 1999. Dynamics of the stream-power river incision model: implications for height limits of mountain ranges, landscape response timescales, and research needs. *Journal of Geophysical Research*, 104, 661-674.
- Whipple, K.X., DiBiase, R.A. and Crosby, B.T., 2013. Bedrock rivers. *Treatise on Geomorphology*, 9, 550-573.
- Wintle, A.G and Murray, A.S., 2006. A review of quartz optically stimulated luminescence characteristics and their relevance in single-aliquot regeneration dating protocols. *Radiation Measurements*, 41, 369-391.
- Wobus, C.W., Hodges, K.V. and Whipple, K.X., 2003. Has focused denudation sustained active thrusting at the Himalayan topographic front? *Geology*, 31(10), 861-864.
- Zhu, L., Wang, C., Zheng, H., Xiang, F., Yi, H. and Liu, D., 2006. Tectonic and sedimentary evolution of basins in the northeast of Qinghai-Tibet Plateau and their implication for the northward growth of the Plateau. *Palaeogeography, Palaeoclimatology, Palaeoecology*, 241, 49-60.